PART 5 – ACQUISITION AND TRACKING

INTRODUCTION AND SUMMARY

Acquisition and tracking will include subtopics of system requirements, performance analysis, tracker functions, tracking performance measured on a probability basis, and component burden relationships.

The advantage promised by laser communication is gained through the use of very narrow optical transmitter beamwidths allowing transmitter power requirements to be correspondingly small. This, in turn, requires very accurate pointing of the laser transmitter. Laser system pointing requirements are sufficiently more severe than microwave that this section deals mainly with optical acquisition and tracking.

The optimum acquisition and tracking system for a particular communication task depends on a host of mission parameters. For instance the transmission of data from a deep space vehicle (DSV) to an earth base receiver requires the spacecraft orientation with respect to a reference coordinate system to be determined. Then the spacecraft must be oriented so as to acquire a cooperative laser beacon at the receiver site. The ground beacon must be pointed to illumine the spacecraft taking proper account of atmospheric irregularities. An optional intermediate step is to have the ground based optical tracker acquire the spacecraft (by means of a broad beam on-board beacon) refining the knowledge of its position so that the ground beacon beamwidth may be narrowed. After the DSV transmitter has been pointed so that it irradiates the earth receiver, the tracking system must continue to point with sufficient accuracy that contact is maintained. The tracking system may be open or closed loop, depending on whether error information required to keep the transmitter beam properly oriented is generated at the receiver or at the transmitter. In either case, the acquisition and tracking system must take into account such factors as:

Relative motion between the tracker and the target.

Coordinate reference errors.

Signal propagation delays.

Aberration effects due to relative acceleration of the transmitter and receiver.

Perturbations of the spacecraft.

Atmospheric effects.

This study of the acquisition and tracking problem begins by considering the requirements imposed on the system by the peculiarities of the mission and the receiver location. Next, the acquisition and tracking system performance is analyzed in terms of these constraints and the system parameters which contribute to the overall pointing error. Then the various functions performed by the general (typical) optical tracker are delineated and a mathematical description of the performance of these functions in the presence of noise is presented. In particular, system performance measures such as probability of detection, probability of

acquisition, probability of false alarm, loss rate, tracking accuracy, etc., are established in terms of the system parameters such as beacon beamwidth, power, receiver FOV, background noise, dark current noise, etc.

Various modes of tracking implementation are discussed. The conventional forms of position encoding which are treated are the following: pulsed beacon (monopulse) system utilizing a quadrant photomultiplier and a CW beacon using pulsed position modulation (PPM), amplitude modulation (AM) and frequency modulation (FM).

Finally, the state of the art and burden of components which significantly affect acquisition and tracking system performance, such as star sensors, sun sensors and attitude control and stabilization devices, is surveyed.

GENERAL ACQUISITION AND TRACKING SYSTEM CONSIDERATIONS

Mission Associated Considerations

SIGNAL PROPAGATION DELAYS

Signal propagation delays over deep space distances require that laser beams be "pointed ahead," typically 0 to 100 microradians.

The acquisition and tracking system configuration is determined by the mission constraints and by the receiver location. Mission related constraints include range, system life, angular motion rates, reference coordinate system errors, and torques produced by equipment or personnel on-board the vehicle which perturb it. Receiver location considerations include atmospheric turbulence and attenuation associated with a ground base, and environmental and operation difficulties posed by a lunar or satellite base.

In the case of earth communication to and from a deep space vehicle (DSV) where significant propagation times are involved, appropriate considerations must be taken of "point ahead" angles. That is, the earth and space transmitters must each be directed toward the point in space where the respective receivers will be when the beams arrive. Thus, a lead angle, α_T, is required for both the earth transmitter and the DSV transmitter. The line-of-sight (LOS) vectors are defined in the figure. These vectors will be called the earth-to-deep space vehicle (E-DSV) and the deep space vehicle-to-earth (DSV-E) vectors, respectively. The E-DSV line-of-sight vector is directed to the DSV from a point in space where the earth was when the received light left the earth on its way to the DSV. Similarly, the DSV-E line-of-sight vector is directed to the earth from a point in space where the DSV was when the light left the DSV. The earth's receiver and DSV's receiver must be directed along the DSV-E and the E-DSV lines-of-sights, respectively.

If atmospheric effects and curved propagation paths are neglected, the earth transmitter axis will be parallel to the E-DSV LOS. Likewise the DSV transmitter axis will be parallel to the DSV-E LOS. Atmospheric effects will cause the transmitted beams to be distorted and bent. This effect is only partially self compensating since the effect is different for a far field wave front than for a near field front. Thus $\alpha_{T(Earth)} \neq \alpha_{T(DSV)}$ in general. This effect must be accounted for if it is desired to update the DSV lead angle from knowledge of the earth's lead angle. The earth receiver and the DSV receiver must be directed along the DSV-E and E-DSV lines-of-sight, respectively.

The position of the transmitter pointing vector relative to the receiver pointing vector may be determined if it is assumed that the lead angle, α_T, is small and that during the propagation times involved, the relative velocity angular direction (aspect angle) is constant. The length of the DSV-to-earth position vector will be approximately equal to that of the earth-to-DSV position vector. If this distance is R, and T is the round trip transit time,

then,

$$T = \frac{2R}{c} \tag{1}$$

where c = speed of light.

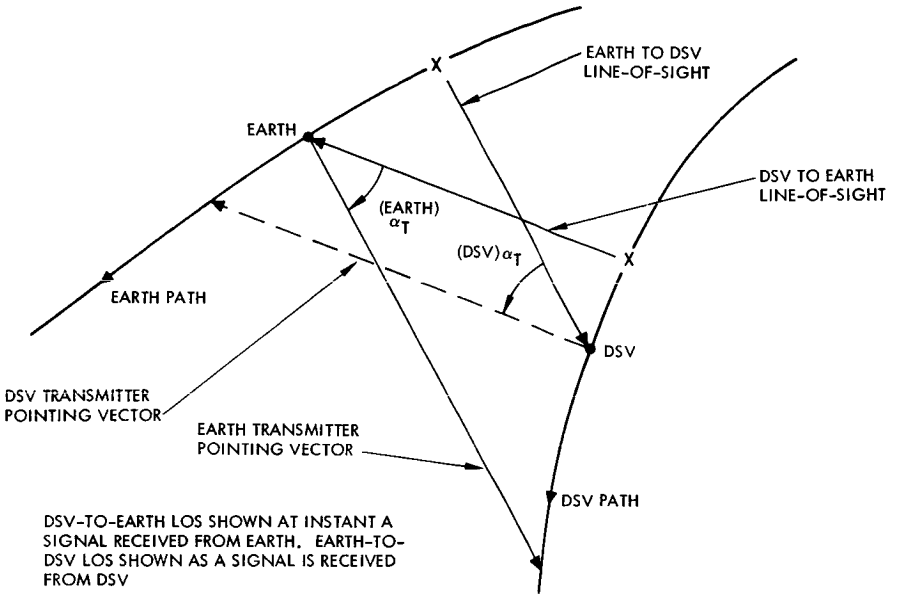

Earth and DSV Line-of-Sight Geometry

SIGNAL PROPAGATION DELAYS

The distance the earth station moves relative to the DSV during the round trip transit time is

$$d_E = V_T T \tag{2}$$

where V_T = the tangential velocity of the earth station relative to the DSV. For small angles, the lead angle may be written as

$$\alpha_T = \frac{d_E}{R} \tag{3}$$

Combining equation 1 and 2 gives

$$R = \frac{cd_E}{2V_T} \tag{4}$$

Substituting equation (4) in equation (3)

$$\alpha_T = \frac{2V_T}{c} \tag{5}$$

and it is seen that the lead angle is independent of the magnitude of the position vector, being only a function of the relative tangential velocity between the transmitter and respective receiver. Since $V_T \ll c$ for interplanetary missions in the foreseeable future, the small angle approximations made previously were valid. Lead angles will range from 0 to approximately 100 μrad during the transfer orbit phase of the mission. For landers and orbiters, lead angle calculations must include the rotation of the planet or the orbital angular velocity. The relative tangential velocity, V_T, is not measured directly but is determined from the range rate and the angular orientation of the LOS. Typically these would be measured from earth using the optical carrier frequency or by using an auxiliary r-f system operating at DSIF frequencies. For instance, the two-way DSIF system presently achieves a range rate accuracy of ±0.03 m/sec while doppler tracking accuracy in the 1970's will be on the order of 10^{-3} m/sec. Uncertainty in the orientation of the LOS introduces an additional error into V_T which is on the order of $V_T \Delta\phi$, where $\Delta\phi$ is the angular uncertainty. For $\Delta\phi = 0.001°$ (17.5 μrad) and V_T = 50 km/sec, ΔV_T due to this angular uncertainty is ≈ 0.88 m/sec. In order to achieve pointing accuracies of 0.001° it is necessary to use optical trackers rather than radio tracking.

RELATIVE MOTION BETWEEN TRANSMITTER AND RECEIVER

Angular rate of the LOS depends upon the range between the transmitter and receiver. Three range zones may be distinguished.

Angular line-of-sight (LOS) which must be accommodated by a space vehicle clearly are a function of the range to the receiving site from the spacecraft. Three general zones may be distinguished based upon acquisition and tracking criteria. These are near earth, near space, and deep space and are indicated in the figure.[1]

High angular LOS rates such as encountered between a ground station and a near earth satellite are typically 3°/sec for a 100 mile orbit. Such LOS rates, limit the viewing time (<10 minutes) and require more rapid acquisition. This in turn demands higher acquisition signal-to-noise ratios and wider transmitter beamwidths. At deep space ranges, LOS rates are much lower 0 to 2°/day typically for a Mars fly-by, which is more compatible with acquisition ease and with narrow beamwidths. In addition, a slew rate requirements are appreciably higher for high LOS rates, ranging from 60°/sec for near earth satellite to 10-20°/minute for a deep space vehicle.

LOS angular rates for the DSV tracker are significantly different for a fly-by mission than for orbiters and landers since orbiters and landers add the rotation of the target planet to their angular rates. This means that the tracking system used on such missions must either be capable of tracking at higher rates or of biasing at the nominal rate, which is known approximately from astronomical data.

[1] N.G. Lozins, "Pointing in Space," Space Aeronautics, August 1966, pp. 76-83.

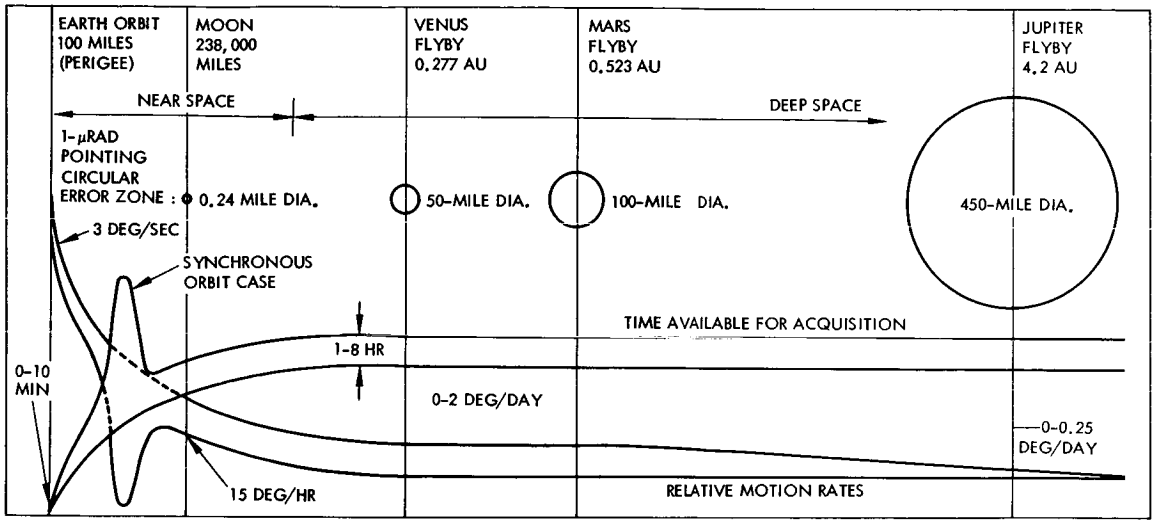

Angular Rates and Available Acquisition Time

Note that there are three range zones which may be distinguished on the basis of range rate and time available for acquisition.

COORDINATE REFERENCE FRAME ERROR

Celestial coordinate reference frames have errors of the same or greater order of magnitude as the pointing accuracy of a laser system.

A fundamental limitation on the orientation of the DSV acquisition and tracking system is the accuracy with which a reference coordinate system can be specified. The available coordinate systems each have peculiarities which must be taken into consideration.

For instance, in the earth-centered equatorial reference system, one of the three orthogonal axes is defined by the line from the center of the earth to the first point of Aries which is that point where the path of the sun crosses the celestial equator from south to north on or about March 22. Currently there is no visually observable star at this location. This point moves westward along the ecliptic at the rate of 50.26 arc-sec per year as a result of the precessional motion of the earth's axis (other motions are also involved). The reference axes form an orthogonal set along this direction, the direction to the north pole, and a third direction normal to these two.

Similar problems arise in the heliocentric system reference system which uses the line from the center of the sun to the first point of Aries as an axis. Deep space acquisition and tracking systems using a celestial reference will have to compensate for these and other stellar motions noted below.

Motions to be considered include both the motions of binary stars and multiple star systems about a common center of gravity, and so-called "proper" motions, which are small changes in stars positions that increase steadily over the passage of years. (Each star has its own peculiar motion, which is called proper motion by astronomers.) For instance, Arcturus and Rigel Kent, two zero-magnitude stars have proper motions which exceed 2 and 3 arc-sec/year, respectively.

In addition to these real motions, there are apparent motions which include the parallactic displacement of nearby stars with respect to the distant stars in the background. This motion is due to the radial displacement of the earth from one side of its orbit to the other. The closer the star, the greater the parallax. The nearest star, Proxima Centuri, has a parallax of 0.763 arc-sec. Space ships venturing beyond 1 AU from the sun would observe proportionately larger values.

The effect of these coordinate errors upon an acquisition and tracking system clearly depends upon the relative size of the transmitted beamwidth to these errors. In the situations where they are comparable and where long flight times are involved, it will be necessary to compensate for these errors by such means as programming pointing corrections or by searching over larger angular sectors during the acquisition.

MANNED VERSUS UNMANNED VEHICLES

Manned and unmanned missions have complementary advantages and disadvantages; in a manned vehicle, the man can correct errors in a tracker but his presence causes disturbances. The unmanned mission has fewer disturbing torques but may need redundancy to provide continuous tracking.

The advantages of a manned mission from an acquisition and tracking point of view are manifold. In conjunction with an on-board computer, man can make very accurate course and attitude correction and navigational sightings. Thus man is better capable of determining the DSV's course, attitude, and position than an earth based observer. Furthermore the astronaut can align an inertial platform reference device and make corrections for its drift. Two other important advantages of manned flight are the facts that continuous tracking and attitude control are not required as are for the unmanned mission. A manned mission has the added advantage of accurate lead angle alignment, eliminating the errors associated with the servo device necessary to the unmanned system. The lead angle may be determined by optical techniques and adjusted when desired. An additional advantage to a manned mission is the ability of the man to perform routine maintenance and repairs; and unmanned mission would require complete redundant systems for the equivalent reliability.

The primary disadvantage of a manned mission is the effect of man motion on the spacecraft, with resulting additional stringent restrictions on the tracking and pointing control system in order to avoid degradation of the tracking and pointing accuracy. For the manned mission this disadvantage may be circumvented and several advantages of the unmanned system acquired if a separate "satellite" vehicle were used for optical communication. If a failure should occur, such a vehicle would be maintained by the astronauts, the lead angle accurately reset, and its platform could be realigned. When communication is desired, the "satellite" vehicle would be separated from the mother vehicle, and maneuvered in space by remote control or tethered to the mother vehicle for convenient retrival.

An unmanned mission will have the restraints of continuous tracking and continuous attitude control. An inertial platform reference device is not feasible for this system since drift correction would be very difficult. In place of a platform, star trackers and sun sensors could be used for attitude reference and control.

The general block diagrams for the "satellite" vehicle for the manned mission and for the unmanned mission are shown in Figures A and B, respectively. For both missions, the electromagnetic transit delay is involved twice in the DSV-E-DSV communication loop. Cross-coupling of the dynamic relationships is indicated by the dotted lines. An inertial platform and rate gyro stabilization is used on the satellite vehicle for the manned missions. Due to offset and drift problems, star trackers (or similar devices) are used for rate and attitude stabilization for the unmanned missions.

The computer shown is intended for the complex navigational and lead angle computations. However much of this burden may be removed by an earth based computer.

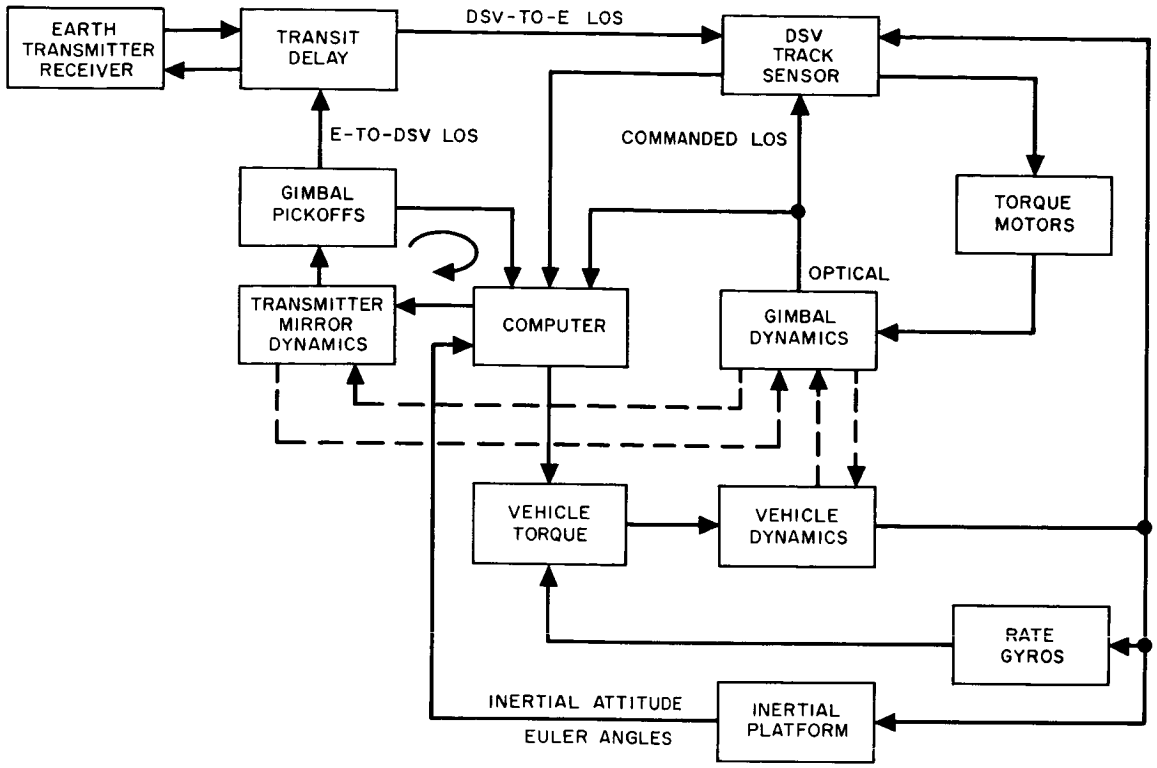

Figure A. Deep Space Vehicle (DSV) Communication Control System Block Diagram for a Manned Mission Communication "Satellite"

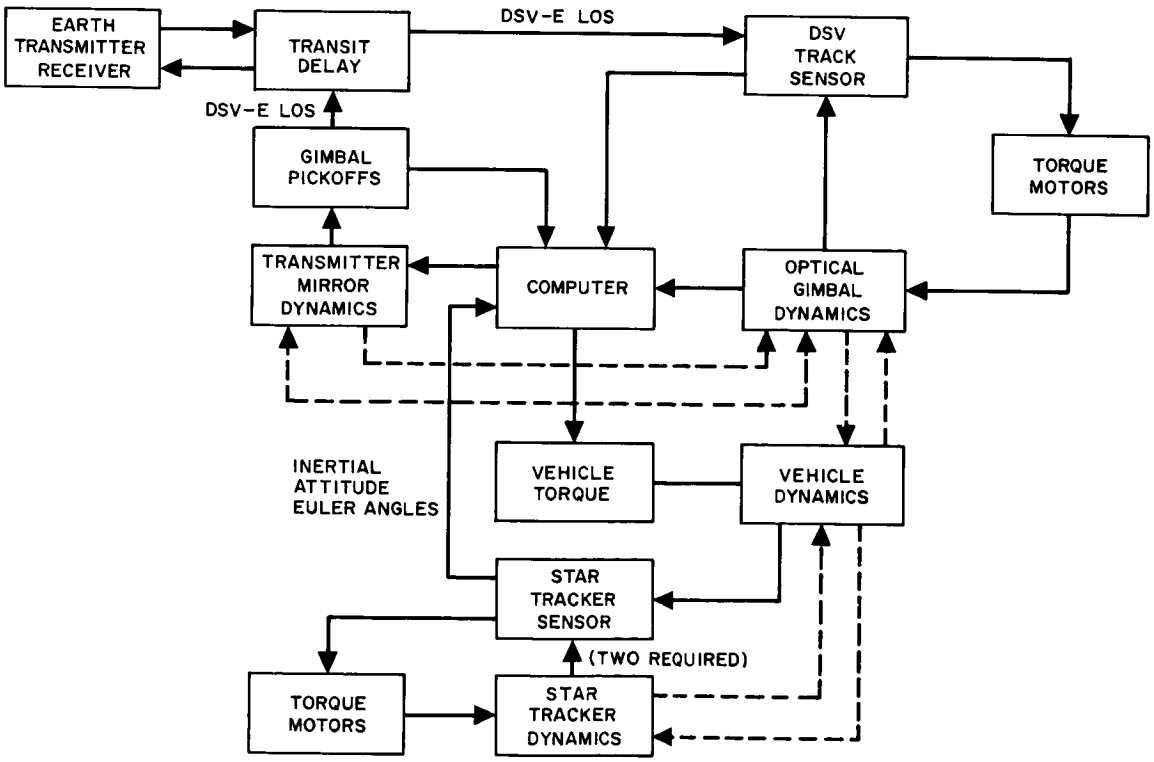

Figure B. Deep Space Vehicle (DSV) Communication Control System Block Diagram for an Unmanned Mission

GENERAL ACAUISITION AND TRACKING SYSTEM CONSIDERATIONS

Receiver Location Considerations

EARTH BASED RECEIVER ATMOSPHERIC CONSIDERATIONS

An earth based receiver for an optical link must cope with atmospheric beam pointing effects including refraction and beam steering.

The deep space link receiver location has considerable bearing on the acquisition and tracking problem. Two possible locations, earth and earth-satellite, each have unique operational and economic advantages or disadvantages. The most significant of these will be considered briefly in this topic and the next topic.

The greatest disadvantage of an earth based receiver for deep space communications is presence of the earth's atmosphere. The first consideration is the attenuation of the optical or radio frequency carrier by absorption and scattering. Cloud coverage, fog, and/or smog may make optical communications impossible for a large percentage of the space mission time. Therefore earth locations must be found where the possibility of such interferences are minimized*.

In addition to attenuation, the atmosphere interferes with optical propagation by refraction, and by such turbulence induced effects as beam spreading, beam steering, and scintillation. Exhaustive measurements of steady state refraction have been made by astronomers. These are summarized in the table[1].

Qualitatively it should be noted that there is a fundamental difference between the fluctuations in signal level during transmission and those during reception. During reception, although diffraction at the spacecraft spreads the beam over a large portion of the earth, all the energy incident on the receiver aperture can be detected if a sufficiently large field stop (detector) is used. However, during transmission, only that portion of the beam that leaves the atmosphere in the direction of the spacecraft is used. There is only a slight spreading of the beam during passage through the atmosphere, but angular or phase disturbances are created because the plane wave front has been distorted. These disturbances may result in a large spreading of the beam after subsequent propagation. Angular divergence here, perhaps not yet affecting beam diameter because of the large initial diameter, will ultimately be the determining factor in beamspread. In antenna phraseology, the top of the atmosphere is still in the near-field region of an optical transmitter. The basic difference between transmission and reception can be summarized as follows: In transmission, cumulative phase fluctuations (which cause angular divergences) are important; however, in reception, only the cumulative amplitude fluctuations (produced by phase fluctuations near the top of the atmosphere) are significant.

Beam steering arises from time-dependent atmospheric inhomogeneties and introduces a random angular error in specifying the true direction of

*Suggestions are given in Part 1 of Volume IV of this report "Background Radiation and Atmospheric Propagation".

[1]Perkin-Elmer Report No. 7846, Contract NAS8-11408, SPO 26471, November 1964.

Average Refraction Angle Versus Apparent Zenith Angle[1] for Visible Light

Apparent Zenith Angle (degrees)	Refraction Angle (minutes and seconds of arc)		Apparent Zenith Angle (degrees)	Refraction Angle (minutes and seconds of arc)	
0	0	0.0	70	2	35.7
5	0	5.0	75	3	30.0
10	0	10.1	80	5	13.1
15	0	15.3	81	5	46.0
20	0	20.8	82	6	26.0
25	0	26.7	83	7	15.0
30	0	33.0	84	8	19.0
35	0	35.7	85	9	40.0
40	0	47.9	86	11	31.0
45	0	57.1	87	14	7.0
50	1	8.0	88	17	55.0
55	1	21.4	89	23	53.0
60	1	38.7	90	33	51.0
65	2	1.9			

EARTH BASED RECEIVER ATMOSPHERIC CONSIDERATIONS

the earth-to-DSV line of sight vector which is superimposed on the predictable steady state refraction. This requires the earth-based transmitter to transmit over a correspondingly wider angle to insure that the DSV is illuminated.

The amount of beam deflection which can be expected depends directly on the strength of the turbulence. As the turbulence goes from weak to strong, beam steering angles typically vary from ±1 to ±15 μrad (rms). Very strong turbulence can produce deflections on the order of ±50 μrad (rms). In addition, the apparent direction of the LOS will vary in time due to quivering at frequencies on the order of a hundred cps or less. These (relatively) rapid angular variations can amount to the same order of magnitude as in the slowly varying part mentioned above. The upper limits quoted refer to daytime conditions. At night conditions are markedly improved due to decreased thermal gradients.

Scintillation introduces random angle noise into the angle trackers with a power spectrum that varies as the -2/3 power of frequency at very low frequencies and has a high frequency cutoff determined by wind velocity and telescope aperture.

EARTH-SATELLITE BASED RECEIVER AND RECEIVER SITE COMPARISON SUMMARY

The advantages and disadvantages of an earth-satellite station are compared with an earth station.

A satellite base offers the possibility of continuously tracking a deep space probe with no outage due to eclipsing or due to atmospheric effects. A synchronous satellite, using a proper inclination angle with respect to the earth's equator, would have a small probability of being occluded by either the earth or the moon during a particular space mission for a time period in the order of months. In any case, not more than two such satellites should be required to provide uninterrupted link performance.

A synchronous satellite, rotating at the same speed as the earth, remains continuously visible from a given earth position.

A synchronous satellite orbit, inclined with respect to the ecliptic plane by an angle somewhat greater than 8.5° ($\sin^{-1}$ 26,500/39,00) will be continuously visible to a deep space probe which is on a line formed by the intersection of the plane of the ecliptic and a plane perpendicular to the synchronous satellite orbit. This is indicated in the figure. As the deep space probe moves off this line there will be periods where the earth will occlude the LOS. Using an orbit with greater inclination will alleviate this, however over a period of time the earth will eventually be in a position to occlude the LOS unless the orbital plane of the synchronous satellite is precessed.

The absence of atmosphere at the earth-satellite greatly reduces acquisition and tracking problems since transmission losses, scintillation, image motion, and scattering effects will be reduced or eliminated. Furthermore continuous view eliminates switchover and reacquisition problems.

Aside from economic considerations, the principal disadvantage of the satellite based receiver is that it imposes on the receiver site acquisition and tracking system the design, reliability, and operating requirements associated with a space vehicle.

The table gives a comparison between the two links considered. Each site considered has definite advantages. A ground base for instance may utilize as much prime power and as large an antenna size as is considered necessary. A satellite base offers no atmospheric effects, a good probability of continuous coverage, and excellent pointing accuracies. The disadvantages are also well defined. A ground base is subjected to atmospheric effects, high background noise during the day, lack of continuous coverage from a single station, frequency reacquisition and long switchover time.

A satellite base is limited by antenna size and prime power, requires more complex and costlier equipment than a ground station, and in the event of occulations poses difficult reacquisition problems. Further, a satellite site requires the acquisition and tracking system to withstand large dynamic loads during boost.

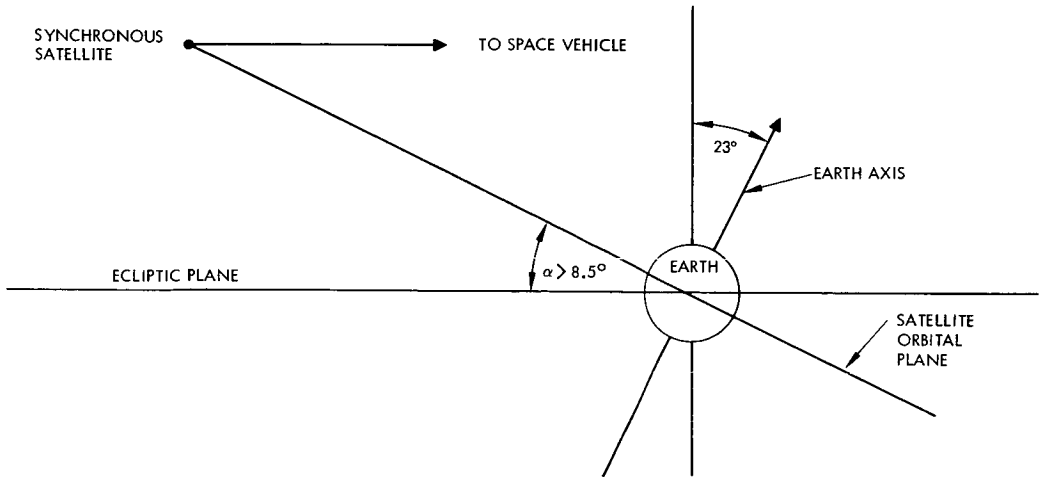

Field of View of a Synchronous Satellite

EARTH-SATELLITE BASED RECEIVER AND RECEIVER SITE COMPARISON SUMMARY

From analysis of this report it would appear that although the earth's atmosphere poses severe problems, they are not insurmountable. That is, a workable deep space system can be built which has its receiving station located on the earth's surface rather than a satellite receiver.

Comparison of Optical Receiver Sites

Base	Advantages	Disadvantages
Earth	Power limited by laser state of art	Pointing accuracy limited by image motion, beam spread
	Antenna size limited by variable flexure of structure	Power reduced by absorption and scattering
	Logistics and maintenance simplified	High background noise during daytime operation
	Sophisticated data processing and trajectory prediction equipment available	Possibility of operation depends on meteorological condition
		Several ground station required for continuous coverage
		Switchover and reacquisition problems difficult
		Long and frequent switchover time
Satellite	No atmospheric effects	Power and antenna size limited in near future by payload requirements
	Low background noise	Monitoring and control ground station required
	Continuous coverage probable from single base	Complex equipment
		No maintenance
	Excellent pointing accuracy	Switchover and reacquisition difficult

INTRODUCTION

In this section the primary emphasis is placed on one-way transmission from an unmanned deep space vehicle (DSV) to a receiving terminal located either on or near the earth.

The station at the DSV end of the communications link and the earth station are similar, in that both consist of input and output devices, a tracker, and signal processing electronics. Three important differences are: higher data rate assumed to be required for DSV-to-earth transmission, limited available space and power in the DSV, and environment of the DSV. As a result of the first two differences, a narrower beam is required for the down link and as a result of the absence of an atmosphere at the DSV, such a narrow transmit beam is possible. Accurately pointing and controlling such a narrow beam (to values as small as 1 microradian) are the major tasks of the acquisition and tracking control system.

In order to insure boresight integrity between the DSV transmitter and receiver, it would be desirable to use the same primary optical system. If the transmitter and receiver use different wavelengths (e. g. different laser modes) separation of the transmitted and received signals can be accomplished spectrally, and the full aperture can be used for each.

The subsections which follow include discussions of the following topics. 1) Acquisition subsystem operational consideration, 2) the tracking subsystem, 3) Signal-to-noise analysis of optical tracking systems, 4) acquisition, 5) detection theory, and 6) angle noise in optical tracking systems.

Subsequent Subsections

- Acquisition subsystem, operational considerations
- The tracking subsystem
- S/N analysis of optical tracking systems
- Acquisition
- Detection theory
- Angle noise error in optical tracking systems.

THE ACQUISITION SUBSYSTEM OPERATIONAL SEQUENCE

The acquisition sequence for the DSV consists of 3 phases: acquisition of inertial coordinates, acquisition of earth beacon, and tracking of earth beacon in narrow beam mode.

The sequence of events during the acquisition of the receiver site beacon by the deep space vehicle (DSV) is outlined in the following paragraphs.

Initially, a beacon at the receiver site capable of providing an adequate signal-to-noise ratio for DSV acquisition will be assumed. Thus the problem of acquisition reduces to orienting the DSV receiver field-of-view so the beacon falls within it.

The spacecraft is oriented in three phases. First it must be oriented such that the earth falls within a solid angle specified by the system gimbal limits. This is accomplished as follows: any large residual angular rates are first eliminated through operation of gas jets controlled by signals from a set of three rate gyros, one for each principal axis. The vehicle will then be oriented to point the telescope directly away from the sun by means of the gas jets and two-axis sun sensors. Roll rate about the telescope axis will be reduced to the limit cycle and held. Attitude signals for the pitch and yaw axes will be generated by the sun sensors, which are nulled when the telescope looks away from the sun. Next is the acquisition of the roll reference star (Canopus or a similar star) by the roll star tracker. This will be accomplished by a command roll rate about the sun line of sight (via gas jets) until the reference star enters the field of view. The generated star tracker error signal is then switched into the roll loop. Care must be taken to select the vehicle search rate small enough that the reference star may be acquired before the star passes through the field of view. Once acquisition of the star line-of-sight is complete an inertial reference has been established. Command signals are now given for a pre-programmed attitude maneuver and the spacecraft is rotated to point the telescope in the vicinity of the earth. (At near earth ranges, the horizon sensor can be used at this point.) When limit cycle operation has been achieved, the system is ready for the second phase of the acquisition.

The second phase of the acquisition consists of searching volume of space by scanning the DSV receiver using the telescope in a wide* angle field-of-view mode. The scan optics of the telescope start at the edge of the solid angle formed by the known uncertainty limits and search toward the telescope axis until the earth beacon is detected. When the beacon is detected, the error signals are switched into the gimbal drives of the telescope and the telescope axis is oriented along the DSV-E line of sight. The system is now in a coarse error detection mode.

*This phase may not be used when the DSV beam is 100 microradians or greater.

In the third phase of the acquisition the space vehicle's communication system is switched from the wide-angle search to the narrow angle track mode. (It may be necessary to do this in several steps if the wide angle tracking error is greater than the telescope's narrow angle field of view.) The system is now in the fine error detection or detection or tracking mode of operation.

The sun sensor can now be switched out of the vehicle pitch-yaw control channels, and be replaced by the tracking error signals, from the beacon. The star tracker must be retained however, since the two-axis control error commands. This marks the completion of the acquisition sequence and tracking control mode begins.

PHASES IN THE ACQUISITION SEQUENCE

- Acquisition of Inertial Coordinates
- Acquisition of Earth Beacon
- Tracking of Earth Beacon

ACQUISITION AND TRACKING SYSTEM PERFORMANCE ANALYSIS

The Tracking Subsystem

THE TRACKING SUBSYSTEM – INTRODUCTION

The Deep Space Vehicle (DSV) tracking loop, its errors and potential error reductions are noted.

The major contributions to pointing error in relation to stabilization and tracking characteristics are defined in this subsection for the DSV and for ground based tracking systems. The possible use of a near earth relay station to circumvent atmospheric effects on the downlink is discussed. The nature of pointing error budgets and interfaces and constraints with other subsystems are discussed for each case.

The relationship of system elements and the major angular error sources are shown in the figure for a tracking system.

The DSV-earth-DSV closed loop indicated by the dashed lines has the potential disadvantages of requiring several separated receivers at each earth-station for continuous coverage and of being able to correct errors which occur at frequencies corresponding to the 2-way transit time. However, this is only servo loop which can enclose the transmitter boresight and lead angle error sources. The transmitter-tracker relative alignment problem is made more difficult by the fact that the variable lead angle adjustment precludes mechanical locking following an in-flight alignment procedure. The major categories of pointing errors, typical causes and means of reducing their effects are summarized in the table.

Accurate pointing of massive structures such as a telescope is most efficiently done by having the entire spacecraft react to the torquing of a small inertia wheel control system. However, in certain applications, e.g., man motions or pointing two telescopes in different direction simultaneously, this is not possible. In such circumstances the telescope must be free to move relative to the spacecraft, and a means of controlling the telescope must be provided. It appears that the most difficult aspect of stabilization to the accuracies required for the DSV is associated with the generation of error signals of sufficient resolution and the alignment of the sensor sensitive axes with the control axes. The extremely precise control required necessitates vehicle configuration that will minimize the external disturbance torque effects as well as internal disturbance torques caused by inertial crosscoupling, equipment motion, temperature gradients, etc. Disturbance torques due to internal moving parts can be reduced by restricting activity during the fine tracking. However, disturbance torques due to inertial crosscoupling can be significant unless care is taken to balance the vehicle such that the inertias in all three axes are approximately equal. In addition, care must be taken to minimize the angular momentum stored in the vehicle.

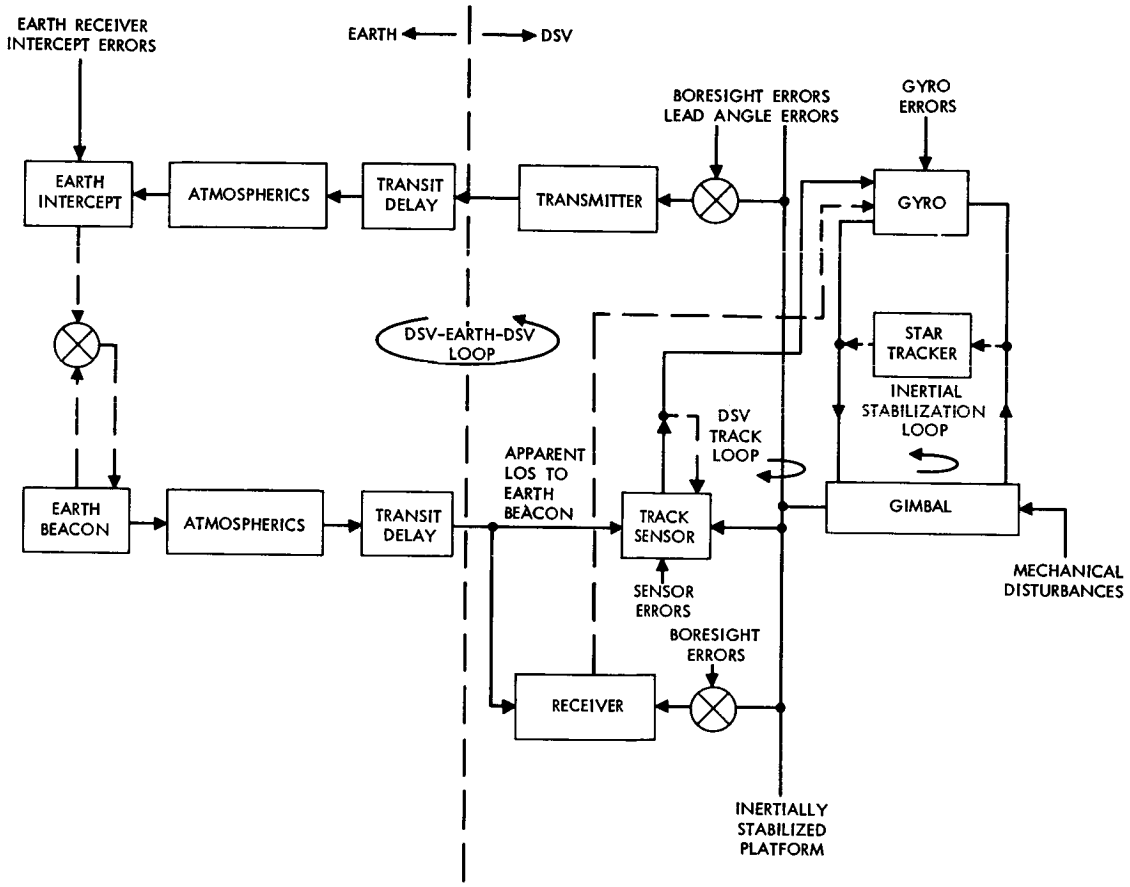

Simplified Relationships of Earth-DSV Tracking Loops and Angle Error Sources

Pointing Error Causes and Means of Correction
for Optical Servo Systems

Pointing Error Cause	Means of Correction
1. Mechanical disturbances of stabilized platform. (Bearing friction and misalignment, gimbal c.g. misalignment, spring torque from leads)	a. Attenuated by inertial stabilization b. Employ focal plane stabilization c. Separate from DSV d. Improve state-of-the-art
2. Stabilization system errors. Gyro drift (static and G-sensitive), resolver inaccuracies, accelerometer, tachometer	a. Feedback compensation b. On-gimbal star sensors c. Track loop design d. State-of-the-art improvement
3. Track errors. Sensor noise, error curve inaccuracies, resolver errors, focal plane tolerances	a. Lower tracking loop bandwidth b. Minimize tracking field-of-view c. Null tracking modes d. Increase beacon power
4. Mechanical alignment errors of optical axes. (Mechanical tolerance, lead angle errors)	a. Require only relative alignment b. Use closed loop where possible c. In-flight alignment/calibration
5. Atmospherics	a. Near earth relay b. Ground site selection c. Spatial averaging by distributed receivers

DSV TRACKING SUBSYSTEM – POINTING ERROR

The interrelationship of several errors associated with the DSV tracker is defined.

The correct pointing angle, in inertial coordinates, is given by the sum of the apparent line of sight (LOS) to the earth beacon, $_{Bd}$, and the lead angle, θ_{ld} (see the figure).

In general, pointing errors may be classified into three categories. These are listed below and illustrated in the figure.

1. Boresight and Lead Angle Errors (ϵ_B) - These errors contribute a static or nearly constant term to pointing error and are especially troublesome since they cannot be enclosed in a closed loop other than a DSV-earth closed loop. The penalty for excessive boresight errors is severe as the result is likely to be loss of transmission for an extended period of time. At ranges of 1 AU or more the round trip transit time exceeds 15 minutes and therefore correcting this error from the earth is slow.

2. Mechanical Telescope Perturbations (ϵ_p) - The steady state response of the stabilization and tracking system may often be sufficient to suppress low frequency mechanical perturbations to a tolerable level. However, due to limited frequency response, high frequency components may cause transients in the inertial telescope pointing angle in excess of desired limits. Since these errors are sensed as apparent line of sight motions by the tracker they will be reduced by the combined action of track and stabilization loops. Under maximum spacecraft maneuvers the tracking system may not be able to contain the pointing error within prescribed limits so that an outage during maneuvers may accrue.

3. Tracking Errors (ϵ_T) - The true tracking error signal, θ_T, of the DSV tracker is given by:

$$\epsilon_T = \theta_{Bd} - \theta_{td} - \psi_{fd}$$

where θ_{td} is the orientation of the telescope axis in inertial coordinates under static conditions, i.e. $\theta_T = 0$, and, ψ_{fd} is the displacement of the tracker look angle (LOS) from the telescope axis (see the figure).

The angle noise in the tracker, originating from such sources as the beacon tracking sensor and the inertial reference sensor of the stabilization system, may be treated by standard Gaussian noise techniques. The angle noise power spectrum is modified by the closed loop response of the tracker and is included as a random term appearing in both θ_{td} and ψ_{fd}. This is considered in more detail in a subsequent topic.

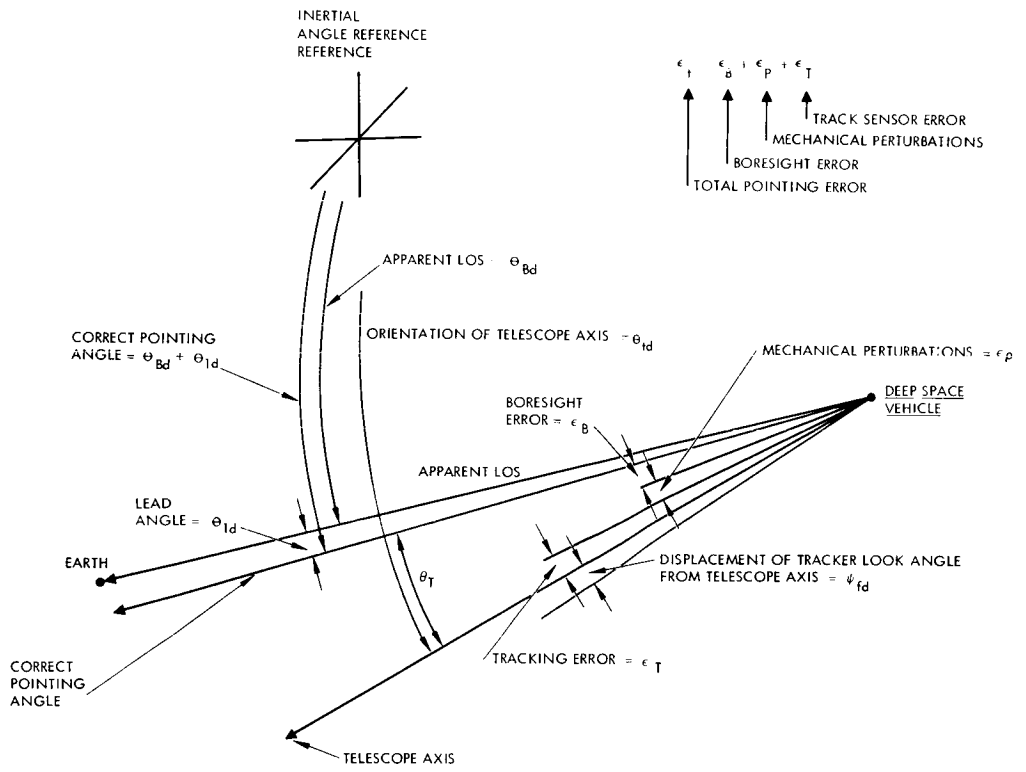

Correct Pointing Angle and Errors Associated with a Tracking System

DSV TRACKING SUBSYSTEM – POINTING ERROR

The total pointing error is then:

$$\epsilon_t = \epsilon_B + \epsilon_P + \epsilon_T$$

where the right-hand terms are the boresight, telescope perturbations, and tracking noise respectively. A typical system pointing accuracy specification therefore would include:

1. An absolute limit on boresight errors in the presence of thermal telescope environment, etc., and the accuracy of lead angle commands.

2. A specification on the tracking and stabilization system which reduces pointing errors as a function of deterministic mechanical disturbances of the telescope including expected rates and the torques due to the attitude control system and spacecraft-earth relative motion. In final form this type of specification may include the mechanical transfer characteristics of the Deep Space Vehicle-tracker-pointer mechanical interface.

3. A specification of the random tracking noise in the tracker to reduce loss rate in the presence of the aforementioned pointing error to be the prescribed level.

DSV TRACKING SUBSYSTEM – DESCRIPTION

The relationships of errors and implementation for a typical DSV tracking system are noted.

The servo loop of a typical vehicle track system using a mechanical inertial stabilization system is shown in Figure A. For simplicity only the outer gimbal loop is shown. The outer gimbal axis is denoted by the subscript d and is considered as part of a three axis system, attached to the inner gimbal of which is the track sensor platform. The three axis gimbal coordinate system is aligned with an i, j, k spacecraft coordinate system with the d axis coincident with the k axis when the inner and outer gimbal angles (and respectively) are zero. The angular track error signal, $_T$, detected by the track sensor is given by the difference between the LOS to the earth beacon, $_{Bd}$, (in inertial coordinates) and the course telescope angle, $_{td}$, plus the fine deflection pointing angle, $_{fd}$.

$$\theta_T = \theta_{Bd} - \left(\theta_{td} + \psi_{fd}\right) \tag{1}$$

The detected error signal is given by the sum of $_T$ and sensor errors, ϵ_t. The track angle error is modified by the fine deflection track closed loop function[1] to give:

$$\theta_T = \frac{s\,(\theta_{Bd} - \theta_{td})}{2 + K_1 K_2 g_1(s)} + \frac{\epsilon_t}{1 + s/K_1 K_2 g_1(s)} \tag{2}$$

The servo compensation function $g_1(s)$ generally has the character of a low-pass (or lag/lead) network. The effect of stabilization errors (spurious telescope motions, ϵ_p due to mechanical disturbances) may thus be reduced by the fine deflection tracking system up to the limiting response frequency of this loop. The frequency cut-off of the fine deflection track loop is limited primarily by the output information bandwidth of the track sensor which as a rule of thumb must be at least 6 times the bandwidth of the track loop to maintain phase margins. As can be seen from Equation (2) however, a high loop bandwidth makes the tracker more sensitive to sensor tracking noise (in proportion to the square root of the track loop bandwidth) so that even when the track sensor and deflection control mechanism are capable of arbitrarily fast reaction, the optimum track loop bandwidth should be limited.

In addition to correction of the track error by the fine deflection loop, the error signals from the track sensor are smoothed and used to correct the telescope pointing angle. The telescope must correct at a rate sufficiently fast to insure that the track angle $_{fd}$ does not exceed the

---

[1] See Figure A for definition of K_1, K_2, $g_1(s)$

dynamic range of the fine deflection loop. This mechanism forms an outer or telescope tracking loop which encompasses the inner or fine deflection loop.

In a typical application the inner or fine deflection tracking loop contains the major contribution to the rms tracking noise. For the case where the angle noise power density, $W\eta(t)$ of the track sensor is essentially white over the frequency response of the track loop, the rms tracker noise is from Equation (2).

$$\epsilon_N = \left[W\eta\,(0)\, 2\pi \int_0^\infty df \frac{|g_1(f)|^2 K_1^2 K_2^2}{|K_1 K_2 g_1(f) + j2\pi f|^2} \right]^{1/2} \qquad (3)$$

$$= \left[W\eta\,(0)\,(\Delta f)_s \right]^{1/2}$$

where $(\Delta f)_s$ is the closed loop bandwidth.

The tracker noise power density at low frequency $W\eta\,(0)$ is related to the solid FOV of the tracker, Ω_R; the tracker voltage signal to noise ratio, SNR_V; and the tracker information bandwidth $(\Delta f)_i$ by:

$$W\eta\,(0) \leq \frac{\Omega_R}{(SNR_v)^2\,(\Delta f)_i} \qquad (4)$$

thus given the track field of view, track loop response time, $(\Delta f)_i$, and rms angle accuracy $j\epsilon_N$, the tracker sensitivity, SNR_v, is determined.

There are two major potential tradeoff quantities in the vehicle acquisition and tracking subsystem: (1) the bandwidth of the closed fine tracking system, f_t, and (2) the field of view of the tracker, Ω_R. The closed track loop bandwidth must be chosen large enough to reduce the residual stabilization error and small enough to avoid a large tracker noise contribution. Similarly the track field must be chosen sufficiently large to reduce tracker loss rate to a negligible level. However, an increased track field of view decreases the angular accuracy of the track sensor since the angle noise component due to sensor noise increases linearly with the size of the track FOV. In addition the errors due to tracker non-linearities and resolver readouts increase with the size of the FOV to be covered.

Sensor Boresight Errors. In a typical image sensor (vidicon, orthicon, image dissector) and non-linearities relating beam position to sweep voltage produce a tracking error which is proportional to the angular track field. In most cases this error is of the order of 1/2 to 1 percent.

DSV TRACKING SUBSYSTEM - DESCRIPTION

The quadrant photodetector depends for angle accuracy on the balance of energy in the blurred image of a point target among the four sections of the field of view. Even in the absence of noise, the null accuracy is limited by the degree to which the gains of the four channels can be balanced. Figure B shows the boresight error as a function of gain imbalance in a single channel. Thus in order to reduce boresight errors to less than 1 percent of the linear response portion of the field of view, gain imbalance must be held to less than 10 percent over the dynamic range of signal levels.

Resolver and Non-Orthogonality Errors. In the following, the method of analysis and parametric relations for tracking errors due to resolver inaccuracies and misalignment of gimbal axes is presented in some detail. Resolver error is the error that exists between the actual resolver shaft position and the indicated shaft position.

Base plate misalignment error is defined to be the angular error that arises when a gimbaled system is mounted on a reference base. The outer gimbal axis of rotation (see Figure C) is taken as the reference for determining these mounting errors and the mount may be misaligned with respect to a similar axis contained in the base. Since angles measured about three orthogonal axes completely specify the mounting misalignment, angles corresponding to roll ($\Delta\alpha$), pitch ($\Delta\beta$), and yaw ($\Delta\lambda$) are used for convenience.

In addition to base plate misalignment, the inner gimbal axis may not be orthogonal to the outer gimbal axis and cause pointing errors. This angle ($\Delta\gamma$) is measured in a plane orthogonal to the gimbal pointing direction.

The line-of-sight of each sensor may be misaligned with respect to the gimbal pointing direction for the mounts. These misalignment angles (Δx and Δy) are measured about an orthogonal set of axes (e and d) contained in a plane orthogonal to the gimbal pointing direction. Δx is measured about the d axis and Δy about the e axis.

Servo error is the error introduced by the tracking servo as a result of base motion inputs and servo noise. These sources of error (with the exception of servo dynamic error) are due to electrical and mechanical inaccuracies (measurement and fabrication) that can only be described in a statistical manner. It is assumed that the error parameters are statistically independent and that each parameter is normally distributed with zero mean.

Since the tracking servo base motion inputs and line-of-sight tracking rates are random with time the servo errors due to these inputs can also be considered to be random variables with zero mean.

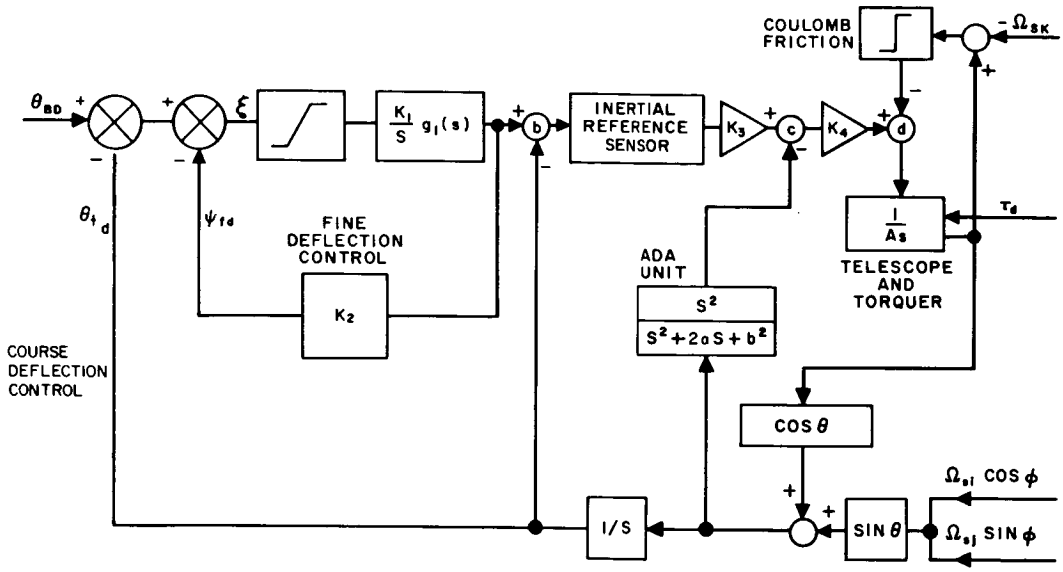

Figure A. Typical Outer Gimbal Servo Loop with Inertial Stabilization

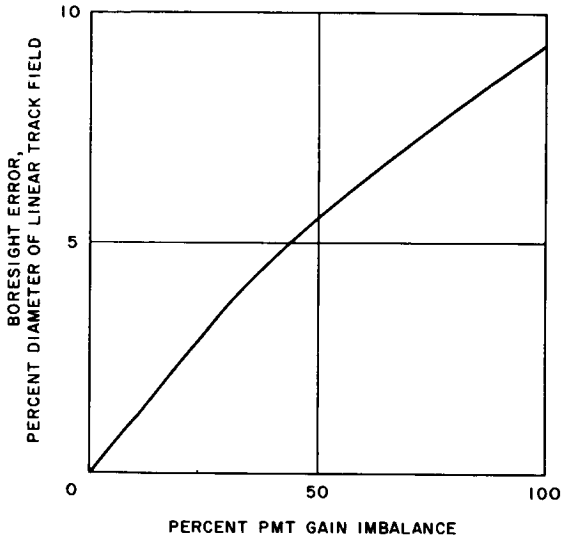

Figure B. Quadrant Detector Boresight Errors

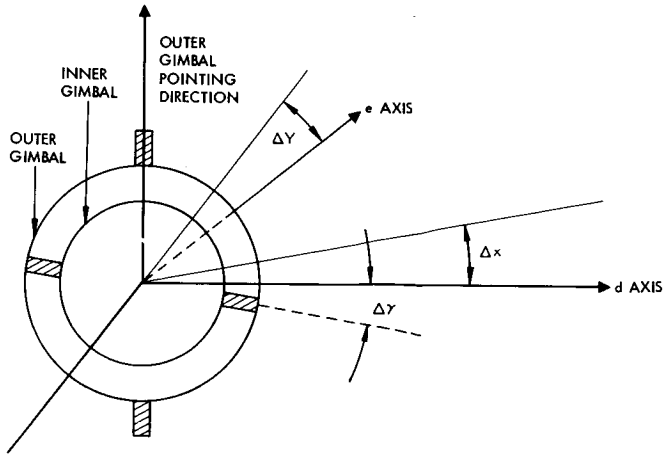

Figure C. Gimbal Alignment Geometry

STABILIZATION SUBSYSTEMS

Stabilization requirements and their effect on the tracking system are reviewed.

The stabilization loop shown in the figure illustrates typical problems in reducing the magnitude of mechanical perturbations to a tolerable level in the 0.1 - 1.0 arc-sec pointing accuracy regions. The disturbances may generally be classed as rate and torque disturbances. Rate disturbances are caused by vehicle maneuvers and the action of vehicle attitude control sensors. Torque disturbances may be caused by vehicle thrusting, meteorite impact or spring torques such as lead connections from the gimbals.

Angular rate disturbances denoted by $\Omega_{s;i,j,k}$ of the vehicle couple into the telescope dynamics primarily through bearing friction which is generally treated as ideal viscous (coulomb) friction and enters the servo loop as a torque at point (d). Disturbing torques may be minimized by placing the telescope mounting coaxial with the main thrust vector. However, a residual moment arm due to misalignment of the telescope center-of-gravity with the center of the gimbal axes remains. In addition, the vehicle structure will have an anisotropic transfer component so that torques directly about the gimbal axis will occur.

The stabilization shown reduces the input mechanical disturbances by (1) comparing the telescope position to an inertial reference sensor, point 6, and (2) by ADA (or accelerometer), point c, feedback loops around the telescope. In the typical stabilization scheme a rate integrating gyro mounted on the gimbal structure is used to sense motions of the telescope in inertial space. The output voltage of the gyro is then used to torque the gimbals so as to null the telescope inertial rate. When, as in the track mode, it is required to move the telescope in inertial space a torquing command is fed to the gyro. The major problems with current gyros are gyro drift and limited reliability. Performance of the best gyros to date is a few hundreths deg/hr (static) drift and greater than 20/million hours failure rate. The contribution of gyro drift to overall pointing and tracking accuracy is minimized by the low frequency error rejection of the closed track loop.

An alternate mechanization of the inertial reference sensor are star trackers mounted on the telescope platform. Since these must have a separate gimbal system to allow narrow field tracking of individual stars the inertial reference frame determined by the star trackers must be referenced to gimbal axis system through a coordinate transformation.

The steady state equivalent input angular rate error, e_{da} (ss), reflected into the track loop at point (a) from input periodic torque disturbances which are lower in frequency than the natural frequency of the stabilization loop is:

$$e_{da}(ss) = \tau_d / K_3 K_4$$

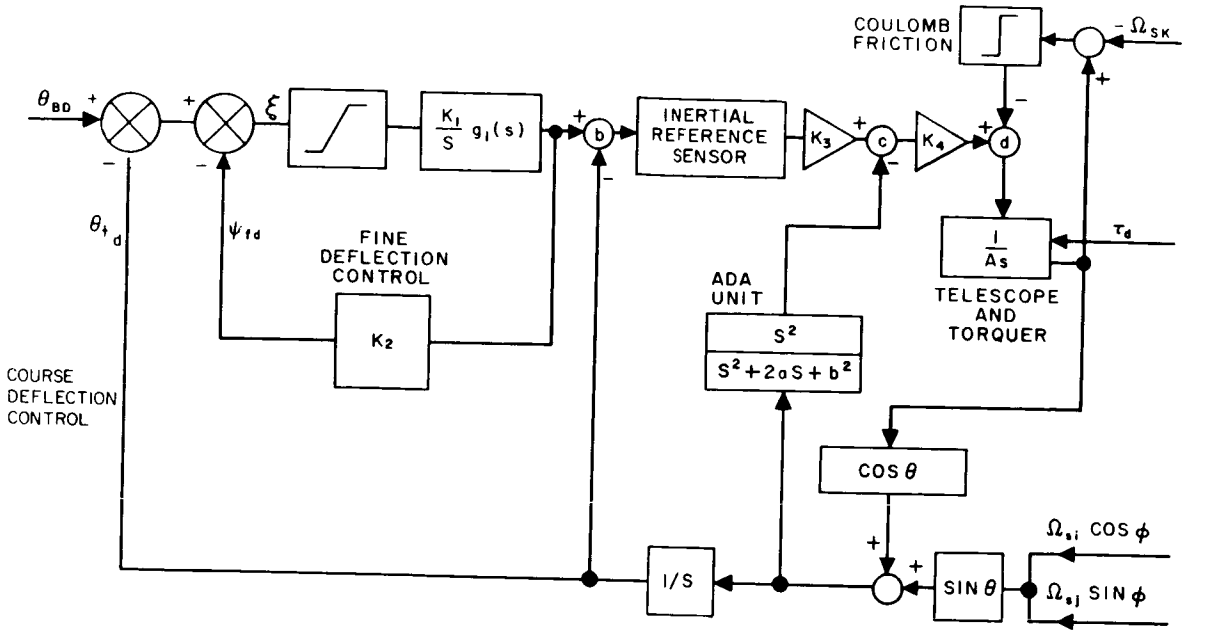

Typical Outer Gimbal Servo Loop
with Inertial Stabilization

STABILIZATION SUBSYSTEMS

thus the limitation on the ability of the stabilization system is to minimize disturbances of this sort depends on the open loop gain (and frequency response) which can be supplied in the stabilization ystem.

Optical Design Constraints. In addition to sensitivity and resolution requirements, the design of systems in which the tracker shares the same aperture with the transmitter and receiver of the optical communication system imposes additional constraints on the optical design:

1. The field angle over which the optics are capable of collimating the transmitter beacon to the desired beamwidth must include in addition to the tracker field of view a range of angles sufficient to allow the transmitter lead angles to be generated. For a typical Mars transfer orbit this amounts to an extra 40 seconds of arc.

2. In systems employing aperture sharing rather than time sharing of earth beacon provision must be made to provide tracker-transmitter optical isolation of a very high degree.

Inertial Reference Unit and Guidance and Navigation Unit Interfaces. Data concerning relative range and range rate must be made available to compute the tracker lead angles. In addition, initial pointing angles for the acquisition process must be referenced to the gimbal coordinates through the gimbal angle readouts.

Vehicle Mechanical Interface. The reduction of high frequency mechanical disturbances transmitted over the optical platform – Vehicle interface is of prime importance to maintaining high pointing accuracy within acquisition and tracking subsystem. Where high pointing accuracy is required during periods of operation of reciprocating machinery, attitude control limit cycling, and thrusting; a solution to the problem is to modify the optical platform mount so as to reduce the high frequency perturbations. This may take the form of soft mounting or mechanically disconnecting the platform. Means must be provided however to allow referencing of spacecraft and gimbal axis coordinate systems.

Boresight Maintenance. The relative boresighting of the tracker and transmitter must be maintained to high accuracy in the thermal and mechanical environment of the spacecraft.

EARTH STATION – POINTING ERROR BUDGET

The error budget is described in terms of statistical and bias errors, the interrelationship is documented and sample normalized loss rate curve presented.

The major sources of pointing error in a ground tracking system are:

1. Atmospheric Scintillation (ϵ_S) - Angle scintillation due to random phase errors is introduced into the spacecraft beacon by the atmosphere. From the point of view of the angle tracker, scintillation introduces random angle noise with a power spectrum which varies as the -2/3 power of frequency near zero frequency and has a high frequency cut off determined by wind velocity which for large aperture telescopes will usually occur at a few cps.

The maximum blur due to atmospheric scintillation imposes a limitation on the tracker FOV. Typically the blur size can vary from 0.5 go 3 arc-sec at night and from 1 to 6 arc-sec for daytime observation.

2. Boresight and Lead Angle Errors (ϵ_B) - The pointing errors due to misalignment of the earth beacon and earth tracker and errors in introducing the beacon lead angle are of the form of bias errors.

3. Tracker Errors (ϵ_T) - Errors introduced in the tracker system such as tracker noise and track sensor boresight errors. The total pointing error is thus

$$\epsilon = \epsilon_S + \epsilon_B + \epsilon_T$$

which is the same form noted in a previous topic that described the Deep Space Vehicle pointing error.

A figure of merit for trackers is loss rate, Λ, defined as the inverse of the mean time between loss of track. The loss rate may be expressed as a function of the tracker error parameters, statistical and biased.

By denoting ϵ_N to be the rms sum of the statistical scintillation and tracker noise contributions to the tracking error, and ϵ_o as the angular radius limit of an earth beacon, the loss rate, Λ, is given approximately by:

$$\Lambda \approx 2\pi f_t \left(\frac{\epsilon_o - \epsilon_B}{\epsilon_N}\right) \exp\left\{-1/2\left[\left(\frac{\epsilon_o - \epsilon_B}{\epsilon_N}\right)^2\right]\right\}$$

where f_t is the closed loop bandwidth of the tracker. (The multiplicative constant will vary somewhat depending upon the filtering used but this formulation is representative.)

The figure plots the loss rate as a function of ϵ_o/ϵ_N using ϵ_B as a parameter and normalized with $f_t = 1$.

The mean time between losses should obviously be large when compared to the largest time lag in the tracking system. This lag is the round trip time, which is in the order of 15 minutes for a Mars encounter. If the mean time to loss is specified as 20 times this, a loss is allowed once for every 18,000 seconds or a loss rate of 5.56×10^{-5}. As may be seen from the figure this requires the ratio of ϵ_o/ϵ_N to be between 6.2 and 9.2 as ϵ_B varies between 0.1 and 0.4.

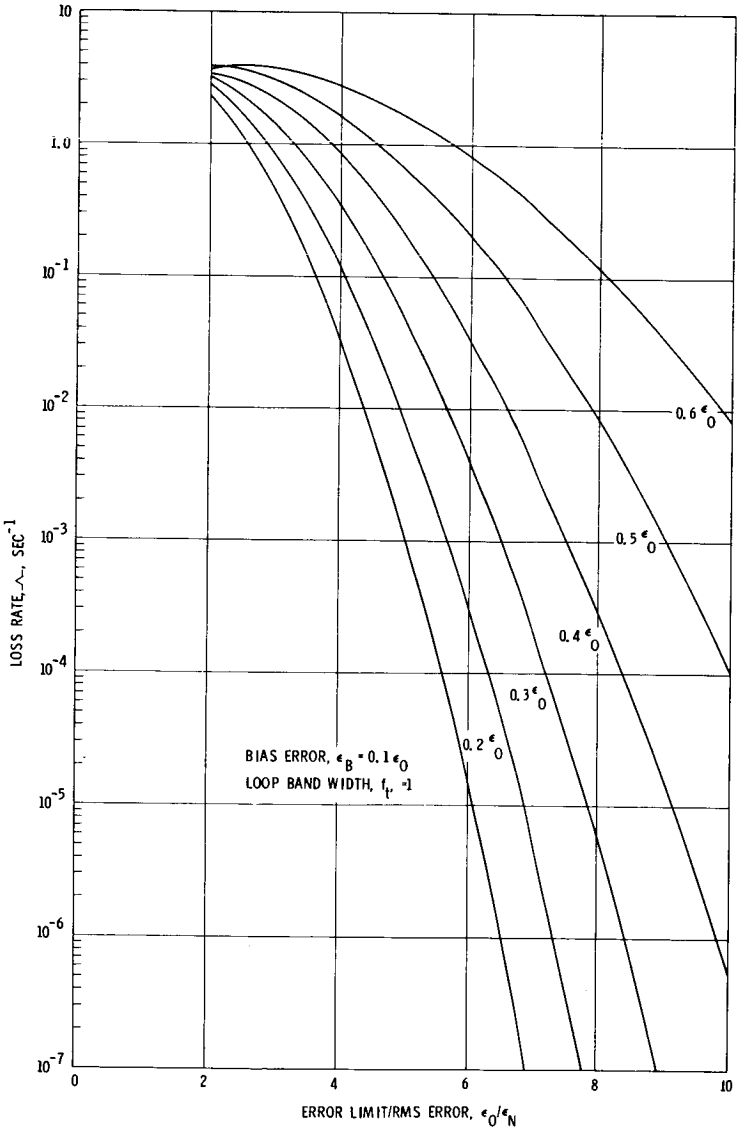

Tracking Loss Rate

SIGNAL TO NOISE RATIOS FOR STAR TRACKERS

Signal to noise examples are given for a star reticle tracker as a function of star magnitude for 3 implementations.

Star trackers operate in the visible spectrum and therefore will use direct detection due to its high efficiency and its simplicity. Beacon trackers may use direct detection or heterodyne detection but due to the simplicity, direct detection operating in the visible light range is favored.

The equation describing the signal-to-noise ratio for direct detection has been developed in Volume II under "Detection Noise Analysis." It is repeated here for convenience.

$$\frac{S}{N} = \frac{\left(\frac{G\eta q}{hf} P_C\right)^2 R_L}{kTB_o + 2qB_oG^2\left(\frac{\eta q}{hf} P_C + \frac{\eta q}{hf} P_B + I_D\right)R_L} \qquad (1)$$

where:

G = detector gain

η = detector quantum efficiency

q = electronic change, 1.602×10^{-19} coulombs/electron

h = Plank's constant 6.624×10^{-34} watt sec . sec

f = light frequency, Hz

P_c = received carrier power, watts

R_L = load resistance, ohms

k = Boltzmann's constant, 1.38×10^{-23} watts/Hz °K

T = Amplifier noise temperature, °K

B_o = Amplifier bandwidth, Hz

P_B = Background received power, watts

I_D = dark current, amps

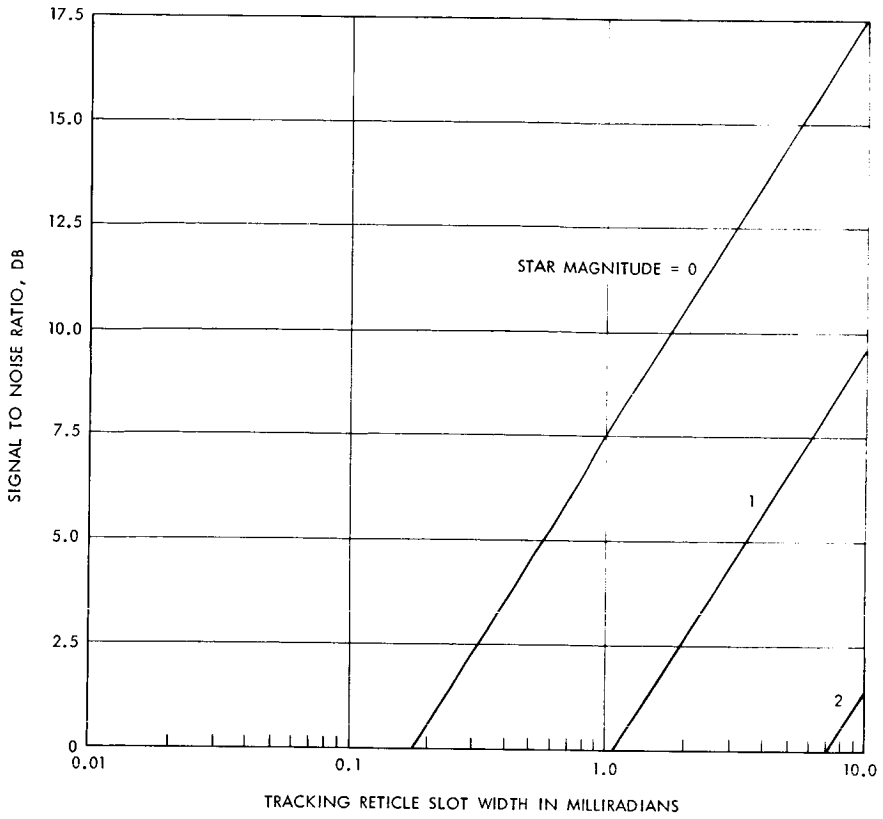

Figure A Sample Signal to Noise Ratio, Using a Photomultiplier Diode (Thermal Noise Limited)

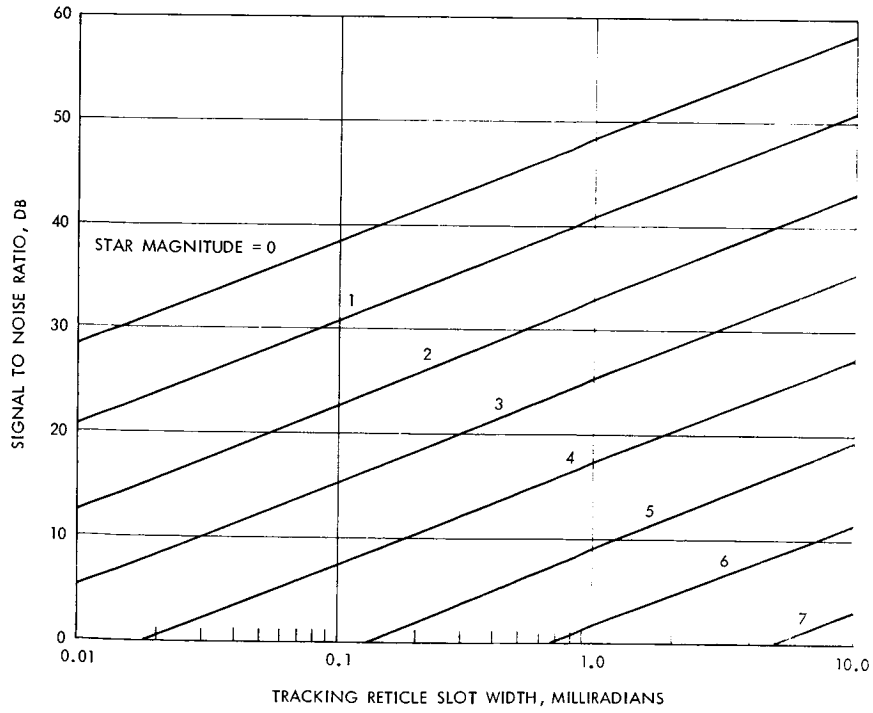

Figure B. Sample Signal to Noise Ratio Using a Photomultiplier Detector (Dark Current Limited)

SIGNAL TO NOISE RATIOS FOR STAR TRACKERS

Symbolically this is

$$\frac{S}{N} = \frac{\text{Signal Power}}{\begin{array}{l}\text{Thermal} \\ \text{noise} \\ \text{power}\end{array} + \begin{array}{l}\text{shot} \\ \text{noise} \\ \text{power}\end{array} + \begin{array}{l}\text{background} \\ \text{noise} \\ \text{power}\end{array} + \begin{array}{l}\text{dark} \\ \text{current} \\ \text{noise} \\ \text{power}\end{array}}$$

The power received from the star, P_c, is

$$P_c = (H_s)(A_o)(B_1) \tag{2}$$

where

H_s = Star irradiance watts/cm^2-micron

A_o = Star tracker effective receiving area

B_1 = Optical filter bandwidth

The video bandwidth of the tracker depends upon the type of tracker used. If a nutating reticle is used, the incoming position is encoded by the reticle rotation. This can be done by allowing the incoming signal to pass through a slit of width W. If the slit is offset by r milliradians, 2 r corresponds to the nutation circle. If the nutation rate is f_s, the time the star is in the slit is t_o or:

$$t_o = \frac{\omega}{2\pi r f_s} \text{ seconds}$$

This time may be related to the required tracking bandwidth as

$$B_o \approx \frac{1}{t_o} = \frac{2\pi r f_s}{\omega} \tag{3}$$

If equation (2) and (3) are substituted into equation (1) and certain parameters values assumed, the signal to noise ratio may be calculated. Values for such a calculation are given in Figure A for a photo diode (G = 1) and for a photo multiplier tube (G = 10^5) in Figures B and C using star magnitude as a parameter. Other assumed parameter values are noted below.

η = 0.585

f = $3 \times 10^8 / .5 \times 10^{-6}$

R_L = 300 ohms

T = 350°K

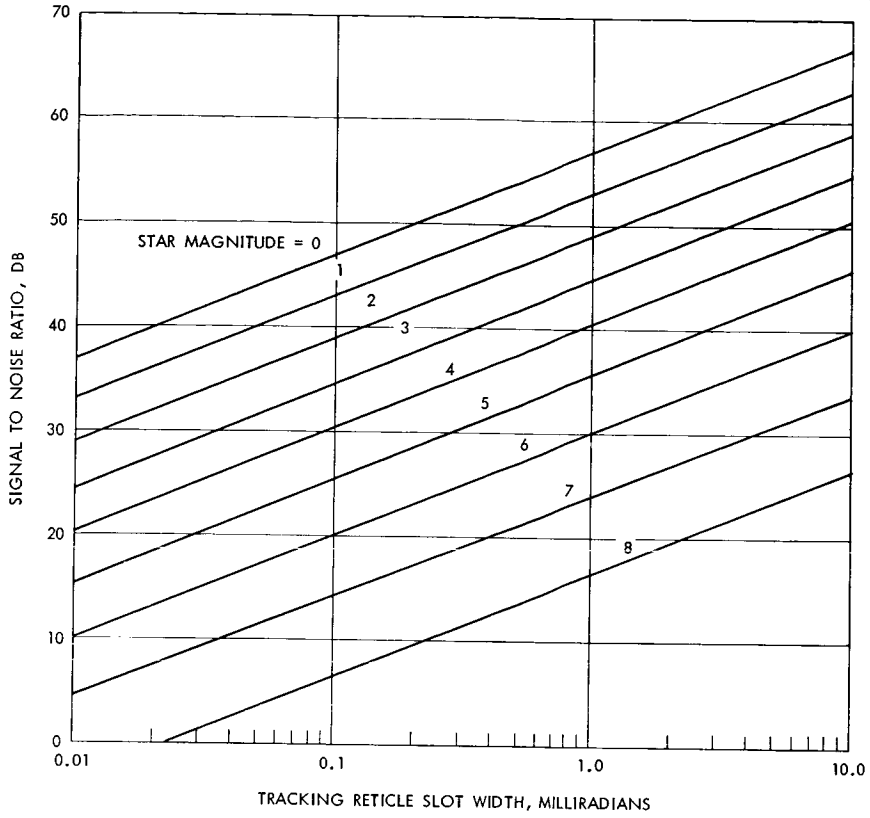

Figure C. Sample Signal to Noise Ratio Using a Photomultiplier Detector (Signal Limited to Background Limited)

r = 5 milliradians

f_s = 32 rev/sec

P_B = equivalent to 6th magnitude star (1.1×10^{-14} watts/cm^2-micron)

I_D = 10^{-8} amps and zero amps (Figure C only)

A_o = 10 cm^2

B_l = 3 microns

H_s = 3×10^{-12} watts/cm^2 - micron (0 magnitude - star)

It should be noted that the signal to noise ratio of Figure A is thermal noise limited while the signal-to-noise ratio of Figure B is dark current noise limited. Figure C which has the dark current set to zero, is signal noise limited for strong signals (near zero magnitude) and background noise limited for weaker signals (6th magnitude and greater). (Note that the background value assumed correspond to a 6th magnitude star.)

ACQUISITION AND TRACKING SYSTEM PERFORMANCE ANALYSIS

Acquisition

MEAN TIME TO ACQUISITION

The mean time to acquire is developed in terms of the statistical and nonstatistical detection parameters.

It is generally desirable to acquire the transmitter-beacon as rapidly as possible. The speed of acquisition is limited by: (1) the possibility of passing over the transmitted signal without detecting it, and (2) the possibility of acquiring false signals produced by noise if the threshold is reduced to increase the sensitivity of the receiver to the transmitted signals.

A quantity $\overline{T}_a$ is defined as the mean time to acquire. The system is to be designed to minimize this number subject to various constraints imposed by other conditions. The average cost, in lost time, due to false acquisitions during the interval required to scan the acquisition field once, is

$$C_o = R_f T_\ell \, (T_\Sigma - T_\sigma)$$

where R_f is the average rate of false target acquisitions, T_ℓ is the lost time due to acquiring a false target, T_Σ is the minimum time to scan the search field of view, and T_σ is the time spent on target during a single scan. The average time needed to scan the acquisition field is then

$$\overline{T}_\Sigma = (T_\Sigma + C_o)$$

If no signal is sensed it is necessary to scan the complete acquisition field again before acquisition can be made. If the decision is "no target" on the second scan, the field scan is repeated, etc. If the target has equal probability, P_o, of being anywhere within the field, the mean time to acquire is

$$\overline{T}_a = \frac{\overline{T}_\Sigma}{2} P_o + \frac{3}{2} \overline{T}_\Sigma P_o (1-P_o) + \frac{5}{2} \overline{T}_\Sigma P_o (1-P_o)^2 + \ldots$$

$$= \frac{\overline{T}_\Sigma}{2} \frac{(2-P_o)}{P_o}$$

The minimum time in which the field can be scanned is

$$T_{\Sigma} = \frac{\Sigma}{R_s}$$

where Σ is the size of the search field of view and R_s the scanning rate. If the receiver field of view is σ, the time spent on target during a single scan, T_{σ}, is

$$T_{\sigma} = \frac{\sigma}{R_s}$$

In addition the number of scan elements, N_s,

$$N_s = \frac{\Sigma}{\sigma}$$

Since the target may be in any one of these elements with equal probability, P_o, this probability is given by

$$P_o = \frac{1}{N_s} = \frac{\sigma}{\Sigma}$$

In terms of the fundamental parameters the mean time to acquire becomes

$$\overline{T}_a = \frac{\Sigma}{2R_s}\left[1 + R_f T_\ell \left(1 - \frac{\sigma}{\Sigma}\right)\right]\left[2\frac{\Sigma}{\sigma} - 1\right]$$

The quantity R_f is dependent on the noise which arrives at the thresholding device, the scan rate, R_s, and the receiver field of view, σ. Sources of noise are the photoelectric detector, background radiation, fluctuations in the signal and background due to atmospheric effects, and the random distribution in time of the photons which constitute the received power. These quantities, the false alarm rate and the probability of detection respectively, are discussed in the following for both the low incident flux level (Poisson) and high incident flux level (Gaussian) cases.

ACQUISITION PROBABILITIES

The acquisition probability is given as a function of the number of angle bins searched, the probability of signal plus noise exceeding the threshold, and the probability of noise alone exceeding the threshold.

The acquisition beamwidth, σ, must scan over the uncertainty solid angle, Σ. Using a simplifying assumption relative to beam overlap, defines K angle bins where $K = \Sigma/\sigma$. If the probability of the noise exceeding the detection threshold is taken as P_N and the probability of the signal plus noise exceeding the threshold is P_S, then probability of acquisition, P_{acq}, may be determined as follows:

$$P_{acq} = \sum_{n=1}^{K} P(m) (1 - P_N)^{n-1} P_S \qquad (1)$$

where P(m) is the probability that the signal is in the $m^{\underline{th}}$ bin. The acquisition implementation used is one where the beam is scanned until a target is detected. Thus the entire frame will not be scanned unless the target is not detected. If a false target is detected the false target angle coordinates are tracked until the nature of the false target is determined. If the simplifying assumption is made that P(m) = 1/K equation (1) reduces to

$$P_{acq} = \frac{P_s}{K} \sum_{n=1}^{K} (1 - P_N)^{n-1} \qquad (2)$$

this is a geometric series which has as the sum

$$P_{acq} = \frac{P_S}{K} \left[\frac{1 - (1 - P_N)^K}{1 - (1 - P_N)} \right]$$

or

$$P_{acq} = \frac{P_S}{KP_N} \left[1 - (1 - P_N)^K \right] \qquad (3)$$

Equation 3 has been plotted for three values of K, the number of angle bins, in Figures A, B and C. In each figure the probability of acquisition, P_{acq}, is given as a function of P_S, the probability of signal and noise exceeding the threshold, using P_N, the probability of noise only exceeding the threshold, as a parameter. P_S and P_N may be a result of several types of statistics, Poisson, Gaussian, etc. Values for P_N and P_S in terms of such statistics are given in subsequent sections.

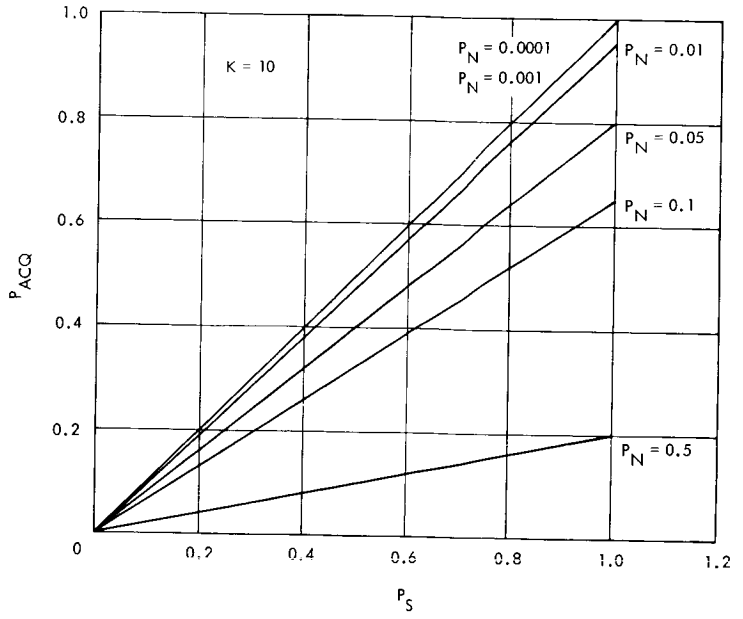

Figure A. Probability of Acquisition when 10 Angle Bins are Used

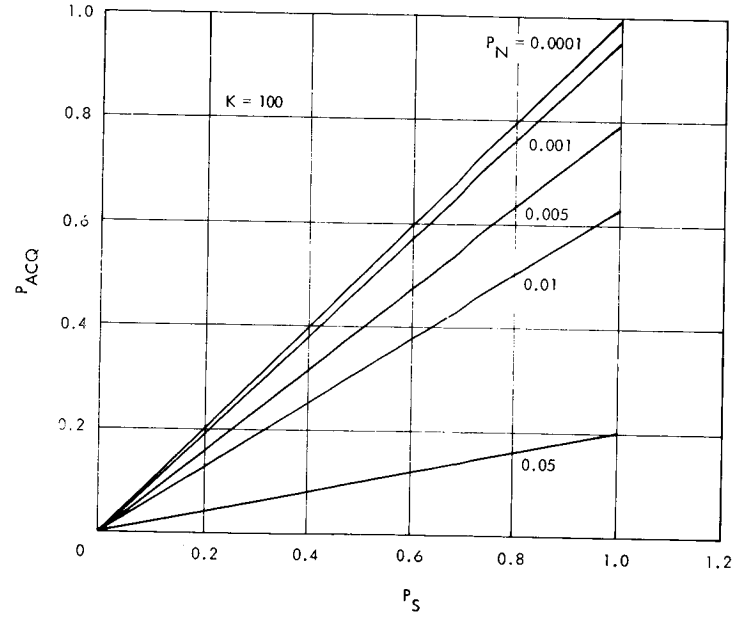

Figure B. Probability of Acquisition when 100 Angle Bins are Used

ACQUISITION PROBABILITIES

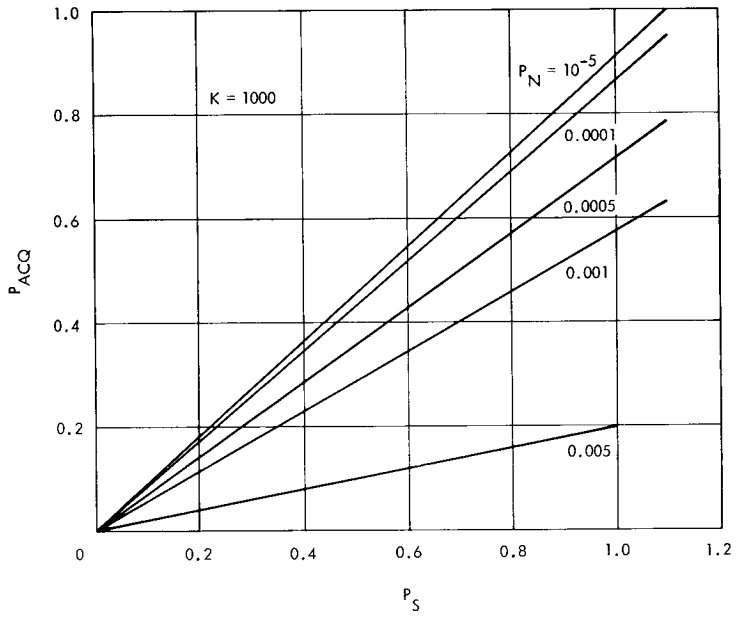

Figure C. Probability of Acquisition when 1000 Angle Bins Are Used

ACQUISITION AND TRACKING SYSTEM PERFORMANCE ANALYSIS

Detection Theory

THE PROBABILITY OF DETECTION AND FALSE ALARM (GAUSSIAN CASE)

The probability of detection for an ideal matched filter detection is derived for Gaussian statistics.

The classical detection problem of a known signal in additive (colored) Gaussian noise may be described mathematically as follows:

Given a finite record of observed data,

$$v(t) = a\, s(t) + n(t), \quad 0 < t < T$$

determine if the known signal s(t) is present or not (i.e., a = 0 or 1) given that n(t) is not necessarily stationary Gaussian noise with vanishing mean and autocovariance function K(u, t). The solution of this problem may be found in a number of textbooks.[1, 2, 3]

The important results are the following:

The optimum detector is a filter with an impulse response

$$h(\tau) = \begin{cases} g(T-\tau) & \text{for } 0 < \tau < T \\ 0 & \text{for } \tau < 0 \text{ or } \tau > T \end{cases}$$

where g(t) is the solution of the integral equation

$$\int_0^T K(u, t)\, g(u)\, du = s(t)$$

[1] C. W. Helstrom, Statistical Theory of Signal Detection, Pergamon Press, New York, 1960.

[2] D. Middleton, An Introduction to Statistical Communication Theory, McGraw-Hill Book Company, Inc., New York, 1960.

[3] Y. W. Lee, Statistical Theory of Communications, J. Wiley and Sons, Inc., New York, 1960.

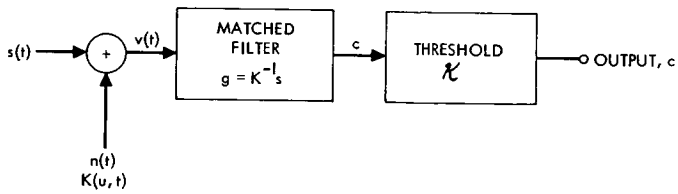

Figure A. Optimum Detector

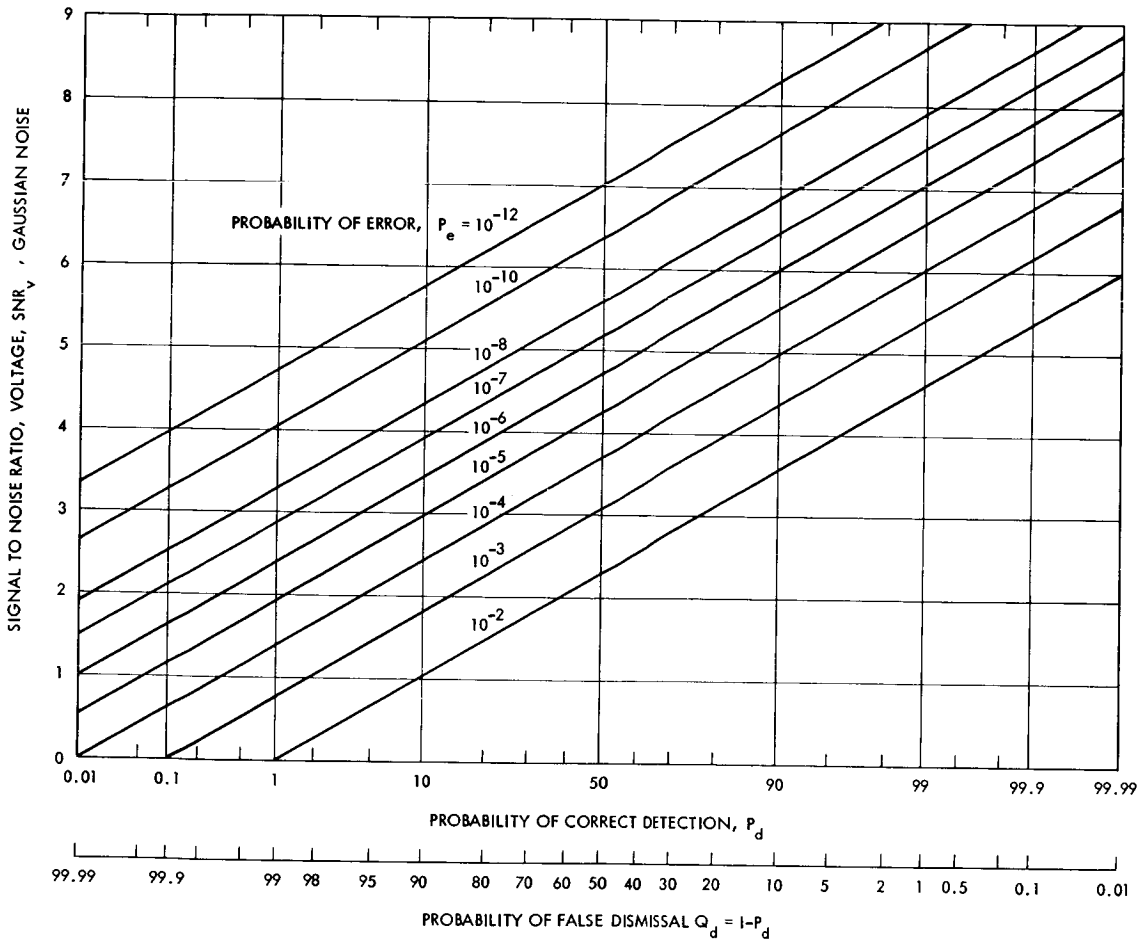

Figure B. General Detection Probability

THE PROBABILITY OF DETECTION AND FALSE ALARM (GAUSSIAN CASE)

followed by a threshold (bias level) given by

$$\kappa = \ln \Lambda_o + \frac{1}{2} SNR$$

where Λ_o depends on the particular decision rule (Bayes, Minimax, Neyman-Pearson), and SNR means signal-to-noise ratio (power). Diagrammatically this is illustrated in Figure A.

If C denotes the output of this filter, then $C > \kappa$ implies s(t) is present while $C < \kappa$ indicates the s(t) is not present. As expected, these results are not always true. Thus, sometimes it is $C > \kappa$ while the signal s(t) is not present. This is a false detection. Similarly, it may happen that $C < \kappa$ while s(t) is present. This is a false dismissal. The probability of false detection for a given threshold level, κ , depends on the SNR and is given by:

$$P_e = P_r \left[C > \kappa \,|\, a = 0 \right] = \frac{1}{\sqrt{2\pi}} \int_{\frac{\kappa}{SNR_v}}^{\infty} e^{-\frac{x^2}{2}} dx$$

Probability of Error

or

$$P_e = \text{erfc} \left[\frac{\kappa}{SNR_v} \right] \text{ which is the (tabulated) error function.}$$

The probability of (correct) detection, P_d, is given by

$$P_d = P_r \left[C > \kappa \,|\, a = 1 \right] = \frac{1}{\sqrt{2\pi}} \int_{\frac{\kappa - (SNR)_v^2}{(SNR)v}}^{\infty} e^{-\frac{x^2}{2}} dx$$

or

$$P_d = \text{erfc} \left[\frac{\kappa - (SNR)_v^2}{(SNR)_v} \right]$$

THE PROBABILITY OF DETECTION AND FALSE ALARM (GAUSSIAN CASE)

Thus given an upper bound for the probability of false alarm, P_e, $\mathcal{K}\sqrt{SNR}$ can be determined and the corresponding value of the probability of detection, P_d, can be obtained for various (SNR_v). The results are given in Figure B.

Indication of Proof. Observe that $\mathcal{C}$ is a Gaussian random variable, for it is the result of a linear operation (namely, integration) performed on the Gaussian random variable $v(t)$. Its mean value under hypothesis $a = 0$ is:

$$E[\mathcal{C} \mid a = 0] = 0$$

while under the hypothesis $a = 1$ is:

$$E[\mathcal{C} \mid a = 1] = \mu$$

The variance of $\mathcal{C}$ under both hypotheses is the same and is found to be:

$$E[(\mathcal{C} - \mu)^2 \mid a = 1] = E[(\mathcal{C} - 0)^2 \mid a = 0]$$

It can be shown for the case under consideration that $\mu = (SNR)_v^2$, i.e., mean value of $\mathcal{C}$ under hypothesis $a = 1$ is equal to the variance of $\mathcal{C}$. Because $\mathcal{C}$ is Gaussian its p.d.f.'s* are given by:

$$p(\mathcal{C}/a = 0) = (2\pi (SNR_v)^2)^{-1/2} \exp - \frac{\mathcal{C}^2}{2(SNR_v)^2}$$

and

$$p(\mathcal{C} \mid a = 1) = (2\pi (SNR_v)^2)^{-1/2} \exp \frac{(\mathcal{C} - SNR_v^2)^2}{2(SNR_v)^2}$$

The false detection probability P_e is:

$$P_e = Pr[\mathcal{C} > \mathcal{K} \mid a = 0] = Pr\left[\frac{\mathcal{C}}{(SNR)_v} > \frac{\mathcal{K}}{(SNR)_v} \mid a = 0\right]$$

*Probability distribution function

The random variable $x = \mathcal{C}/(SNR_v)$ has unit variance.

Hence:

$$P_e = Pr\left[x > \frac{\mathcal{K}}{(SNR)_v}\,\middle|\, a = 0\right] = \frac{1}{\sqrt{2\pi}} \int_{\frac{\mathcal{K}}{(SNR)_v}}^{\infty} \exp -\frac{x^2}{2}\, dx$$

or

$$P_e = \text{erfc}\ \frac{\mathcal{K}}{(SNR)_v}$$

In a similar way the correct detection probability P_d is:

$$P_d = Pr[\mathcal{C} > \mathcal{K} \,|\, a = 1] = P\left[\frac{\mathcal{C} - (SNR_v)^2}{(SNR)_v} > \frac{\mathcal{K} - (SNR_v)^2}{(SNR)_v}\,\middle|\, a = 1\right]$$

$$= \frac{1}{\sqrt{2\pi}} \int_{\frac{\mathcal{K} - (SNR_v)^2}{(SNR)_v}}^{\infty} \exp\left(-\frac{x^2}{2}\right) dx$$

or

$$P_d = \text{erfc}\ \frac{\mathcal{K} - SNR_v^2}{(SNR)_v} = \text{erfc}\left(\frac{\mathcal{K}}{SNR_v} - SNR_v\right)$$

The error function, erfc x, is extensively tabulated in many publications under various forms. Here the form

$$\text{erfc } x = \int_x^{\infty} e^{-t^2/2}\, dt$$

is used.

PROBABILITY OF DETECTION AND FALSE ALARM (POISSON CASE)

A means for determining the probability of detection and probability of false alarm using Poisson statistics is given.

For this case, the approach of Woodbury[1] is followed. Since both the signal and noise photons are governed by Poisson statistics, the average number of received signal photons N_R is $\overline{N_R}$ and the average number of received noise photons N_N is $\overline{N_N}$. The probability of detection, P_d, is defined as the probability that the number of signal plus noise events, $N = N_R + N_N$, be equal to, or greater than, a certain threshold, M, when the laser signal is present.

$$P_d = \sum_{X=M}^{\infty} \exp\left(-\overline{N}\frac{(\overline{N})^X}{X!}\right)$$

where the distribution of N is taken to be Poisson. Figure A plots M versus N with P_d as a parameter.

The probability of false alarm, P_e, per cell is defined as the probability that the number of noise events N_N is equal to or greater than M:

$$P_e = \sum_{X=M}^{\infty} \exp\left(-\overline{N}_N\frac{(\overline{N}_N)^X}{X!}\right)$$

This relationship is given in Figure B, where the M (threshold) is given as a function of $\overline{N}_N$, with P_e as a parameter.

[1] E. J. Woodbury, Annals of the New York Academy of Sciences, 122, 661 (1965).

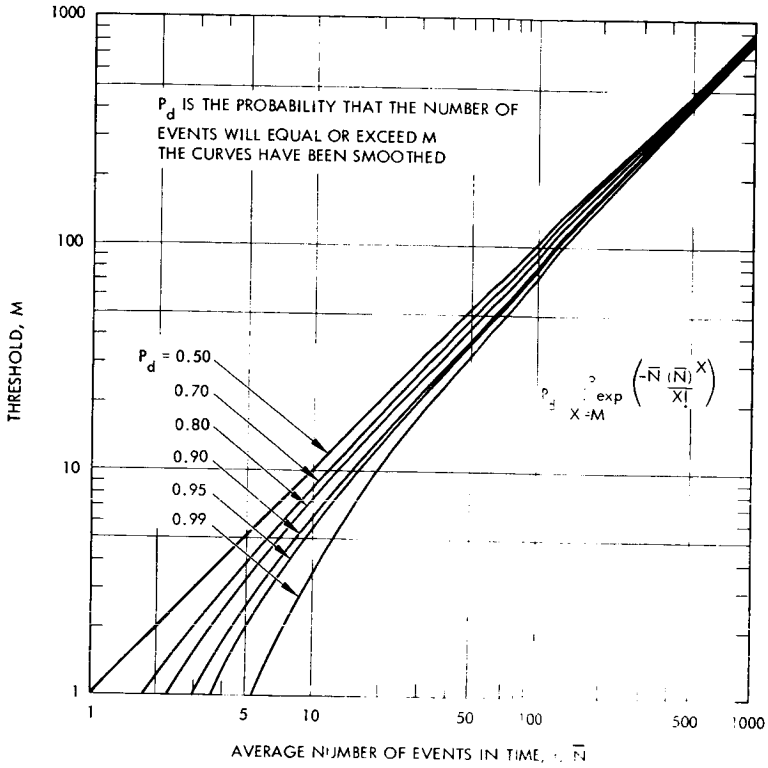

Figure A. Threshold as a Function of Average Number of Events, $\bar{N} = \bar{N}_R + \bar{N}_N$ in Time t, Dwell Time

Note: When it is desired to detect with a given probability, P_d, an event which emits on the average $\bar{N}_R$ photons, in the presence of $\bar{N}_N$ noise photons in t seconds, the threshold should be set at a number, M. Under these conditions there is always a probability of false detection, P_e, given in Figure B.

PROBABILITY OF DETECTION AND FALSE ALARM (POISSON CASE)

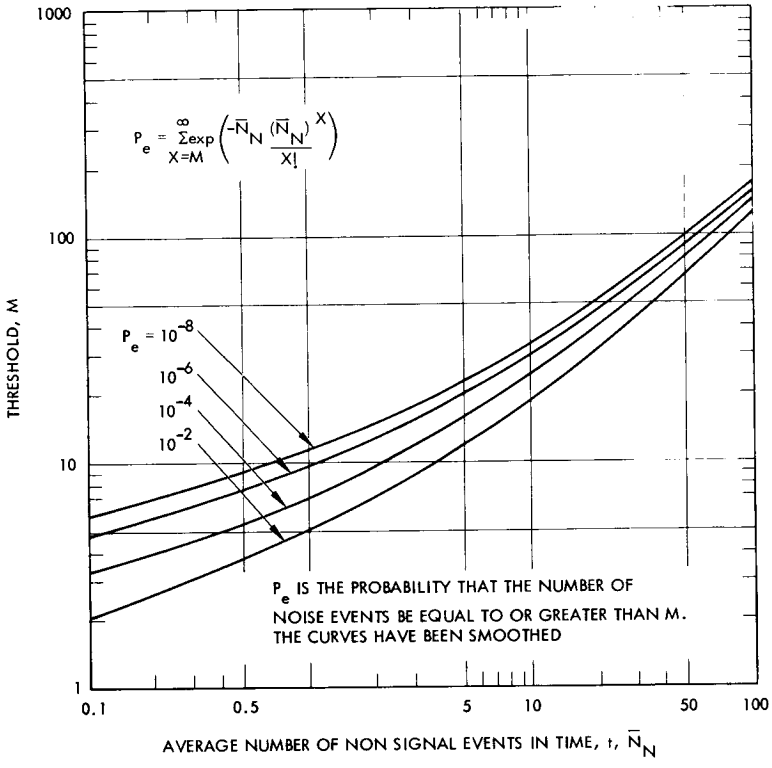

Figure B. Threshold as a Function of Average Number of Noise Events in Time t

Note: This curve may be used to estimate the probability of false detection, P_e, when the threshold of the decision mechanism has been set at M (see Figure A). The knowledge of the average number of noise photons, $\bar{N}_N$, determine P_e.

ACQUISITION AND TRACKING SYSTEM PERFORMANCE ANALYSIS

Angle Noise Error in Optical Tracking Systems

INTRODUCTION

The rms angle tracking error has a form which is relatively independent of the specific tracking implementation.

Angle tracking systems may be classified into the following four general categories:

Quadrant Angle Tracking Systems

Frame Scanning Angle Tracking Systems

Beam Lobing Angle Tracking Systems

Reticle Angle Tracking Systems

In a quadrant angle tracking system, the pulsed or continuous wave (CW) carrier is tracked by defocusing the received beam onto a four quadrant sensor. The relative strengths of the four sensor signals give the off-axis angle deviation.

A frame scanning system consists of a moving sensor describing a raster or spiral scan, or an array of point sensors such as vidicon elements which are sequentially examined. The coordinates of the detected image determine the tracking angle. Because of the time sampling nature of the sensor, the system is usually limited to use with CW carriers.

In a beam lobing system the received beam is focused to a spot which is mechanically rotated about its axis to illuminate four "cross-hair" slit sensors. The relative time position of detections from the sensors determines the tracking angle. Beam lobing systems are usually limited to operation with CW carriers.

The reticle system intensity modulates a received CW or pulsed beam by a rotating "pin wheel" type of transparency. The relative position of the beam on the reticle produces an AM or FM signal, depending on the reticle code. The modulation is detected using the scanning frequency and phase to yield the tracking angle and off axis magnitude.

The following topics present a description of the various angle tracking systems and an error analysis of their performance. One reservation must be made; the relations given are derived under the assumption of Gaussian statistics. This condition is achieved when the number of photons utilized in the decision process is sufficiently large to assume the law of large numbers. For low photon levels the relations will not be a function of the signal-to-noise ratio, but some function of the signal and noise power.

Angle Tracking Systems

- Quadrant
- Frame Scanning
- Beam Lobing
- Reticle

General Form of Angle Error Equation

$$\epsilon_\theta = \frac{k_\theta}{(SNR)_v}\left(\frac{\Delta f_s}{f}\right)^{1/2}$$

INTRODUCTION

The random angular position error of an optical tracker is measured by the RMS tracking angle noise error, ϵ_θ, given by a function of the following form:

$$\epsilon_\theta = \frac{k_\theta}{(SNR)_v}\left(\frac{\Delta f_s}{f}\right)^{1/2}$$

where

$(SNR)_v$ = voltage signal-to-noise ratio

Δf_s = servo noise bandwidth

f = pulse repetition rate (or modulation frequency)

and

k_θ = modulation (resolution coefficient)

k_θ depends upon the nature of the specific tracker and is in a sense a measure of the ultimate geometrical accuracy limitation which the particular position encoder places upon the tracker, such as angular diameter of the Airydisk, angular width of the reticle slit, etc.

A description of the monopulse system used for the basic analysis is given in the following. In addition, CW system utlizing pulse position modulation (PPM), amplitude modulation (AM) and frequency modulation (FM) are discussed and the corresponding forms for these cases are given.

MONOPULSE QUADRANT TRACKING SYSTEM

The bias error due to unbalance of photomultiplier detectors is desired.

The monopulse system consists of a pulsed (laser) beacon and a quadrant photomultiplier (PM) tracker. The receiving optics form a diffraction limited spot at the apex of a four-sided prism which reflects portions of the blur circle onto separate photomultipliers, as shown in Figure A.

The error signal is derived by comparing the amount of energy in each of the four PM channels. In order to determine the error in the X and Y coordinates the following differences are found:

$$\epsilon \text{ Coordinate Error: } (S_1 + S_2) - (S_3 + S_4) = \Delta\epsilon$$

$$\theta \text{ Coordinate Error: } (S_1 + S_4) - (S_2 + S_3) = \Delta\theta$$

where S_i = signal from ith quadrant.

When the center of the "blur circle" falls at the apex of the beam splitting prism, the error signals are zero. Clearly both the absolute sensitivity of each of the PMs (considered in this topic) and the noise (considered in the next topic) will limit the ultimate accuracy of the system so that the center of the blur circle will perform excursions about this mean null position.

Bias Error Cassed by Photodetector Gain Unbalance. The voltages generated at each of the photodetectors are given by

$$V_1 = \frac{H\,G_{D1}}{(\pi\delta^2/4)}\left[\pi\delta^2/16 + f(\epsilon, \theta)\right] \tag{1}$$

$$V_2 = \frac{H\,G_{D2}}{(\pi\delta^2/4)}\left[\pi\delta^2/16 + f(+\epsilon, -\theta)\right] \tag{2}$$

$$V_3 = \frac{H\,G_{D3}}{(\pi\delta^2/4)}\left[\pi\delta^2/16 + f(-\epsilon, -\theta)\right] \tag{3}$$

$$V_4 = \frac{H\,G_{D4}}{(\pi\delta^2/4)}\left[\pi\delta^2/16 + f(-\epsilon, +\theta)\right] \tag{4}$$

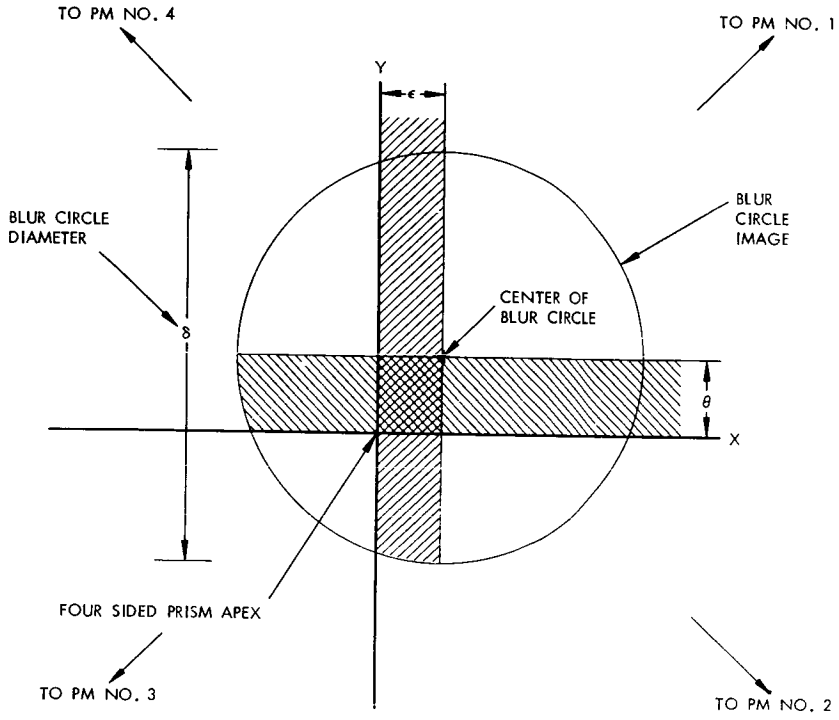

Figure A. Blur Circle and Quandrant Photomultiplier (PM) Geometry

MONOPULSE QUADRANT TRACKING SYSTEM

where H is the total radiant energy incident on the system, G_{Dn} is the gain of the nth photodetector, and δ is the diameter of the blur circle. The function, $f(\epsilon, \theta)$ is the incremental area of the blur circle in a quadrant as a function of ϵ, θ; at boresight, $f(0, 0) = 0$. The bias error is determined by forming the steering signals and setting them equal to zero, thus,

$$\Delta \text{ azimuth} = (V_1 + V_2) - (V_3 + V_4) = 0 \tag{5}$$

$$\Delta \text{ elevation} = (V_1 + V_4) - (V_2 + V_3) = 0 \tag{6}$$

Substituting Equations (1) to (4) into Equations (5) and (6) yields after some algebraic manipulation

$$0 = 1/4\left[G_{D1} + G_{D2} - G_{D3} - G_{D4}\right] + \frac{4}{\pi\delta^2}\left[G_{D1} f(\epsilon, 0) + G_{D2} f(+\epsilon, -\theta) - G_{D3} f(-\epsilon, -\theta) - G_{D4} f(-\epsilon, +\theta)\right] \tag{7}$$

and

$$0 = 1/4\left[G_{D1} - G_{D2} - G_{D3} + G_{D4}\right] + \frac{4}{\pi\delta^2}\left[G_{D1} f(\epsilon, \theta) - G_{D2} f(+\epsilon, -\theta) - G_{D3} f(-\epsilon, -\theta) + G_{D4} f(-\epsilon, +\theta)\right] \tag{8}$$

The exact function $f(\epsilon, \theta)$ is rather complex. However for small angles a good approximation is

$$f(\epsilon, \theta) \approx \frac{\epsilon\delta}{2} + \frac{\theta\delta}{2} \tag{9}$$

Substituting Equation (9) into Equations (7) and (8) yields

$$0 = \left[G_{D1} + G_{D2} - G_{D3} - G_{D4}\right] + b_o\left[G_{D1}(\epsilon + \theta) + G_{D2}(+\epsilon - \theta) - G_{D3}(-\epsilon - \theta) - G_{D4}(-\epsilon + \theta)\right] \tag{10}$$

and

$$0 = \left[G_{D1} - G_{D2} - G_{D3} + G_{D4}\right] + b_o\left[G_{D1}(\epsilon + \theta) - G_{D2}(+\epsilon - \theta) - G_{D3}(-\epsilon - \theta) + G_{D4}(-\epsilon + \theta)\right] \tag{11}$$

where b_o is the modulation index given by

$$b_o = \frac{8}{\pi\delta} \tag{12}$$

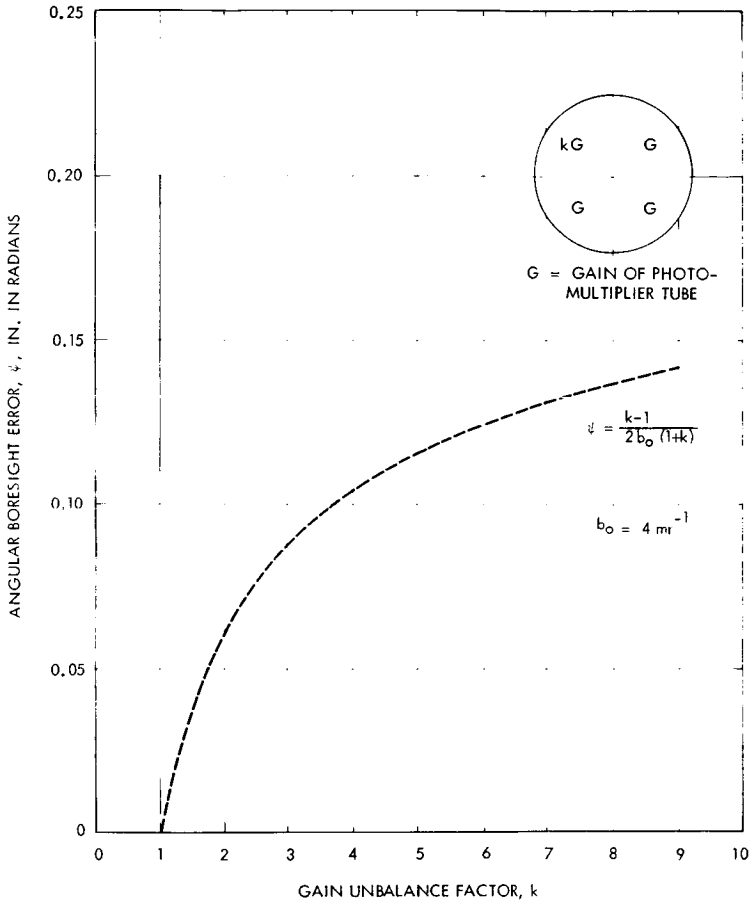

Figure B. Total Error Bias, ψ, Produced by PMT Gain Unbalance

MONOPULSE QUADRANT TRACKING SYSTEM

Equations (10) and (11) are a set of linear simultaneous equations in ϵ and θ which may be easily evaluated for any photodetector gains. For example let

$$G_{D1} = G_{D2} = G_{D3} = G$$

and

$$G_{D4} = kG \tag{13}$$

Solving for the bias gives

$$\epsilon = \frac{k - 1}{2b_o (1 + k)}$$

and (14)

$$\theta = -\left[\frac{k - 1}{2b_o (1 + k)}\right]$$

The total bias angle is

$$\psi = \sqrt{\epsilon^2 + \theta^2} = \frac{k-1}{\sqrt{2}\, b_o(1 + k)} \tag{15}$$

where

ψ = total error bias produced by the gain change

k = gain unbalance factor

b_o = the modulation coefficient before the gain change occurred.

This equation takes into account the elevation and azimuth component biases and the effect of the gain factor on the modulation coefficient, b_o, of the system. The result is plotted in Figure 3 for $b_o = 4\ mr^{-1}$. The gain balancing techniques presently used in the PMTs will hold the gain factor to below 1.7 and hence the bias error to less than 0.05 mr for this example.

ANGLE NOISE ANALYSIS OF MONOPULSE QUADRANT TRACKING SYSTEM

Signal and noise relationships for a monopulse quadrant tracking system are derived.

A block diagram of a typical monopulse quadrant tracking system is shown in the figure. It consists of entrance optics which form a diffraction limited spot at the apex of a four sided prism which reflects portions of the blur circle onto four separate photomultipliers. The photomultipliers convert the optical signal into electrical signals which are then processed by a series of amplifiers and filters. The four quadrant signals are used to derive the azimuth and elevation tracking error signals by combining their sums and differences. These error signals in turn control the entrance optics in such a manner as to seek their cancellation. The object of this section is to consider the angular accuracy of which such a monopulse trackup system is capable. This will be done in the following steps. First the process by which the beacon signal is converted to electrical tracking error signals is described. Second, the effect of noise being introduced in this process is observed. Third, the loop error signal is derived and fourth, the angular noise error spectrum is evaluated.

Signal Process

The optical signal power captured by the entrance optics is

$$S_T = H(t)A_o \tag{1}$$

where H(t) is the beacon irradiance and A is the optics aperture. Assuming small position errors the signal captured by any one of the four photomultipliers is given by

$$S_i = \frac{H(t)A_o}{\frac{\pi\delta^2}{4}} \left[\frac{\pi\delta^2}{16} + \left(\epsilon_i(t) + \theta_i(t)\right)\frac{\delta}{2}\right] \tag{2}$$

where δ is the diameter of the blur circle and $\epsilon_i(t)$ and $\theta_i(t)$ are the time dependent quadrant position errors of the blur circle defined in the figure. To simplify the analysis and with no loss in generality it will be assumed that only an azimuth error, ϵ_i, exists. Thus for $\theta_i = 0$ the quadrant signals are

$$S_1 = S_2 = H(t)A_o\left[\frac{1}{4} + \frac{2}{\pi\delta}\epsilon(t)\right] \tag{3}$$

$$S_3 = S_4 = H(t)A_o\left[\frac{1}{4} - \frac{2}{\pi\delta}\epsilon(t)\right]$$

The photomultiplier converts the optical signal power into electrical voltages which are then amplified by the AGC amplifiers. The signal is then filtered. If the optical beacon were cw, a simple low pass filter with sufficient bandwidth to follow the signal fluctuations induced by the tracker would be used. If the beacon is pulsed the filter would consist of a sample and hold circuit consisting of a switch which is turned on and off at the beacon pulse rate, and a low pass filter. At the filter output the LaPlace transform of the signal voltages are

$$E_i(s) = G_D B(s) S_i(s) \tag{4}$$

where G_D is the gain of the photomultiplier assumed to be independent of frequency and $S_i(s)$ and $B(s)$ are the respective Laplace transforms of the optical signal in the i^{th} quadrant and the filter.

The Laplace transform of the voltage signals thus depends on the beacon modulation and the type of filter employed. If the beacon is a cw signal of irradiance H, the Laplace transform is

$$E_i(s) = G_D A B(s) H A_o \left[\frac{1}{4s} \pm \frac{2}{\pi\delta} \epsilon(s) \right] \tag{5}$$

where $\epsilon(s)$ is the Laplace transform of the two dependent azimuth position error. If the beacon is a pulsed signal and the detector filter consists of a sample and hold type network, the signal voltage is

$$E_i(s) = \left\{ P \right\} G_D A A_o \left[\frac{1}{4s} \pm \frac{2}{\pi\delta} \epsilon(s) \right] \tag{6}$$

where $\left\{ P \right\}$ is the value at which the holding network peaks and is given by

$$\left\{ P \right\} = \left\{ H(t) \oplus B(t) \right\}_{PK} \tag{7}$$

In both the cw and pulsed beacon cases, the signal voltage can be expressed as

$$E_i(s) = K \left[\frac{1}{4s} \pm \frac{2}{\pi\delta} \epsilon(s) \right] \tag{8}$$

where K is a constant derived from either equations (5) or (6).

After filtering, the signal voltages are combined in the sum and difference networks. The sum signal is given by

$$\sum_i E_i(s) = \frac{K}{s} \tag{9}$$

Finally the difference signal is given by

$$\Delta_i E_i(s) = \left(E_1 + E_2 \right) - \left(E_3 + E_c \right) = \frac{8}{\pi\delta} K \epsilon(s) \tag{10}$$

ANGLE NOISE ANALYSIS OF MONOPULSE QUADRANT TRACKING SYSTEM

Noise Analysis

Together with the signal, the photomultiplier generates an irreducible noise voltage which like the signal voltage, is amplified and filtered. The noise power at the output of the photomultiplier will be assumed uniformly distributed across the frequency spectrum of the signal. Its spectral density is thus independent of frequency and of N_D volt^2 per cycle. At the filter output, the Laplace transform of the mean square noise voltage is given by

$$\overline{V_n(s)}^2 = N_D B(s)B(-s) \tag{11}$$

If the filter has a noise equivalent bandwidth W_N, the mean square noise voltage is

$$\overline{V_n(t)}^2 = N_D W_N \tag{12}$$

The power signal to noise ratio of the total beacon signal received is obtained from (10) and (12)

$$(SNR) = \frac{\left(\Sigma E_i(t)\right)^2}{V_n(\epsilon)^2} = \frac{K^2}{N_D W_N} \tag{13}$$

Loop Error Signal

Since all of the devices following the photomultiplier are linear, the signal and noise voltages are added to one another. The total difference network azimuth error signal is

$$\Delta E_T = \Delta E_i(s) + \sqrt{4\overline{V_n(s)}^2} \tag{14}$$

This signal is transformed to the azimuth pointing error angle $\epsilon(s)$ by the servo. The angle is then given by

$$\epsilon(s) = -\Delta E_T G(s) \tag{15}$$

where G(s) is the transfer function of the feedback loop. Substituting (10) and (14) into (15) yields

$$\epsilon(s) = -\left[K \frac{8}{\pi\delta} \epsilon(s) + 2\sqrt{\overline{V_n(s)}^2}\right] G(s) \tag{16}$$

Solving for the azimuth pointing angle gives

$$\epsilon(s) = \frac{-2(G(s)\sqrt{\overline{V_n(s)^2}}}{1 + KG(s)\frac{8}{\pi\delta}} \tag{17}$$

RMS Angular Noise

The RMS angular noise may be obtained from

$$\left|\epsilon(\overline{j\omega})\right|^2 = \frac{1}{W_o}\int_o^{W_o} \left|\epsilon(j\omega)\right|^2 d\omega \tag{18}$$

where W_o is the equivalent noise bandwidth of the feedback loop transfer function and

$$\epsilon(j\omega)^2 = \left.\frac{4G(s)^2\,\overline{V_n(s)^2}}{\left[1 - KG(s)\frac{8}{\pi\delta}\right]^2}\right|_{s=j\omega} \tag{19}$$

It is interesting to note that if the servo loop is designed to make

$$KG(s)\frac{8}{\pi\delta} \gg 1$$

equation (19) becomes

$$\left|\epsilon(j\omega)\right|^2 = \frac{1}{\left(\frac{8}{\pi\delta}\right)^2 \frac{K^2}{\overline{V_n(s)^2}}} \tag{20}$$

which in turn, after substitution of (13) becomes

$$\left|\epsilon(j\omega)\right|^2 = \frac{1}{\left(\frac{8}{\pi\delta}\right)^2 (SNR)} \tag{21}$$

ANGLE NOISE ANALYSIS OF MONOPULSE QUADRANT TRACKING SYSTEM

Substitution of (21) into (18) yields the familiar result

$$\left| \bar{\epsilon} \right|^2 = \frac{1}{b_o^2 \, (\mathrm{SNR})}$$

where b_o is modulation index defined as $8/\pi\delta$.

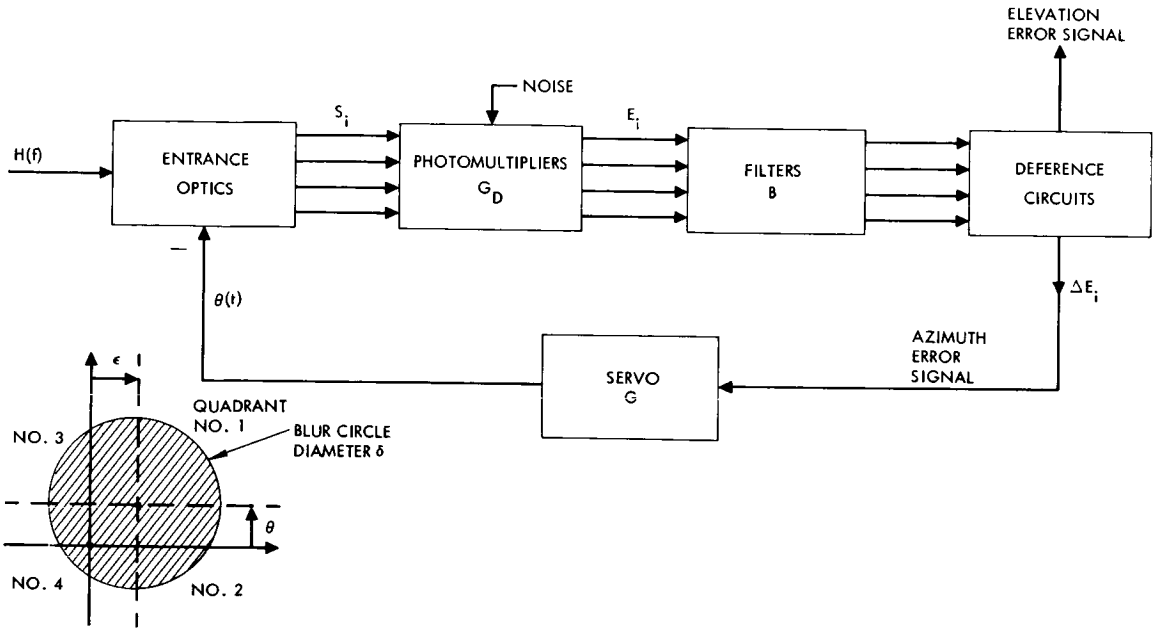

Monopulse Quadrant Tracking System Block Diagram

BEAM LOBING PPM TRACKING SYSTEM

The total tracking error is derived for a PPM tracker.

The operation of the beam lobing pulse position modulation (PPM) tracking system system is illustrated in Figures A, B, and C. The image of a point source (or target) at boresight is deflected by a rotating prism (Figure A) so that it describes a periphery just touching the outer ends of the sensor cells (dotted circle in Figure B). The image of a target off boresight, but within the field of view, is described by a periphery with the same radius as before, but centered at the point where the image would be without the prism. When the target image passes over a cell (slit) a pulse, called a "target pulse," is realized. The duration, τ, of the target pulse is the time the nutating image requires to cross the cell. The position of the target pulse thus generated is varied with respect to four fixed and equally-spaced reference pulses. From Figures B and C, it is clear that at least two target pulses are needed for locating the target position with respect to boresight, giving the yaw (x) and pitch (y) angles. There are four separate detection channels – one corresponding to each cell.

The pulse position modulation, measured between the reference pulses and the signal pulses (see Figure C), is used to obtain the pitch and yaw signals. The error in tracking is due to the error in measuring the time at which the blur circle passes the sensor.

From Figure C it is seen that the error in the x axis, x, is:

$$x = R \sin \omega t \tag{1}$$

and

$$\Delta x = -\Delta t \left[R\omega \cos \omega t \right] \tag{2}$$

when the tracking error is small, i.e., ωt is close to zero,

$$\cos \omega t \cong 1$$

and

$$\Delta x = -R\omega \Delta t = -\frac{2\pi R}{T} \Delta t \tag{3}$$

where

T is the period of nutation

Δt is an error in determining the time when the light spot crosses the detector due to noise

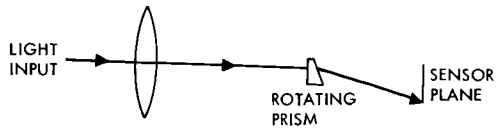

Figure A. Optical Schematic of Beam Lobing PPM System

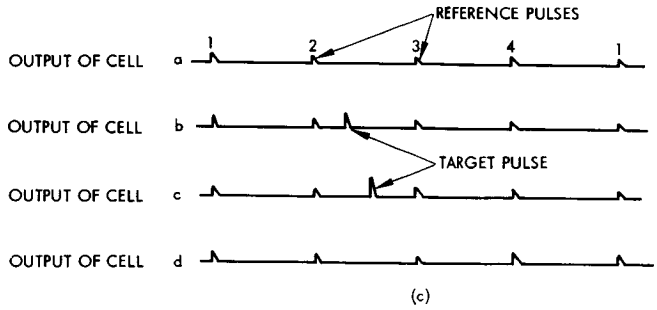

Figure B. Image Plane Geometry of PPM Beam Lobing System

BEAM LOBING PPM TRACKING SYSTEM

The noise uncertainty, Δt, can be reduced to a minimum value (for a given signal to noise ratio) by using a matched filter. To find the value of Δt, consider first the time required for the blur circle to cross the detector, τ.

$$\tau = \frac{\Delta l + f}{\omega R} \tag{4}$$

for an optimum filter Δt is then

$$\Delta t = \sqrt{\frac{N}{S_P}} \frac{1}{\sqrt{\frac{3}{2\tau}}} = \sqrt{\frac{N}{S_P}} \sqrt{\frac{2}{3}} \sqrt{\frac{\Delta l + f}{\omega R}} \tag{5}$$

where N is the noise power spectural density at the output of the photodetector and S_P is the peak signal measured at the same place.

The position uncertainty in the x direction Δx, is then

$$\Delta x = -\frac{2}{3} \frac{\sqrt{\omega R(\Delta l + \delta)}}{S_P / \sqrt{N}} \tag{6}$$

and the uncertainty error in the y direction will be the same. The total error, $\epsilon_P = \sqrt{2}\,\Delta x$ since $\tau = (\omega/2\pi)$

$$\epsilon_P = \frac{4}{3} \sqrt{\pi(\Delta l + \delta)R}\ (1/T)\ (S_P/\sqrt{N}) \tag{7}$$

Equation (7) holds for white thermal noise. In the background limited case, noise is proportional to the square root of the signal and the total error is

$$\epsilon_P = \frac{4}{3} \sqrt{\pi(\Delta l + \delta)R}\ (1/\sqrt{S_P T}) \tag{8}$$

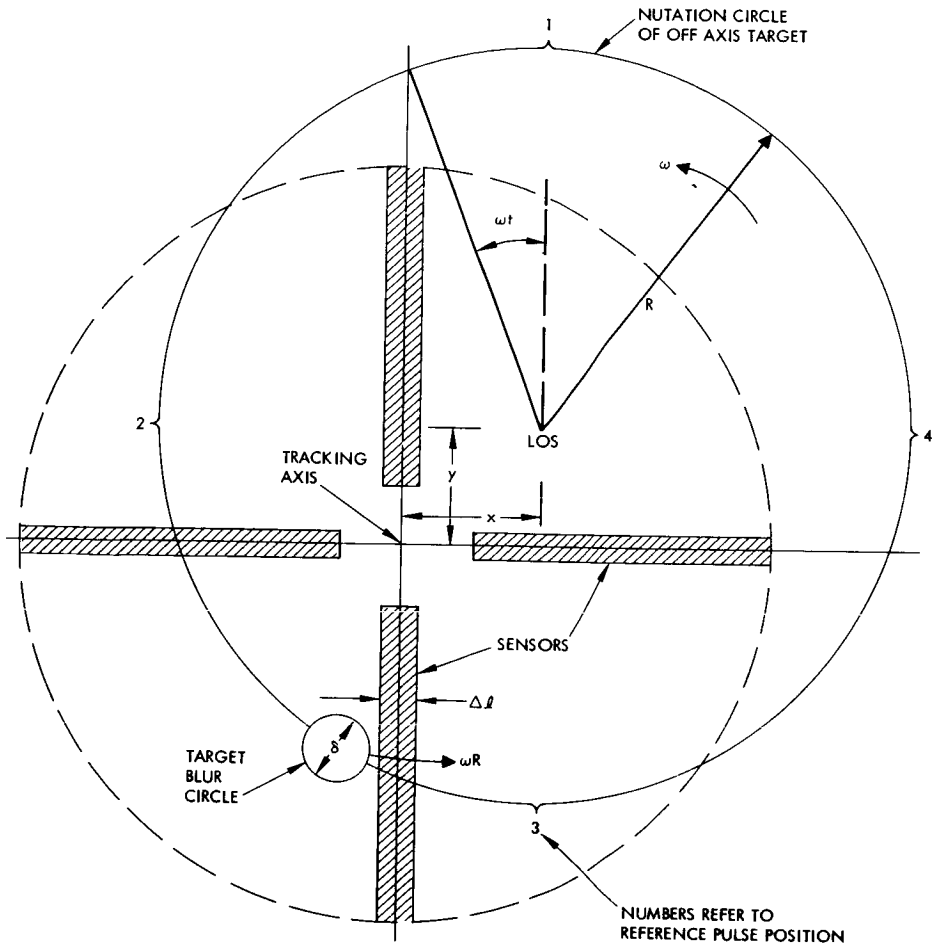

Figure C. Beam Lobing PPM Tracking System Outputs

AM RETICLE TRACKING SYSTEM

The implementation and performance of an AM reticle tracking system is described.

Figure A illustrates a block diagram of an AM Reticle tracking system. The received beam passes through a rotating reticle such as the one shown in Figure B and is focused on the photodetector. The reticle intensity modulates the beam in such a manner that the angular position of the beam from the reticle axis, which is boresighted to the optical reference system, may be determined by the electrical detection system following the photodetector. With the reticle shown in Figure B, if the beam is not passing through the center of the rotating reticle, the radiant power on the detector surface will be of the general form of Figure C. The frequency spectrum of this signal consists of a fundamental modulation frequency dependent upon the angular slit spacing and angular velocity of the reticle, plus harmonic sidebands. The narrow band filter passes only the fundamental and the first pair of sidebands. Next, the demodulator shifts the spectrum to zero frequency. The filtered output of the demodulator ideally is a sine wave whose amplitude is a function of the radial displacement of the beam, and whose phase is proportional to the beam displacement along orthogonal axes. The reference for the phase detectors is the frequency corresponding the reticle rotation rate. The beam displacement voltages are used to control servo motors which reposition the optical sensor to the beam center.

The performance analysis of the AM tracking is complicated by the fact that the signal modulation is not a monotonic function of the radial error. As the beam moves from the center of the rotating reticle to the outer edge, initially the target spot will be partially covered, then partially uncovered by slits resulting in only partial modulation. Furthermore, at certain radial positions the rate of covering and uncovering of the spot will be nearly equal and the percentage of modulation will drop. These modulation perturbations, however, are reasonably small and may be ignored in a first order analysis.

Even assuming Gaussian noise statistics at the optical detector output, the analysis of the angle error fluctuations is difficult because the electrical receiver contains nonlinear elements. It has been shown[1] that the tracking error due to detector noise is

$$\underline{\text{Large Signal Input}} \quad \epsilon_t = \frac{K\pi a_i \left(\frac{f_c}{f_m}\right)}{2\left(\frac{S}{N}\right)_v}$$

[1] P. E. Mengers, "Tracking Accuracy of Infrared Trackers," General Electric Report No. R59ELC100 Defense Electronics Division, December 1959.

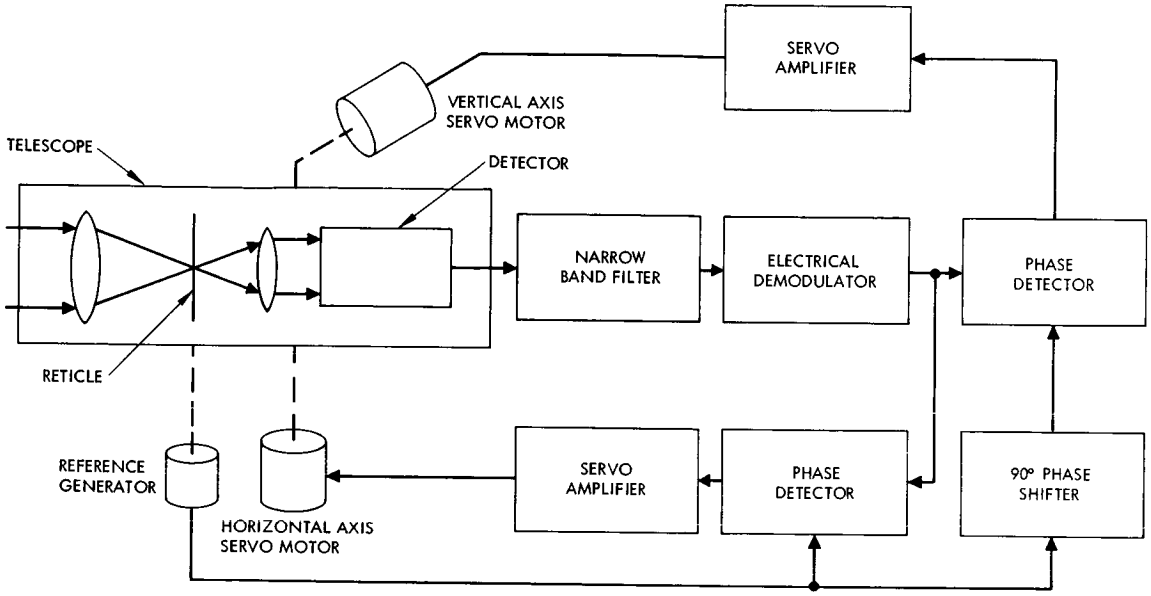

Figure A. AM Tracking System, Block Diagram

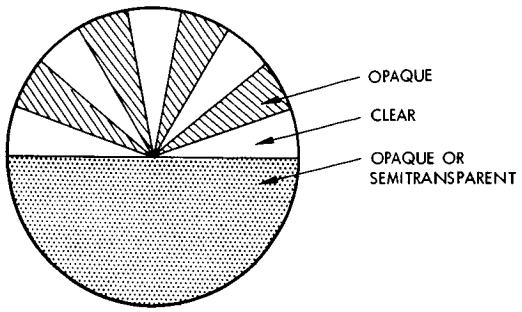

Figure B. Simple Optical AM Reticle

AM RETICLE TRACKING SYSTEM

$$\underline{\text{Small Signal Input}}\ \epsilon_t = \frac{K\pi\alpha_i\left(\frac{f_c}{f_m}\right)}{2\left(\frac{S}{N}\right)_v^{1/2}\left(2^{1/8}\right)}$$

where

α_i = angular size of image

f_c = reticle rotational frequency

K = 0.64

f_m = modulation frequency

$\left(\frac{S}{N}\right)$ = receiver output voltage signal-to-noise ratio

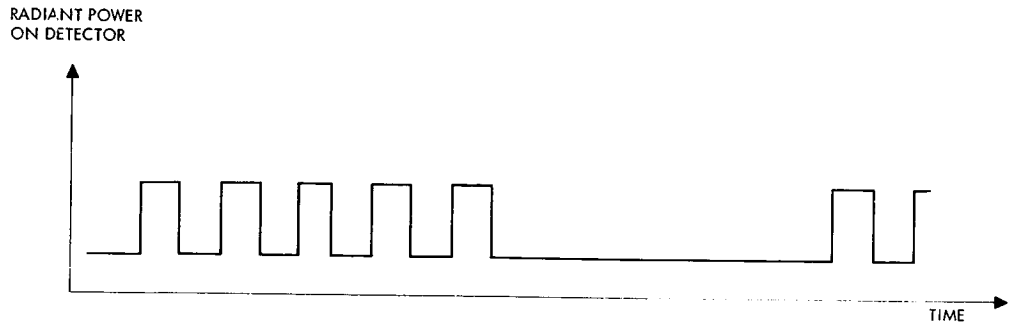

Figure C. Radiation Signal After Modulation by AM Reticle

FM RETICLE TRACKING SYSTEM

Typical FM reticle implementation is shown and the noise error signals are documented.

An FM reticle tracker operates in a similar manner to the AM reticle tracker. One type of FM reticle consists of slits which are shifted slightly as a function of the radial distance from the center of the reticle. The result is a frequency modulation about the mean chopping frequency. Another type of FM reticle consists of a reticle with evenly spaced slits rotated off-axis to the received beam as shown in Figure A. Figure B illustrates the relationship of the instantaneous frequency to the angular position. The tracking error fluctuations have been shown[1] to be:

$$\text{Small Signal Case } \epsilon_t = \frac{2\,\alpha_m \left(\frac{\omega_d}{\omega_F}\right)}{\left(\frac{S}{N}\right)}$$

$$\text{Large Signal Case } \epsilon_t = \frac{2\,\alpha_m}{\left(\frac{S}{N}\right)}$$

where

α_m = maximum angular displacement of beam

$\Delta F_i = \frac{\omega F}{2\pi}$ = IF input filter bandwidth (halfwidth)

$\Delta F_d = \frac{\omega_d}{2\pi}$ = predetection filter bandwidth (halfwidth)

$\left(\frac{S}{V}\right)$ = receiver output voltage signal to noise ratio.

[1] P. E. Mengers, "Tracking Accuracy of Infrared Trackers," General Electric Report No. R59ELG100 Defense Electronics Division, December 1959.

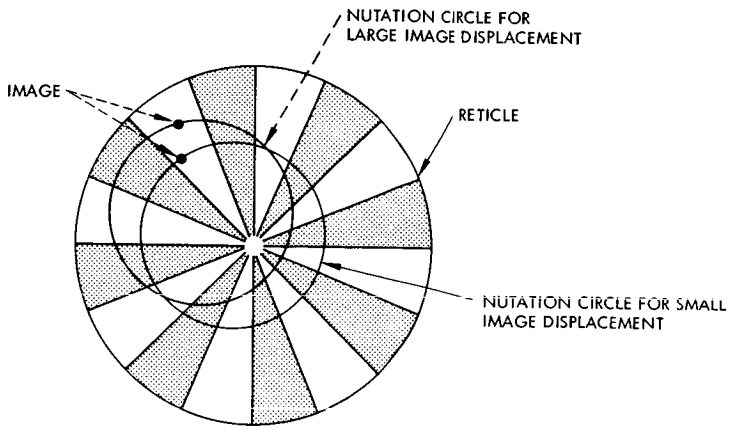

Figure A. Nutation Circle and Reticle Relative Geometry

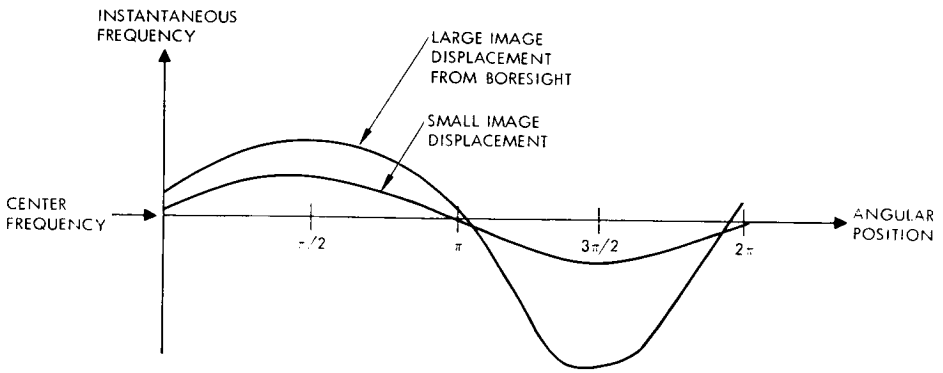

Figure B. Instantaneous Frequency as Function of Rotation of Reticle Axis About Boresight for a FM Precessional Reticle

COMPONENT PERFORMANCE AND BURDEN RELATIONSHIPS

Attitude and Tracking Sensors

Component Performance and Burden Relationships
Attitude and Tracking Sensors*

SUN SENSORS

Attitude sensors are introduced and the first of these, sun sensors, are described.

Active sensors are required for stabilization since gyroscope devices are unsuitable for extended missions due to their short life (under 1000 hours typically) and unpredictable drift errors. Similarly ambient field sensors e. g., magnetic field, are unsuitable because field lines are not predictable with sufficient accuracy and are too weak to be of use in interplanetary space.

Three basic types of attitude and tracking sensors are of interest with respect to the acquisition and tracking systems. They are:

1. Sun Sensors
2. Star Sensors
3. Planet Sensors

Sun sensors are described in this topic while star and planet sensors are described in subsequent topics.

The sun is the most common attitude reference for non-earth oriented vehicles. The principal advantage of the sun as a reference is the relative ease with which it may be acquired as a consequence of its high intensity. One significant disadvantage is that solar activity may shift the center of radiance by as much as 0. 75 arc second. ** Among the various types of sun sensors which have been used to date are the following.

Shadow Masked Sun Sensors. These consist of shadow masked arrays of photovoltaic or photoconductive cells as indicated in Figure A. The cells are connected as differential pairs such that the output electrical signal changes sign at a center null point. These sensors are small and simple and are capable of null accuracies of the order of 0. 1 degree. The chief sources of error are stray light and unequal aging and thermal drift between cells.

Lens Type Sun Sensors. The important design parameters of lens type sun sensors are the focal length and the distance between the reticle and the detector, indicated in Figure B. The use of a lens allows an "angular gain" over that obtainable with the shadow mask. Two units such as are indicated in Figure B are used to provide null positioning.

Null accuracies from 0. 01 to 0. 1 degree can be obtained using these sensors.

*Much of the material of this section is found in "Optical Attitude Sensors for Space Vehicle Applications: Descriptive Survey of Recent Literature and Error Studies" M. S. Thesis by James Harold Spotts, 1965, UCLA.
**Observed from 1AU.

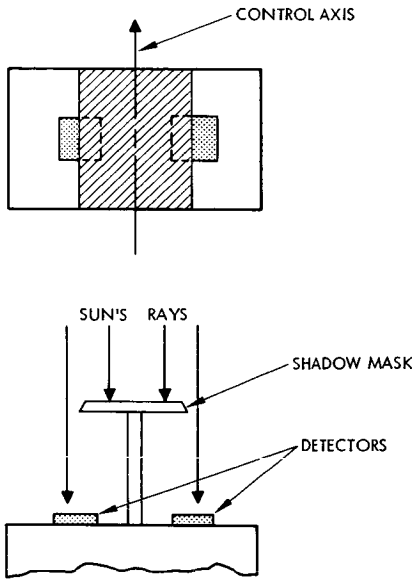

Figure A. Simple Shadow Mask Sun Sensor

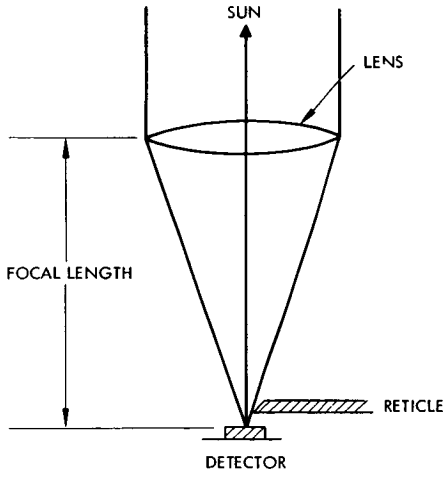

Figure B. Simple Lens Type Sun Sensor

SUN SENSORS

"Critical Angle Prism" Sun Sensor.[1] Generally for higher accuracies, more complex systems are needed. However, null accuracies from 0.001 to 0.01 degree can easily be obtained using the critical angle prism sensor, a simple device composed of a glass prism and two photovoltaic cells, shown in Figure C. This sensor makes use of the fact that when the sun is in the null plane, almost all of the light will be reflected in the prism and will not reach the photo detector. Due to the critical angle, deviations from the null create a sharp error signal in the differentially connected photo cells. Null accuracies of the order of 30 arc seconds have been obtained. Sun sensors of this type have been proposed for use in the AOSO and claim accuracies as 1.3 arc seconds or 0.00036 degrees.

Digital Sun Sensors. Many stabilized vehicles do not require a sun sensor for attitude stabilization but use the sun as a reference for initial attitude determination. The digital sun sensor, shown in Figure 7, actually encodes the sun angle for digital communication. If the field of view of the digital sensor is 0 degrees and if n cells are used, then the resolution is $/2^n$ degrees. The only limiting factor is the angle subtended by the sun, approximately 0.5 degree at 1AU.

Two digital sun sensors are used on the Saturn Meteoroid Satellite and on the gravity gradient stabilized version of the ATS. They have field of view of 128° x 128° and 1 degree resolution.

[1] Seward, Harold H. "A Sunfinder for an Interplanetary Vehicle." Massachusetts Institute of Technology Instrumentation Laboratory Report, E-965 (Revision A), Dec. 1960.

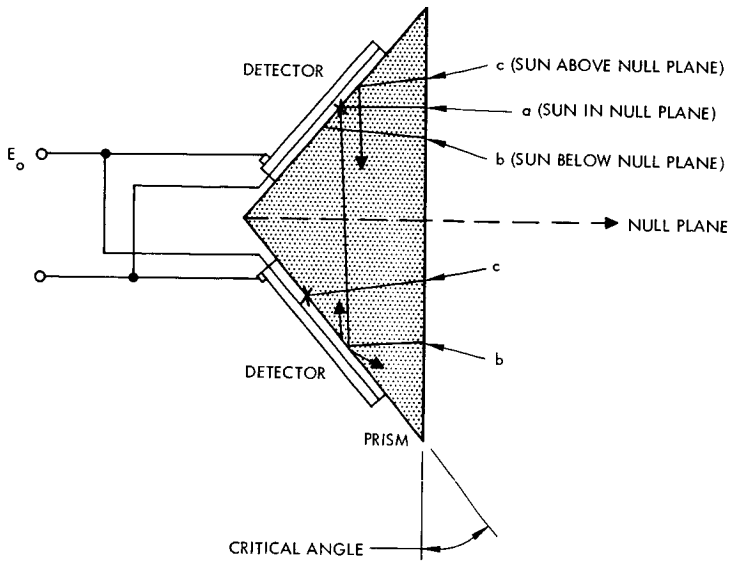

Figure C. Critical Angle Prism Sensor Design

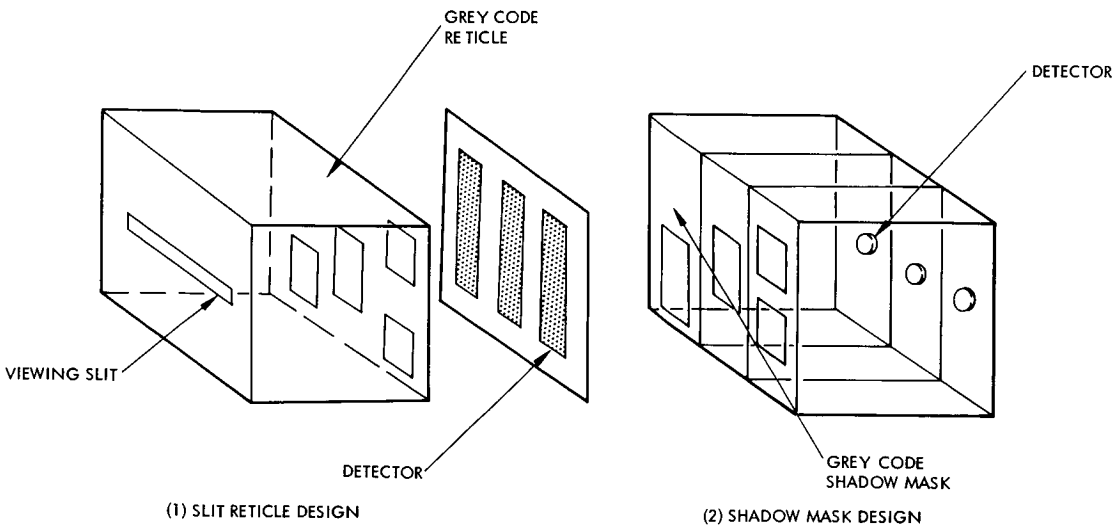

Figure D. Digital-Type Sun Sensors

CONVERSION CHART FOR ANGULAR MEASURE

A conversion chart for degrees, minutes, seconds, milliradians and microradians is given.

In this section various forms of angular measure are used. While each usage is appropriate, relative sizes are not always appreciated. For this reason a single conversion chart has been constructed which relates degrees to minutes, seconds, milliradians and microradians.

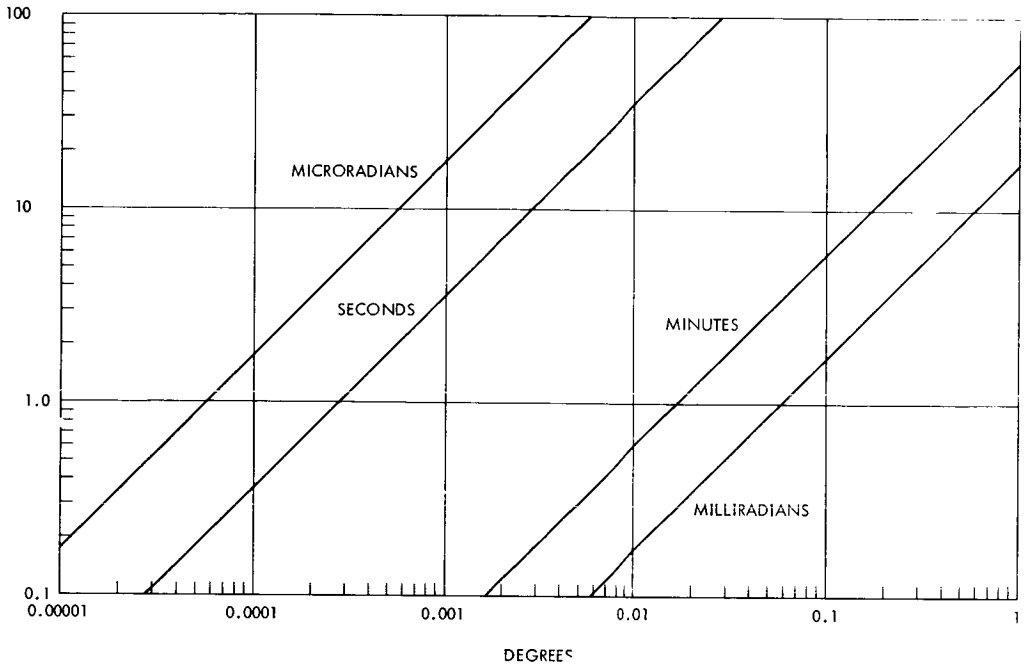

Conversion Chart for Angular Measure

STAR SENSORS

Scanning techniques used with conventional photomultiplier are described and accuracy vs weight is given for certain space designs.

There are three principal classes of star sensors, according to the type detector used: (1) the conventional photomultiplier, (2) the image detector, and (3) the quadrant photomultiplier. Photomultiplier tube tracking are discussed in this topic. Further description of photomultipliers, image dissectors and quadrant photomultipliers are discussed in the next topic.

A star appears essentially as a point source. (The apparent angular size of useful stars ranges from 0.0068 arc second for Sirius to 0.0410 arc second for Antares.) Hence the limitations of star tracker accuracy are mainly due to the background noise and internal instrument errors. By using larger optics, the signal to noise ratio (S/N) of the sensor output can be increased and higher angular discrimination achieved. Additional discrimination can be obtained by measuring differences in intensities and spectral densities. Also several sensors may be used to discriminate by recognizing a certain pattern of stars.

Initial acquisition is difficult due to the small angular size of the stars and the small angular beam of the star tracker. Scanning during acquisition is required and may be provided internally in the tracker or by maneuvering the vehicle. Mirror and vibrating reed scanning techniques are depicted schematically in Figures A and B. The table lists detailed specifications of some typical instruments. Values from this table and other data is plotted in Figure C.

Comparison Matrix of Star Sensors

Candidate Instrument	Performance (at Synchronous Altitude)		Interface Considerations	Reliability	Weight, Power and Size	
Star (Polaris) sensors (Polaris is a +2.1 magnitude star)						
1. ITT Federal Labs. OAO Boresighted Star Tracker	1. Star magnitude sensitivity 2. Field of view 3. Accuracy (rms) 4. Gimbaled (electronically) 5. Two axis capability	+6 10 arc minutes 1.5 arc seconds ±1.5 degrees 15 arc second steps	1. Small field-of-view-acquisition may be difficult. Also may be difficult to constrain vehicle motions within field of view in normal operation 2. Precision and gimbaling capability not required. 3. High weight of system.	1. To be used on OAO. 2. Reliability number not available. 3. All digital circuitry.	1. Weight 2. Power 3. Size	25 pounds ±28 volts dc ±10 volts, 7.7 watts (diameter) 3 x 15 inches 5 x 11 x 12 inches electronics
2. ITT – Dual Mode Star Tracker	1. Sensitivity 2. Field of view 3. Accuracy (rms) 4. Not gimbaled 5. Two axis capability	+3 8 x 8 degree acquisition, 32 x 32 minute track ±5 arc seconds	1. Adequate field of view for acquisition. 2. More precise possibly than required.	1. No moving parts – all electronic gimbaling 2. Reliability number not available.	1. Weight 2. Power 3. Size	9.5 pounds ±26 volts dc, 8.0 watts 5 x 10.5 x 5 inches
3. ITT – Electro-Optical Housing Head for Star Tracking	1. Sensitivity 2. Field of view 3. Accuracy (rms) 4. Not gimbaled 5. Two axis capability	+2.5 magnitude 1.0 x 1.0 degree ±9 arc seconds	1. Small field of view relative to 2 above – acquisition more difficult.			
4. Kollsman Instrument Company. Gimbaled Seeker	1. Sensitivity 2. Field of view 3. Accuracy (rms) 4. Gimbaled (mechanically) 5. Two axis capability	+2 magnitude 1 x 1 degree ±5 arc seconds ±43 degrees, two axis	1. Excessive weight – high precision and gimbaling not required for Polaris one or two axis sensing.	1. OAO flight instrument 2. Reliability number not available.	1. Weight 2. Power 3. Size	42.5 pounds 12.9 watts Not available
5. Bendix Corporation Star Sensor (Proposed for SERT-III Mission)	1. Sensitivity 2. Field of view 3. Accuracy 4. Not gimbaled 5. Single axis design	+2.1 magnitude 10 x 10 degrees <0.1 degree	1. Proposed sensor with off-the-shelf components – sensor development program necessary to a certain degree.	1. Proposed design utilizing off-the-shelf components – hence reliability not available. 2. Reliability development program required.	1. Weight 2. Power 3. Size	5.0 pounds 8.0 watts 4 x 7 x 10 inches
6. ITT Sensor Design (Proposed for SERT-III)	1. Sensitivity 2. Field of view 3. Accuracy 4. Single axis design 5. Information not available. Sensitivity capability possibly questionable.	+2.1 magnitude 10 x 10 degrees 0.012 degree	1. Similar to (2) above except single axis; however, some development required.	1. Proposed design utilizing off-the-shelf components; reliability not available.	1. Weight 2. Power 3. Size	8.0 pounds Not available 2-1/4 diameter x 8.5 inches

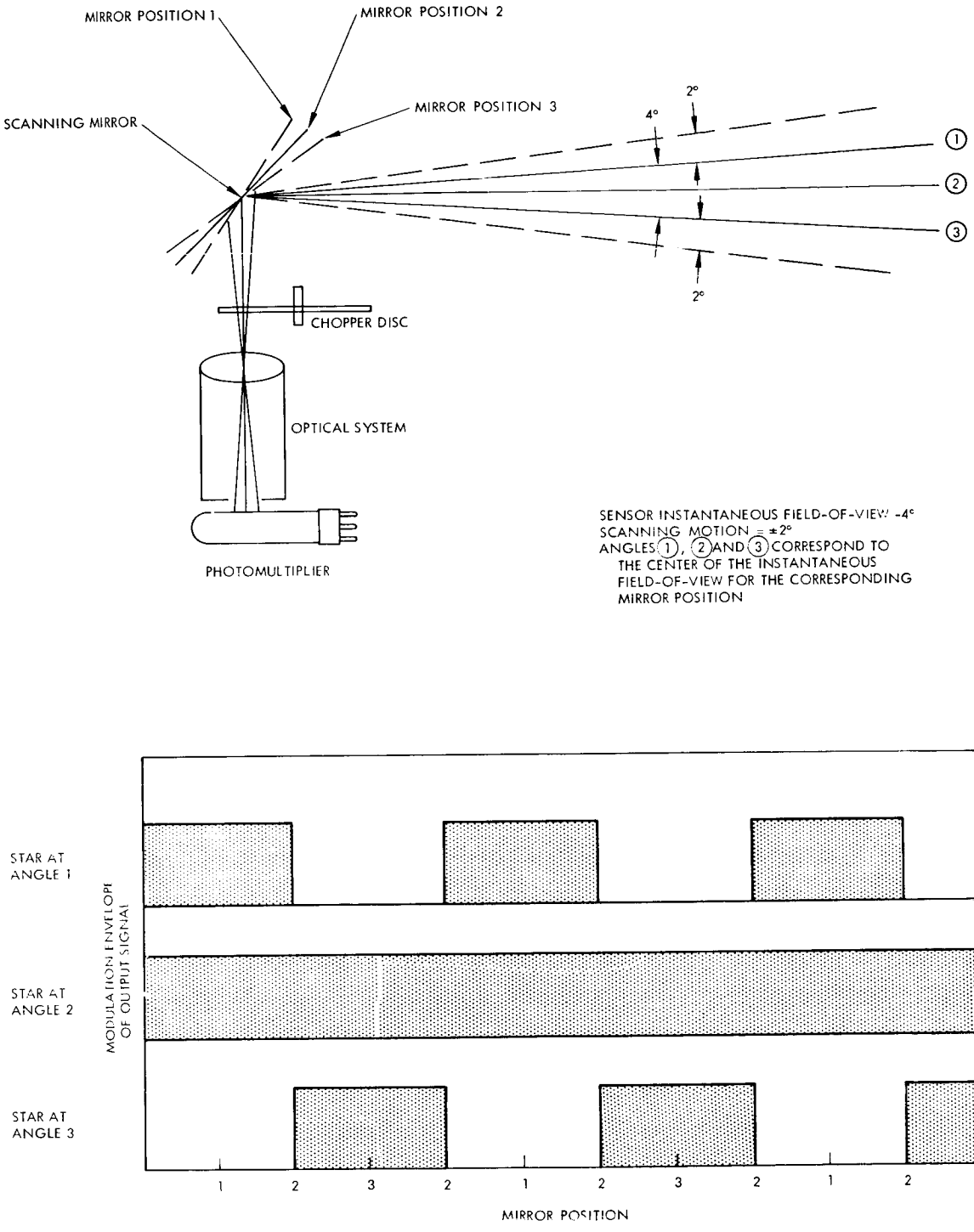

Figure A. Scanning Mirror Star Sensors

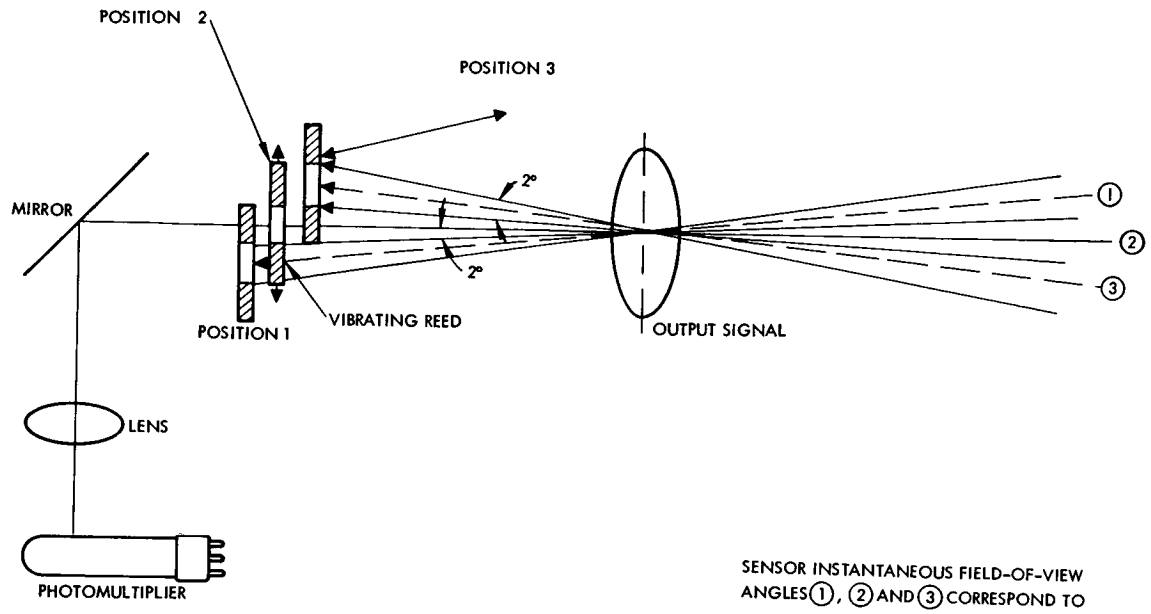

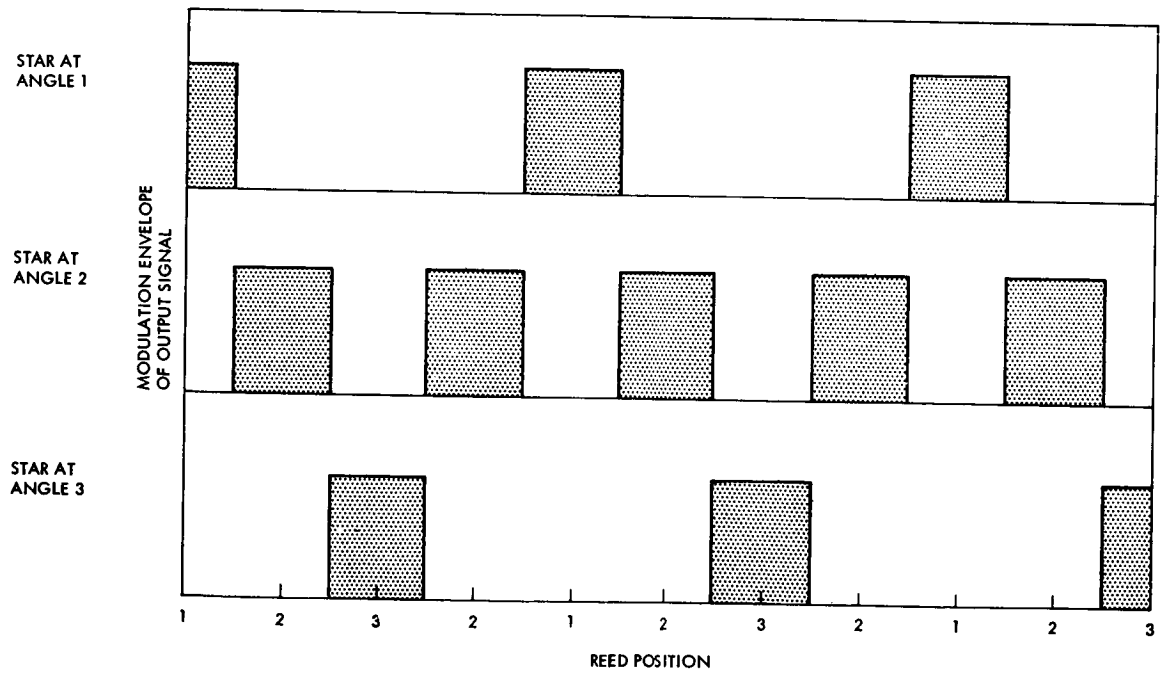

Figure B. Vibrating Reed Star Sensor

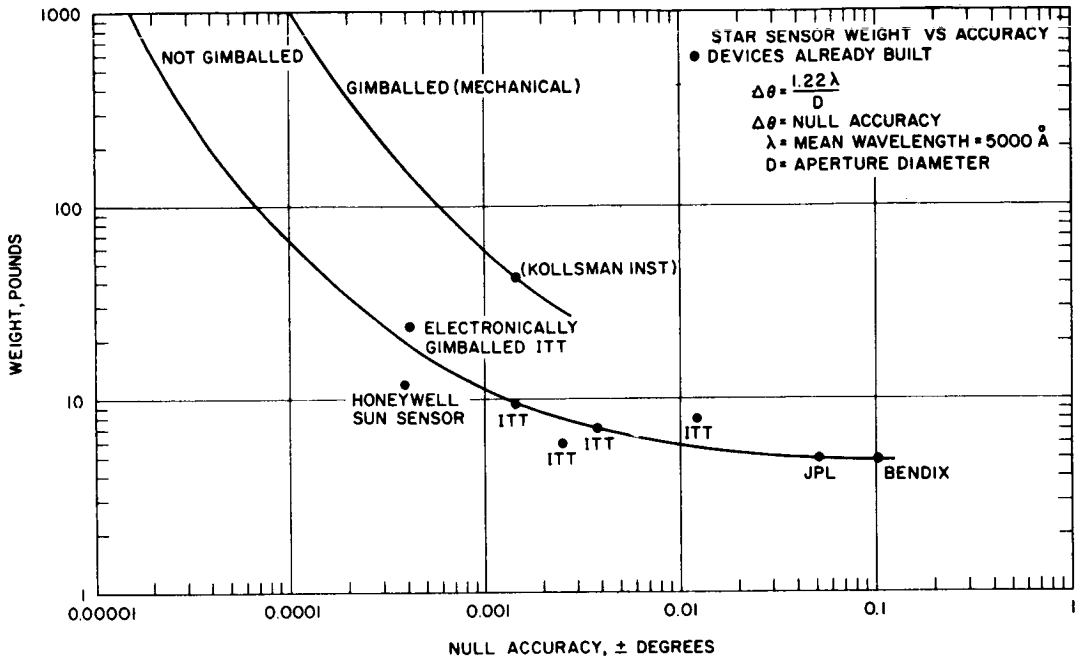

Figure C. Star Sensor Weight versus Accuracy

STAR TRACKER DETECTORS

Examples of star tracker implementation using photomultiplier, image dissector, and quadrant photomultiplier are given

Photomultiplier Tube. The conventional photomultiplier tube detector has been widely used in star sensors. Since only the magnitude of the energy incident on the photocathode is sensed, scanning is required to give position information. To avoid dc drift, modulation is provided either by a chopper or by the mechanical scanning.

A one-axis Canopus sensor of this type is used on Surveyor. Error signals are generated by comparing the modulation envelope of the sensor output with a reference signal square wave. The Surveyor sensor was designed for a null accuracy of approximately 0.1 degree with a 4 x 5 degree instantaneous field of view (FOV).

On the orbiting astronomical observators (OAO), six photomultiplier trackers are used, each having 1 degree FOV. Only three of the six trackers are required to lock on their guide stars for vehicle acquisition. This system is capable of 30 arc second accuracy for second magnitude or brighter stars. High accuracy (±0.1 arc second) star sensing with a 2 arc minute FOV is provided by the 80 cm Cassegrain telescope used for astronomical observations.

Image Dissector. The image dissector tube detector (Figure A) allows mechanical scanning and modulating to be performed electronically. It consists of a scanning section and of a photomultiplier. A one axis Canopus sensor of this type having a null accuracy of 0.1 degree was used on Mariner II. It had a total field of view of 4 degrees in roll and 32 degrees in pitch and an instantaneous field of view of 0.86 degree in roll and 10.6 degrees in pitch.

The boresighted star tracker used on the OAO incorporated two image dissector tube and had a null accuracy of 2 arc seconds. It had a total field of view of 3 degrees and an instantaneous field of view of 10 arc minutes.

Quadrant Photomultiplier. The quadrant photomultiplier (Figure B) uses four photocathode segments. The segments are sequentially sampled and the currents are then compared to obtain the attitude signal. The Canopus sensor of this type used on the Advanced Orbiting Sun Observatory, AOSO, had a null accuracy of ±0.5 arc minute.

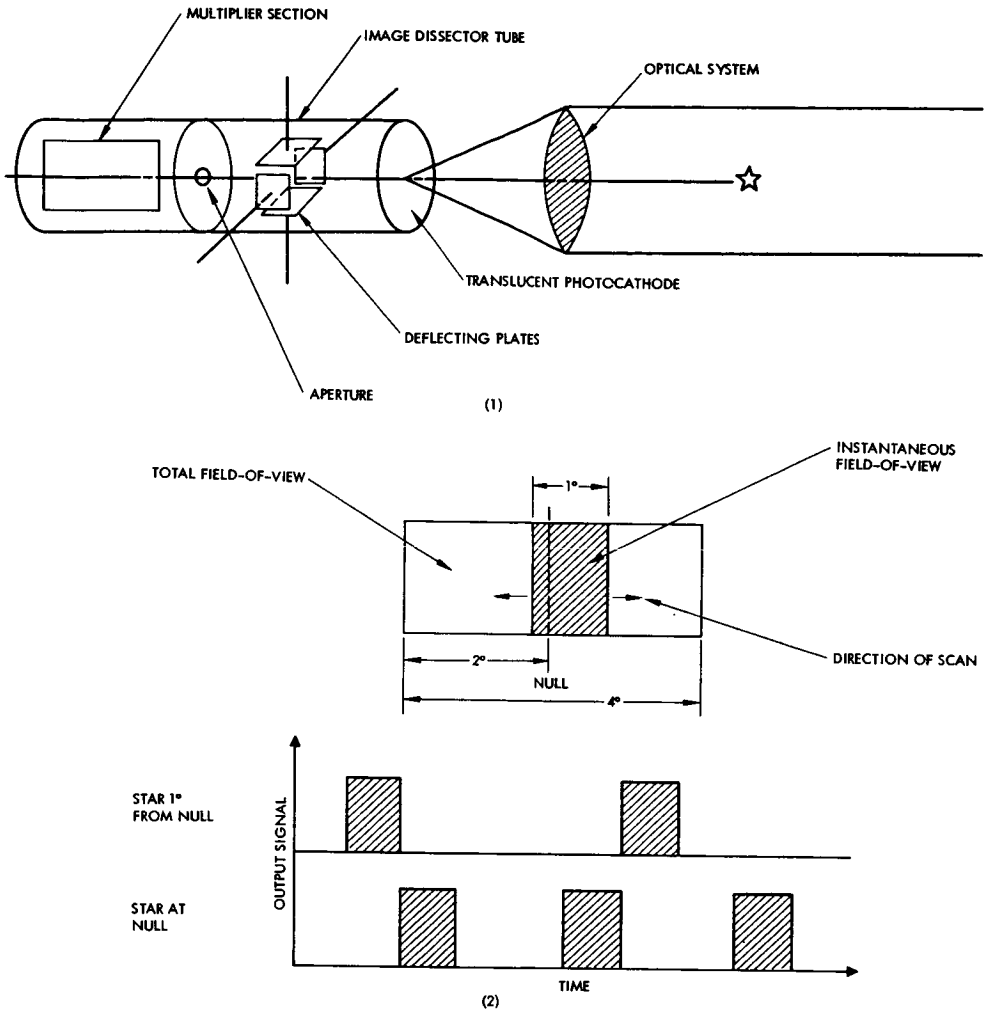

Figure A. Image Dissector Star Sensor

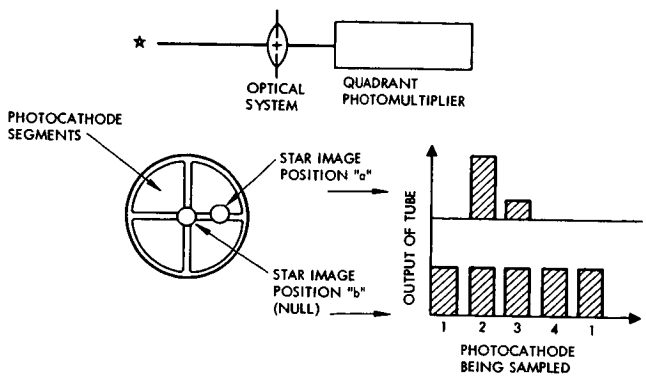

Figure B. Schematic Diagram of a Quadrant Photomultiplier Type of Star Sensor

PLANET SENSORS

The principle of operation for Planet Sensors is described and several implementations are schematically illustrated.

Planet sensors are applicable to bodies subtending angles greater than 0.25 degree. As a result of the larger angular size of the target object, target irregularities are the dominant error source. Planet sensors may be conveniently grouped according to their spectral response as visual or infrared.

Visual Sensors. The Ranger vehicles used shadow masked photomultiplier tubes to sense the earth at ranges of 90,000 miles. These sensors (Figure A) were designed to have a linear range of 2.5 degrees and a null accuracy of ±0.1 degree. Similar performance was reported for the Mars sensors used on Mariner II.

Infrared Sensors. Horizon scanners (Figure B) utilize a scanning sensor with a small field of view. Pulses are generated when a body enters or leaves the field of view. The Mercury capsule used two such sensors, each having an instantaneous field of view of 2 x 3 degrees and providing an accuracy of ±1/2 degree. Nimbus used a similar system to provide accuracy of ±1/2 to ±1-1/2 degrees. Horizon scanners of various types are compared in the table.

Edge trackers (Figures A and C) lock onto the space-target boundary and oscillate the sensor field of view about this edge. Attitude information thus obtained is based on the average mirror orientation. Three sensors of this type provide 2-axis information for the OGO, with accuracies of better than 1 degree at altitudes from 100 miles to 100,000 miles. Contemporary infrared planet trackers are not capable of accuracies much better than ±0.5 degree.

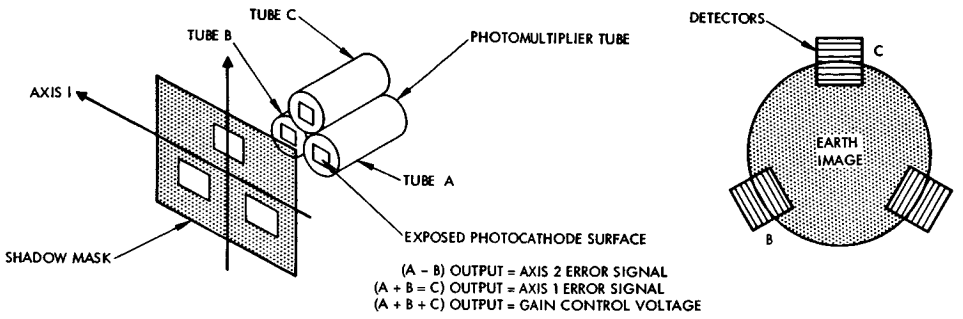

Figure A. Ranger Earth Sensor Schematic

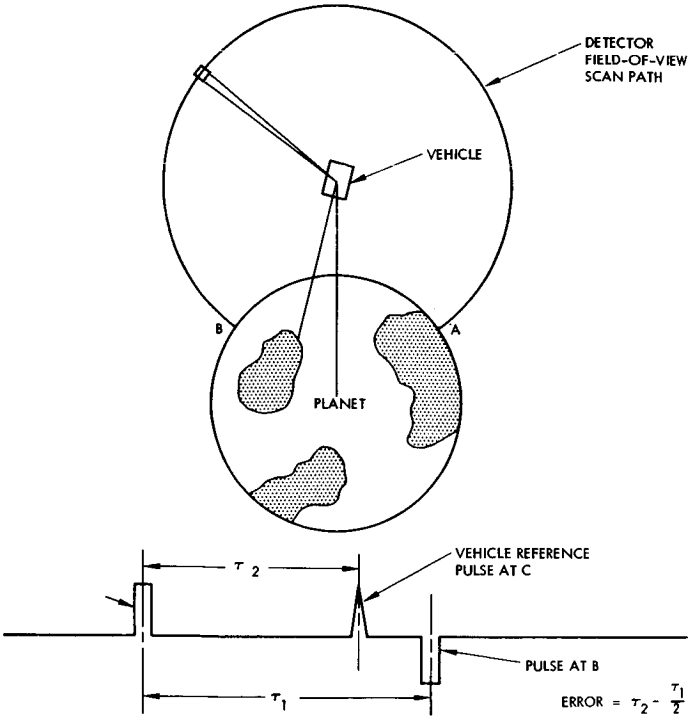

Figure B. Operating Principle of Horizon Scanners

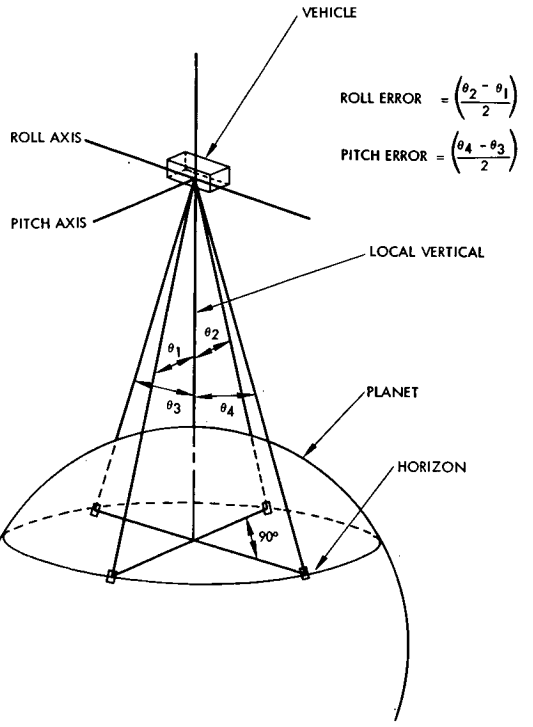

Figure C. Operating Principle of Edge Tracker Devices

Comparison Matrix of Horizon Scanners

Candidate Instrument	Performance (at Synchronous Altitude)		Reliability	Weight, Power and Size	
Earth Horizon Scanners					
1. Advanced Technology Labs (ATL) Gemini Horizon Scanner	1. Altitude range 2. Accuracy 3. Scanning 4. Field of view 5. Two axis capability 6. Accuracy versus tilt angle	50 to 2000 n. mi. 0.1 degree Azimuth, edge tracking 92 to 102 degrees above vertical – 1.4 x 1.4 degrees instantaneous 8 to 22μ bandpass ±20 degrees allowable at 850 n. mi. – accuracy degrades with tilt angle	1. MTBF = 25,000 hours estimated. 2. Currently flying on Gemini and classified projects.	1. Weight 2. Power 3. Size	4.5 pound sensor 4.2 pound electronics 10 watts at 26 volts 4-18 x 5-3/4 x 5-1/8 inches
2. ATL OGO Horizon Scanner	1. Altitude range 2. Accuracy 3. Scanning 4. Field of view 5. Two axis capability 6. Accuracy versus tilt angle	100 n. mi. to 80,000 n. mi. 0.1 - 0.2 degree Edge tracking–two heads per axis 1.4 x 1.4 degrees instantaneous 90 degrees above vertical acquisition 8.5 to 20 microns bandpass Error increases above 5.0 degrees tilt angle maximum tilt is 6.0 degrees	1. 0.874 reliability for 1 year 2. In production, flight experience on OGO program.	1. Weight 2. Power 3. Size	13.2 pounds 9.8 watts 7 x 6 x 2.5 inches each dual head 7 x 5 x 3 inches electronics
3. ATL Advanced OGO Horizon Scanner	Performance identical to (2) above except that: 1. Accuracy 2. Two axis capability	<0.05 degree 14 to 16 microns bandpass	1. 0.9934 reliability for 1 year. 2. Scheduled to fly on later OGO's – in qualified testing.	1. Weight 2. Power 3. Size	10.0 pounds 6.0 watts 7 x 6 x 2.5 inches each dual head 7 x 5 x 2 inches electronics
4. Barnes All Altitude Horizon Sensing System – Model 13-160	1. Altitude range 2. Accuracy 3. Scanning 4. Field of view 5. Two axis capability 6. Accuracy versus tilt angle	100 to 22,000 n. mi. 0.1 degree instrument <0.1 - 0.2 degree system error Three edging tracking heads, one per sensor 70 degree acquisition scan, 0.5 x 3.0 degrees instantaneous 1.8 to 20 microns bandpass Similar to 2.6 above	1. MTBF not available.	1. Weight 2. Power 3. Size	4 pounds sensor head each 7 pounds 4.0 watts average 12.0 watts maximum 5 x 6.5 x 5 inches each 13 x 8.5 x 4 inches electronics

COMPONENT PERFORMANCE AND BURDEN RELATIONSHIPS

Passive Attitude Control Techniques

Active Attitude Control Devices

INTRODUCTION

Types of control techniques are introduced and accuracy ranges are given.

Attitude control techniques are classified as active or passive, depending on whether they consume energy or not. Passive control techniques produce restoring torques by use of such natural forces as:

Solar radiation pressure

Gravity gradients forces

Magnetic forces

Aerodynamic forces

Active attitude control devices use:

Spin stabilization

Reaction wheels

Momentum wheels

Reaction jets

Passive attitude control techniques other than solar pressure are limited in use to regions near planets. Restoring torques produced by natural forces are relatively quite small compared to those of active devices so that the equilibrium time, to correct significant vehicle displacements, may be too long for a primary attitude control system and an optical communication system. Attitude control techniques are summarized in the table. Accuracy limitations of the above attitude control techniques and others are summarized in the figure[1].

Spin Stabilization has an accuracy range to 0.2 degree and passive control techniques produce angular accuracies of 2 to 4 degrees.

[1] "High Accuracy Attitude Control for Space Astronomy," D.C. Fosth and W.H. Zimmerman, JACC 1967, pp. 753-761.

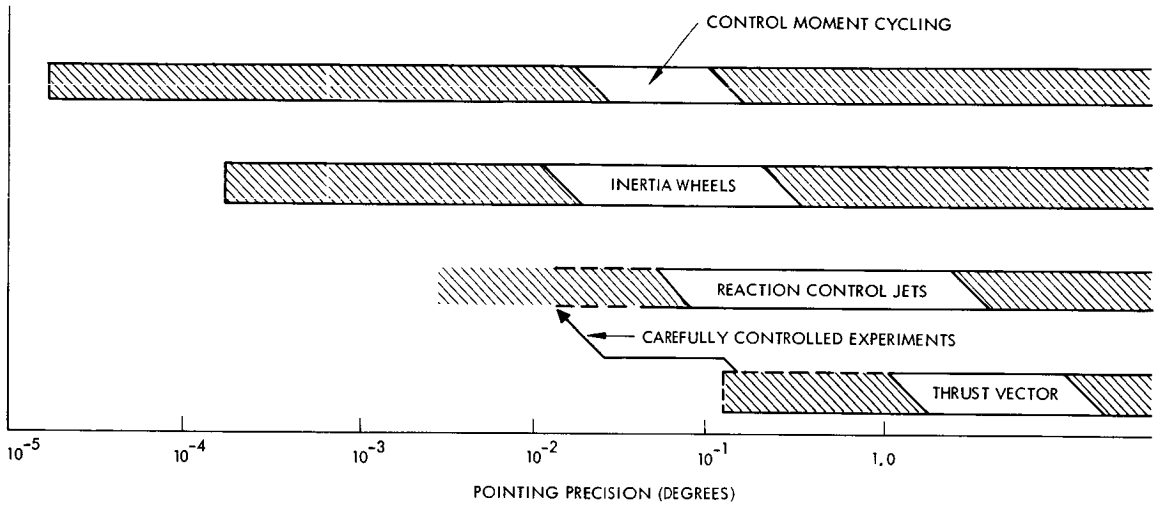

Accuracy Comparison of Space Type Actuators

Comparison Matrix of Attitude Control Techniques

Candidate Systems	Performance Considerations	Interface Considerations	Reliability Considerations	Weight Considerations
I. On-Off reaction jet systems	1. Limit cycle mode of operation causes average attitude errors to be one-half the deadband plus sensor errors. 2. System fuel consumption susceptible to sensor noise and disturbance torque magnitude. 3. System provides maneuver capability and acquisition capability for small fuel weight penalty. 4. Duty cycle inversely proportional to attitude deadband (for small disturbance torques), hence fuel consumption in steady state possibly large.	1. Sensor and sensor physical alignment errors add to system attitude errors. 2. System requires either low thrust levels and small thrust misalignments for orbital Δv maneuver jets (or auxiliary control mode during Δv maneuvers). 3. Force levels may be selected to perform some transfer orbit control; however, if supplemental apogee propulsion is required, spin stabilization will be required during apogee thrusting.	1. Relatively simple, reliable system. 2. Extensive space flight experience exists. 3. Cold gas system requires no ignition—only solenoid valves and pressure regulation are active elements. 4. Liquid propellant requires ignition, and zero-g feed system.	1. Fuel weight may be excessive, especially if cold gas selected as propellant.
II. Magnetic control systems	1. Missing control axis will result in poor pointing accuracy at certain times in orbit. 2. Magnetic control introduces cross-coupling between axes in most cases. 3. Weak earth field requires large coils with reasonable control torque magnitudes. 4. Somewhat complex signal processing is required on board spacecraft. 5. Lifetime is not limited by fuel supply provided power remains available throughout mission.	1. System requires extremely low thrust from orbital Δv maneuver thrustors due to rather weak control forces. 2. Acquisition performance is relatively poor with primary magnetic control. 3. Sensing of earth's magnetic field is required in addition to other 3 axis attitude sensing. 4. Large power supply required to produce sufficient control torque. 5. Mounting of coils may present alignment and configurational problems.	1. No moving parts, but electronic circuitry is more complex than reaction jets. 2. Limited space flight experience exists. 3. Thermal heating of coils may introduce lifetime degradation.	1. Weight of large coils may be excessive. 2. Weight of additional power supply may be excessive.
III. Reaction wheels with reaction jet momentum removal	1. Cyclic disturbance torques and maneuvers can be performed for no additional fuel penalty. 2. Precise accuracy (limited to sensor accuracy) and attitude stability can be achieved. 3. Tracking accuracy can be better than for other candidates by proper design. 4. Reaction jet system provides acquisition capability and back-up attitude control capability (until fuel is depleted). 5. Some crosscoupling is introduced via the angular momentum vector of the wheels.	1. Low Δv maneuver thrust levels and misalignments are required. 2. Sensing for three control axes must be provided, however, system is somewhat less sensitive to sensor noise than reaction jet system. 3. Separate transfer orbit control and control during apogee thrusting (if required) may be required. 4. Any number of maneuvers for experiments may be performed with no weight penalty.	1. Wheels and motors in each axis constitute some moving parts; electronic circuitry is also more complex than for reaction jet system. 2. High speed bearing in motor-flywheel sets may degrade lifetime. 3. Some space flight experience will or does exist (Nimbus, OAO, OGO).	1. Weight tradeoff must be performed versus all reaction jet systems for 2-year lifetime.

Comparison Matrix of Attitude Control Techniques (Continued)

Candidate Systems	Performance Considerations	Interface Considerations	Reliability Considerations	Weight Considerations
IV. Reaction wheels with magnetic momentum dumping.	1. Same as III-1, 2, 3, 5 above. 2. Back up attitude control capability does not exist essentially due to II-1, 2, 3, 4; signal processing is not set up for primary attitude pointing. 3. Momentum dumping only reduces the crosscoupling and missing axis difficulties somewhat.	1. Same as III-1, 3, 4 above. 2. Same as II-3, 5 above.	1. Same as III-1, 2, 3 above for wheel portion. 2. Momentum dumping circuitry more complex than for reaction jet momentum dumping.	1. Same as II-1, 2 above. 2. Total system weight including wheels larger than for III since momentum unloaded expected to require only small fuel weight.
V. Momentum bias system with reaction jet momentum removal	1. Momentum vector stiffness allows rather gross Δv maneuver thrust levels and misalignments. 2. Reaction jet system provides acquisition capability; wheel and jet may be used from possible transition from spin stabilized transfer orbit mode to non-spinning operational mode. 3. Most cyclic angular momentum due to disturbances can be stored without fuel penalty. 4. Passive dumping is sufficient in roll-yaw axes; active only (electronically) in pitch axis.	1. Only two axis earth sensing may be sufficient due to inertial stability and fact that roll error (relative to earth) becomes yaw error 90 degrees later in orbit. 2. Large Δv thrust levels and misalignments are tolerable. 3. Experiment maneuvers will be limited in N-S direction.	1. One wheel instead of three; however, larger wheel may have more bearing lifetime problems. 2. Control circuitry is least complex of all candidates. 3. No space flight experience.	1. Wheel weight and structural support weight may be large. 2. Fuel weight will be excessive if frequent reorientation maneuvers are required.
VI. Gyro torquers with reaction jet momentum removal	1. Same as III-1, 2, 3, 4. 2. Performance essentially identical with reaction flywheels.	1. Same as III-1, 2, 3, 4.	1. Mechanical motion of constant speed gyros replaces speed variations of flywheels. 2. Six spinning masses rather than three (unless two axis gimbal used with one set of 2 gyros). 3. No appreciable space flight experience (scheduled for one classified military project but program cancelled).	1. Same as III-1.

SOLAR RADIATION PRESSURE

Solar pressure values and usefulness to spacecraft control are described.

Solar Radiation pressure may be used in attitude control at distances greater than 300 miles from the earth. The radiation pressure at a solar distance of 1 AU is approximately 10^{-7} lb/ft^2 and varies inversely with the square of the solar distance. The solar radiation torque on a vehicle is given by

$$L_s = C_r A_s \left| \vec{b} \times \vec{P}_S \right|$$

$$= C_r P_S A_s b \sin \psi_s$$

where

L_s = solar-radiation torque

A_s = area of solar sail

b = distance from center of mass to center of pressure of vehicle and solar sail

ψ_s = angle of incidence of solar radiation on sail surface

P_s = solar-radiation pressure

C_r = coefficients of radiation force

According to Thompson,[1] the angle ψ_s, is kept small, typically in the range of 10 degrees. Chin[2] provides a table of coefficients, C, which are a function of both vehicle geometry and surface reflectivity (see the table.)

The figure shows solar radiation torque as a function of effective length of lever arm with effective area as a parameter. Studies have indicated that for a typical 1000-pound vehicle at 1 AU having a 50 ft^2 stabilizer, a 5 degree disturbance would be reduced to less than 1 degree error in about 12 minutes. Attitude control by radiation pressure has the advantage of extreme reliability. The principle disadvantage is that restoring torques are so weak that equilibrium times are long and accuracy is limited to 1 degree. Another disadvantage is that large deployed areas of sail are required.

---

[1] W. T. Thompson, "Passive Altitude Control of Satellite Vehicles," Guidance and Control of Aerospace Vehicles, edited by C. T. Leondes, McGraw-Hill, 1964.

[2] T. H. Chin, "Spacecraft Stabilization and Altitude Control," Space/Aeronautics, June 1963.

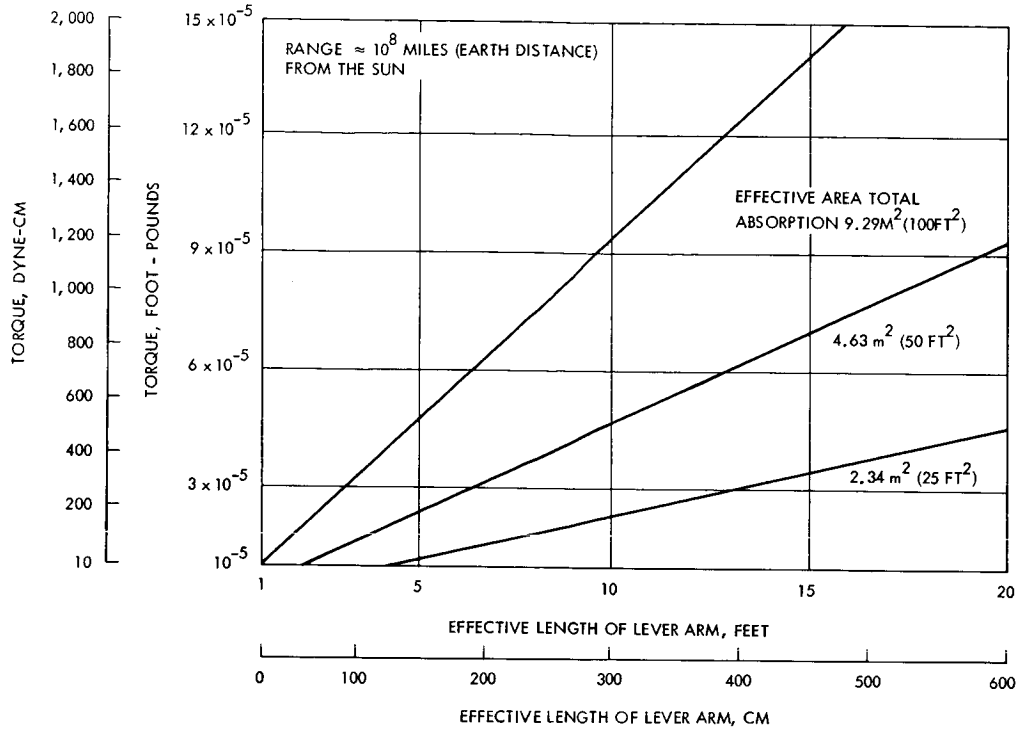

Solar Radiation Torque as a Function of Lever Arm Effective Length

(Note: Pressure varies as the inverse square of the distance to the sun.)

Coefficient of Solar Radiation, Cr

Vehicle Geometry	Coefficient
Plane surface	$0 < C_r < 2$
Sphere	$0.75 \leq C_r \leq 1.25$
Cylinder	$0.862 \leq C_r \leq 1.471$
Cone or paraboloid	$0 \leq C_r < 2$

One step beyond passive stabilization is the use of movable solar vanes to trim the vehicle in response to sensed attitude information. This system was used on Mariner C. The same disadvantages remain, however, as for the case of the completely passive system.

GRAVITY GRADIENT FORCES

Torque and natural period equations are given for gravity gradient attitude control.

Unless the gravitational force acts along a line passing through the center of mass, a torque tending to rotate the satellite will result. The conventional gravity gradient configuration is shown in the figure. The gravity gradient torque, L_g, is:

$$L_g = \frac{3}{2} \omega_o^2 (I_x - I_z) \sin 2\theta_\ell \quad \text{(dyne-cm)}$$

where

I_x = moment of inertia about the x axis

I_z = moment of inertia about the z axis

ω_o = orbit angular rate = $\sqrt{\frac{GM_e}{r^3}}$

G = gravitational constant

M_e = mass of earth

r = distance from center of earth

θ_ℓ = angle of libration, angle between the symmetric axis of the satellite and the local vertical

The natural period of oscillation (libration period) of the gravity-stabilized satellite is given by

$$T_{||} = \frac{2\pi}{\sqrt{\frac{3\,GM_e}{r^3}(1 - I_z/I_x)}} \text{ seconds}$$

in the plane of the orbit and by

$$T_{\perp} = \frac{\pi}{\sqrt{\frac{GM_e}{r^3}(1 - I_z/I_x)}} \text{ seconds}$$

normal to the plane of the orbit.

Typical values for an orbit period of 100 minutes are $T_{||}$ = 57.8 minutes and $T_{\perp}$ = 50.0 minutes.

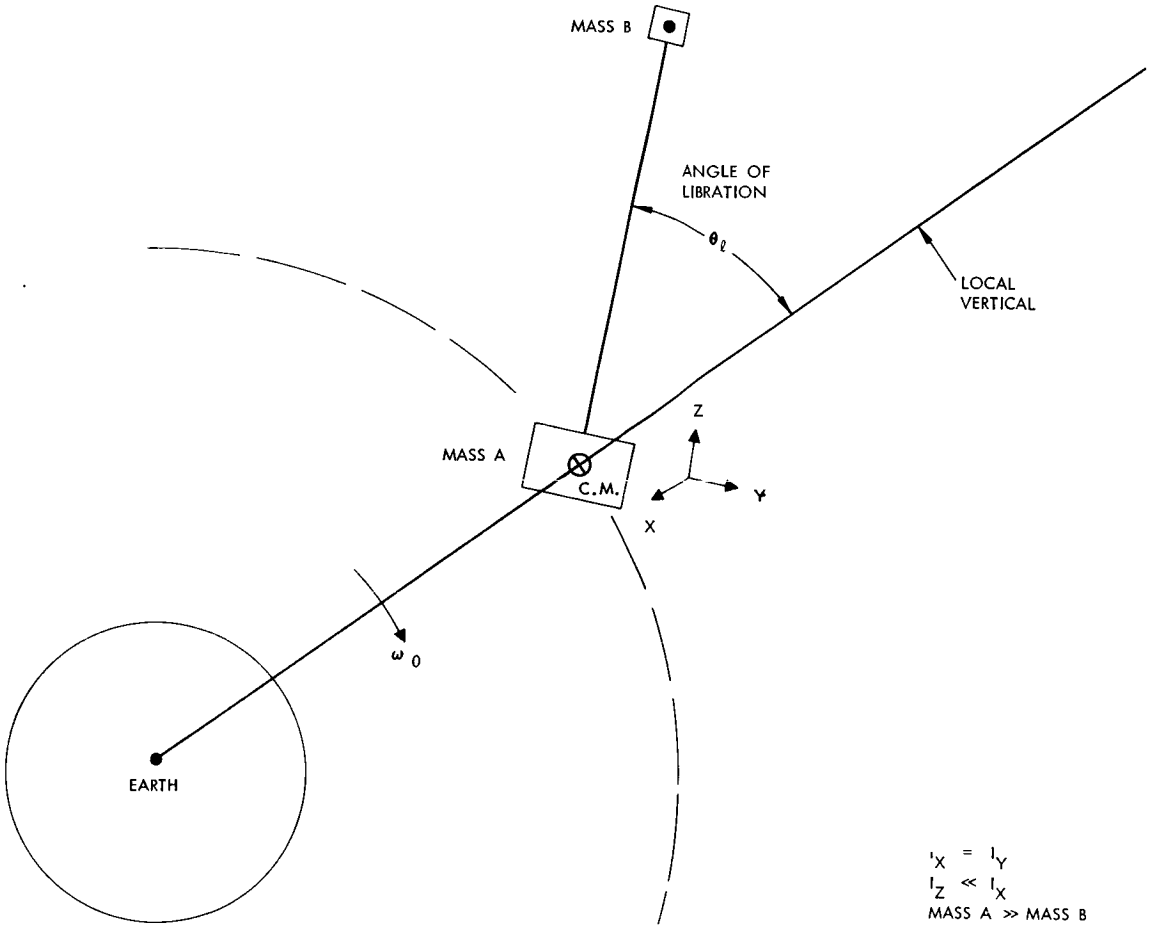

Gravity Gradient Schematic

The principle advantage of gravity gradient stabilization is its extreme simplicity. Its disadvantages are that restoring torques are small so that even with adequate damping, accuracy is limited to the order of ±1 degree. [1]

[1] E. I. Ergin, "Current Status of Progress in Attitude Control, AIAA Guidance and Control Conference, Cambridge, Massachusetts, August 12-14, 1963.

MAGNETIC FORCES

Magnetic forces are described and altitude variations documented.

Torques are produced by the interaction of the earth's magnetic field with magnetic elements on the vehicle. The earth's magnetic field is that of a magnetic dipole with its axis precessing about the earth's spin axis. The total earth magnetic field intensity as a function of altitude is plotted in the figure.[1] The axial and normal components of the dipole field are given by

$$H_{axial} = 0.38 \frac{(1 - 3\cos^2\delta_m)}{(r/r_e)^3}$$

$$H_{normal} = 0.461 \frac{\sin^2\delta_m}{(r/r_e)^3}$$

H_{axial} = the axial component of field intensity (oersteds)

H_{normal} = the normal component of field intensity (oersteds)

δ_m = the angle between the earth's magnetic dipole axis and the radius vector to the satellite

r = the distance to the satellite from the center of the earth (centimeters)

r_e = the radius of the earth (6.371×10^8 cm)

The torque tending to align the magnetic dipole of the on-board magnetic elements with the local magnetic field is given by

$$L_m = MH \sin\phi$$

where

M = magnetic dipole moment of the vehicle

H = local magnetic field intensity

ϕ = angle between the local magnetic field and the dipole moment of the vehicle

[1] E. I. Ergin, "Current Status of Progress in Attitude Control, AIAA Guidance and Control Conference, Cambridge, Massachusetts, August 12-14, 1963.

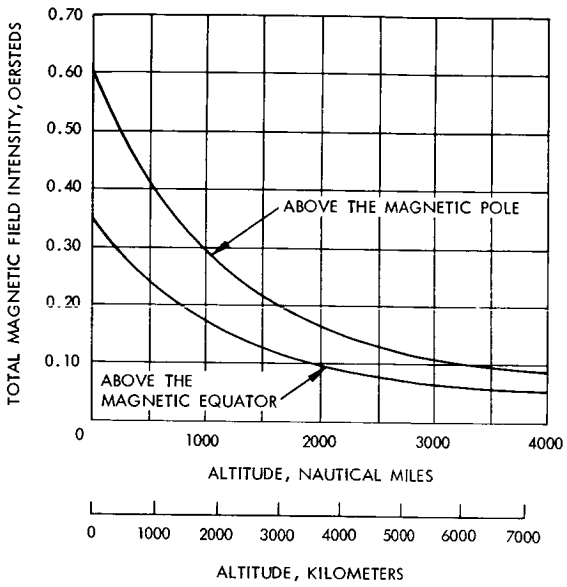

Figure A. Field Intensity Versus Altitude for Earth's Magnetic Field

MAGNETIC FORCES

In the case of the TRAAC satellite in a 500 mile orbit, H = 0.3 oersteds and M = 10^3 resulting in a maximum torque of L_m = 300 dyne cm. Since the earth's field precesses with its spin rate, the torque will, in general vary from one orbit to the next as well as being a function of position during an orbit, and may in fact require the expenditure of considerable on-board power. Thus, this is not strictly a passive control method.

Variable torques can be produced by current carrying coils. For a coil centered about the Z body-axis of a satellite the magnetic torque is given by

$$\vec{L}_m = \frac{\pi r_c^2 i}{10} n (B_y \hat{u}_x + B_x \hat{u}_y)$$

$\hat{u}_x$ and $\hat{u}_y$ = unit vectors

r_c = radius of coils (cm)

i = current (amps)

B = flux density(gauss)

n = number of turns

The maximum torque as a function of altitude over the magnetic equator is plotted in Figure B. The Tiros II and III used current loops to precess the satellite spin axis during the orbit. Significant control torques can be achieved by this technique at altitudes up to 10,000 miles with accuracies as great as 0.1 degree. Such accuracies however presuppose corresponding accuracy in knowledge of the magnetic field direction. Lack of such knowledge along with the variations of the magnetic field as the spacecraft traverses its orbit limit the usefulness of magnetic stabilization where high accuracy is required.

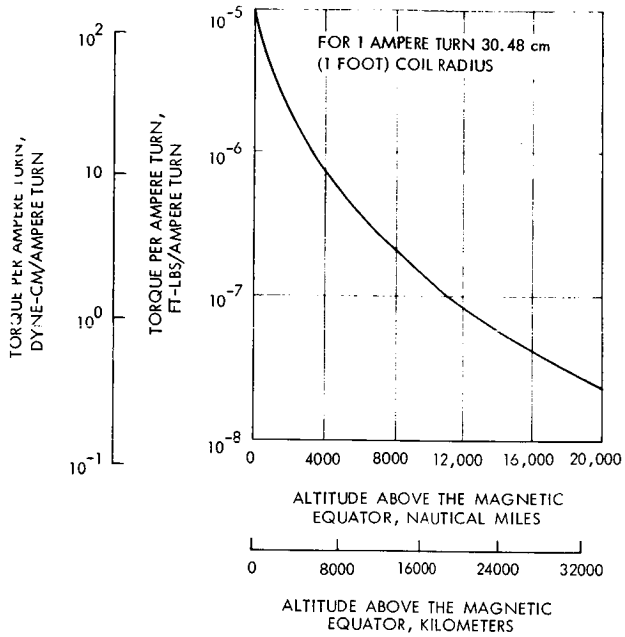

Figure B. Maximum Torque Versus Altitude (at Magnetic Equator)

REACTION WHEELS

A reaction wheel control system can produce very good control at the cost of system complexity.

Reaction wheels produce a torque on the vehicle in response to an equal but opposite accelerating torque applied to the wheel itself. In doing so, the reaction wheel also acquires and stores angular momentum from the vehicle. Since there is a practical limitation on the moment of angular momentum which may be stored in the wheel, excess momentum must be periodically "dumped" by decelerating the wheel while applying a compensating torque by a coarse attitude control device, typically a reaction jet. Since the reaction wheel provides reaction torque only about its axis of rotation, a separate wheel is generally required for each of the three control axes. This requirement may be circumvented by utilizing gyroscopic crosscoupling between two wheels to provide torques about a third axis. Inadvertent crosscoupling is, in fact, a complicating design consideration for three wheel systems. Reaction wheel size is determined by the angular momentum storage capacity required and driving motor considerations. Figure A depicts wheel weight as a function of angular momentum for wheels of various radii. Figures B and C show wheel weight as a function of maximum speed for wheels of several radii. Figures A through C are based on a constant input torque of 2.71×10^{2} dyne-cm (2×10^{-5} ft-lb). Figure D shows momentum capacity versus buildup time for several constant input torques. In a typical system application 705 Kg (1550-pound) communication satellite vehicle was stabilized to within ±0.25°/axis with 15.2 cm (6-inch) diameter 2.26 Kg (5-pound) reaction wheels. Momentum dumping with 4000 rpm wheels was required every 48 hours. Fuel weight required for momentum dumping for a 3-year period weighed only 1.6 Kg (3.54 pounds).

Reaction wheels are accurate and reliable. Tracking errors less than ±0.5 arc second and accuracies of ±0.1 are second are predicted. Bendix reports 10,000 hour lifetimes for their present wheels and predicts future lifetimes of several years.

The disadvantages of a reaction wheel control system are its relative complexity with motors and wheels continuously operating, the electrical power requirements, and potentially the system weight (a reaction jet system is also required). Crosscoupling may also be a problem as the wheels possess a net angular momentum vector which introduces additional cross-coupling between the control axes.

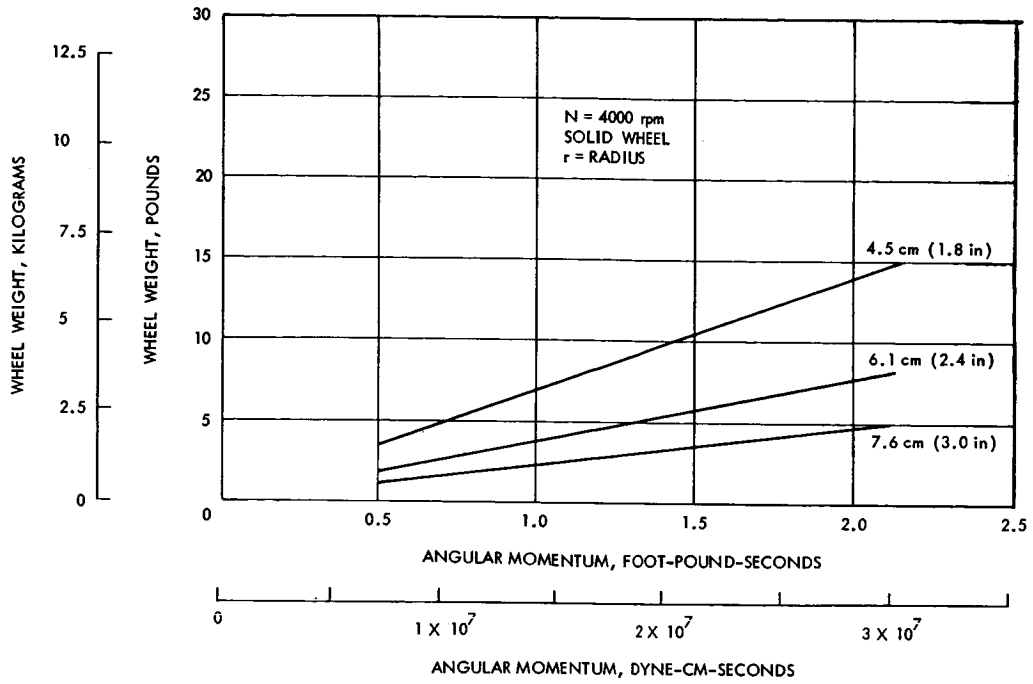

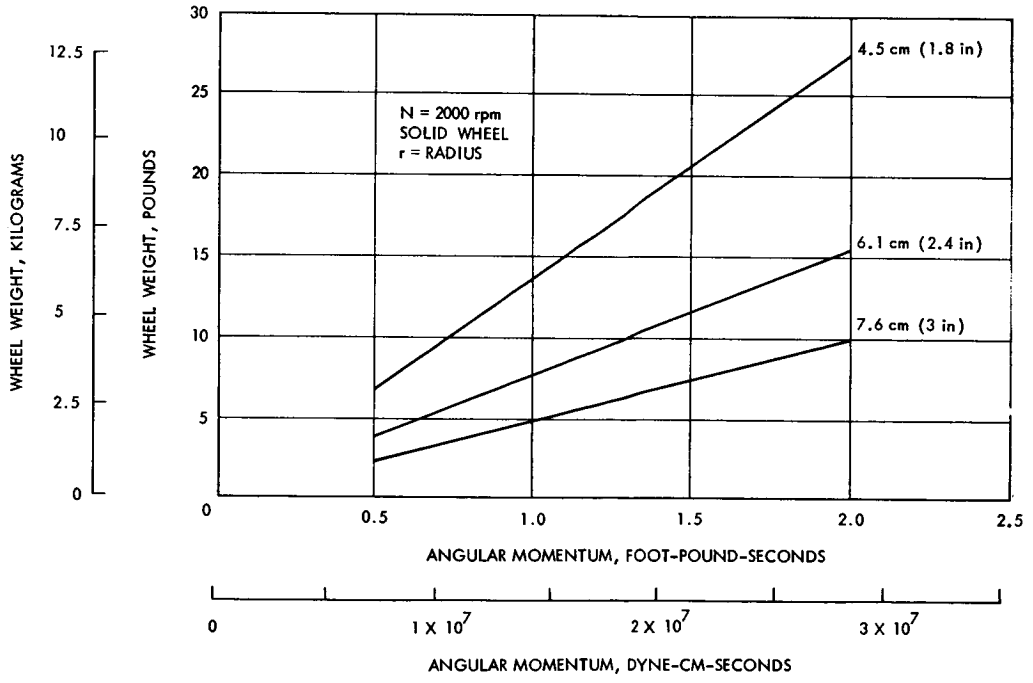

Figure A. Weight Versus Maximum Allowable Momentum Storage (max) in Reaction Wheel

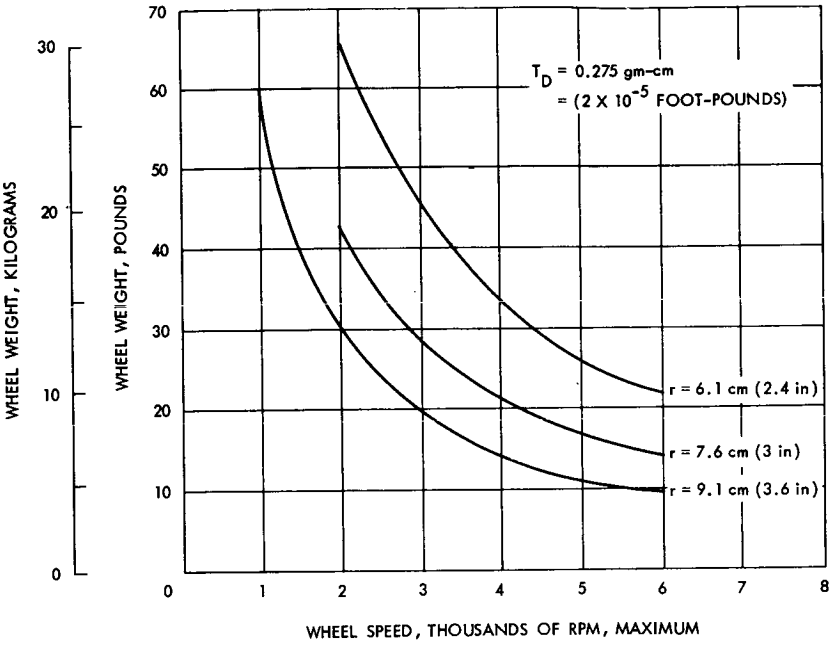

Figure B. Weight as a Function of Speed for 5-Day Reaction Wheel Dumping

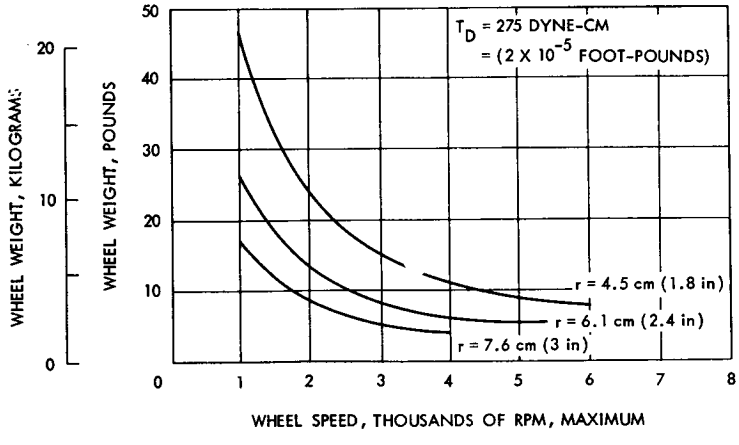

Figure C. Weight as a Function of Speed for 1-Day Reaction Wheel Dumping

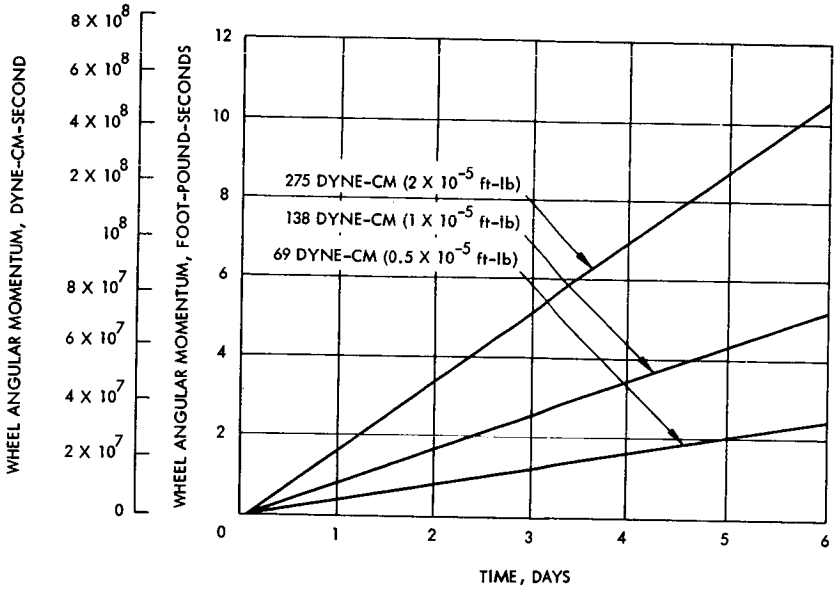

Figure D. Momentum Capacity as a Function of Time for a Constant Torque

MOMENTUM SPHERES AND FLUID FLYWHEELS

Momentum spheres and fluid flywheels are described and actual design are compound with reaction wheels.

Variations on the reaction wheel principle include the reaction sphere and the fluid flywheel. In place of individual flywheels for each vehicle control axis, a momentum sphere provides, in a single device, control torques for all three axes. As suggested by its name, the momentum sphere consists of a spherical rotor suspended by magnetic or electrostatic forces so that it is free to rotate about any axis. Driving motor elements are provided at mutually orthogonal locations and are excited in accordance with the control torques required for their respective axis. The sphere then rotates at a velocity and about an axis which are the result of the past history of vehicle torque requirements. As with other momentum transfer devices, the momentum sphere will saturate and requires resetting. A characteristics advantage of the momentum sphere is the lack of gyroscopic coupling from one axis to the other regardless of the component of momentum about any axis that may be stored in the sphere.

The fluid flywheel has been developed by GE for the Advent communication satellite. It is functionally equivalent to a conventional reaction wheel, however, the reaction torque is provided by circulating a liquid through a closed circular tube. In certain applications, this can be quite advantageous. The fluid within the tube is essentiall the rim of a flywheel, yet the tube itself is a static element. As a matter of fact, it is not necessary that the tube follow a circular path; it can follow the overall outline of the vehicle. Therefore, the inertia of the fluid, the required momentum is reached at a low fluid velocity, which minimizes flow losses. Ideally, a low density fluid with low viscosity is desirable. The low density increases the inside diameter of the tube for a given mass per foot, which further reduces the flow losses for a given velocity

With conducting fluids, the circulating pump can be of the Faraday type in which a driving dc current flows across a diameter of a section of the tube which is in the gap of a strong magnet. (ac pumps are also possible.) dc pumps are characterized by a high pumping head at low velocities or in equivalent terms a high stall torque. Since it has no wearable moving parts, it is, in principle, capable of very high reliability. A typical reaction wheel, reaction sphere, and fluid flywheel are compared in the table.

Device	Size and Burden	Reliability	Development Status	Advantages	Disadvantages
Wheels (3)	15.5 cm (6-inch) diameter 13.6 kg (30-pound) weight 15 watts	Improved materials the reliability fairly good. Still subject to mechanical failure (mainly bearing).	Used on OGO and OAO. Developed for several immediate applications.	Highly accurate, proven.	Crosscoupling effects.
Spheres	15.5 cm (6-inch) diameter 9.06 kg (20-pound) weight 10 watts	Questionable reliability. Major problem is the sphere suspension system.	None developed for space use. A few experimental models now in existence.	No cross-coupling. Lighter weight.	Subject to suspension system failure. Development status.
Fluid	15.5 cm (6-inch) diameter 16.3 kg (36-pound) weight 7 watts	Highly reliable (no moving parts).	Developed by GE for Advent Communication Satellite.	Low power consumption. High reliability. Simple control system. Fast response.	Crosscoupling effects. Development status.

Comparison of Momentum Storage Devices

MOMENTUM WHEELS

Momentum wheels are similar to reaction wheels except they are larger. Typical values of weight and momentum are given.

Momentum wheels provide restoring torques about the axis of rotation in a manner identical to the reaction wheel. However, they differ from the latter in having much greater momentum storage capacity so that they also provide gyroscopic stability about the remaining two axes. Orientation of the vehicle about the spin axes is controlled by applying torque to the momentum wheel just as if it were a reaction wheel. Although the other two axes are gyroscopically stabilized, another torquing device such as a reaction jet or reaction wheel must be used to process them to the proper attitude as well as to correct for drift and disturbing torques.

The advantage of the momentum wheel system is the much greater attitude stiffness compared to the reaction wheel system. Disadvantages are the greater weight and volume of the wheel and its required supporting structure and the potentially high power requirements for its driving motor. Some typical momentum wheel control system weights are shown in Figure A and B.

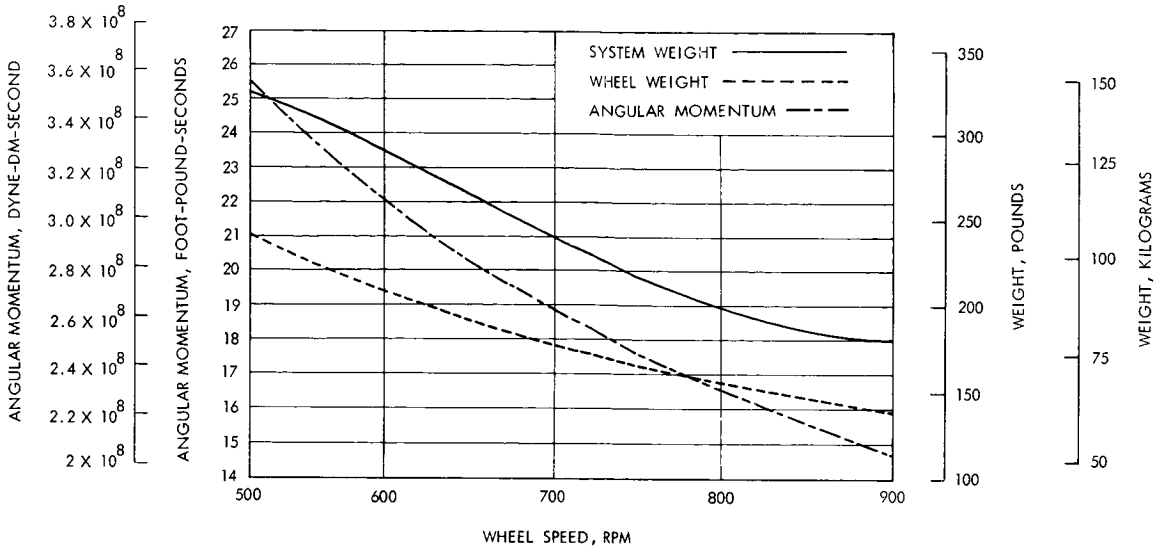

Figure A. Momentum Wheel System Weight and Angular Momentum Versus Wheel Speed for Constant Wheel Diameter, 152 cm, (5 feet)

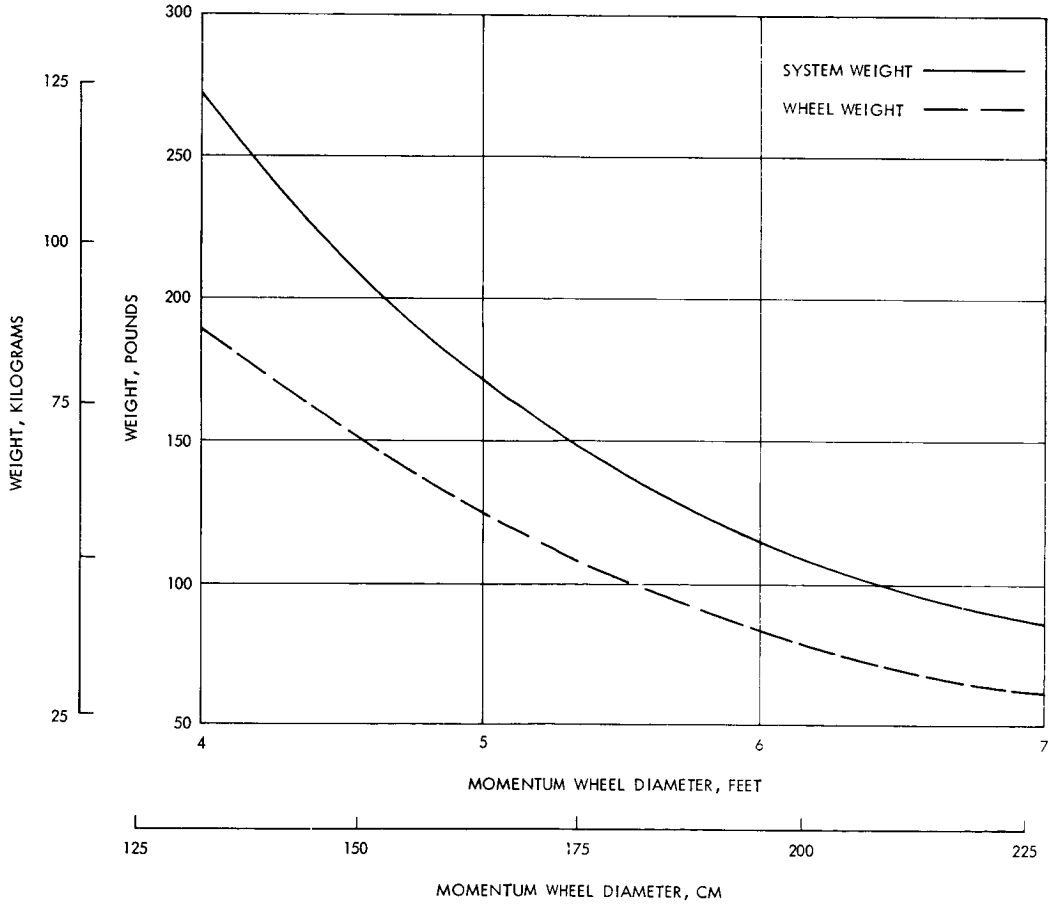

Figure B. Momentum Wheel System Weight Versus Wheel Diameter for Constant Wheel Speed (500 rpm) and Angular Momentum, 1.82×10^5 gram-cm-sec, (13.24 Foot-Pound-Seconds)

REACTION JETS

Reaction jets are widely used in attitude control. Typical system weights are given for cold gas systems, monopropellant systems and bipropellent systems.

Reaction jet systems, using gas or liquid propellant, constitute a simple, reliable, and space proven means of attitude stabilization. Reaction jet systems are customarily operated in an on-off mode characterized by limit cycle operation in which the jets are energized when the error in vehicle orientation exceeds a pre-determined limit.

For stability, velocity information is added to the attitude sensor signal. In the usual case of the two sided or "hard" limit cycle the vehicle enters a "deadband" angle between the limit positions with a velocity sufficient to coast across the deadband and emerge from the other side, whereupon the torquers are energized and the vehicle again crosses the deadband, etc. In a properly designed system the velocity with which the deadband is entered each time is less than that at which it left the deadband so that deadband rates decrease until a minimum value or limit cycle rate is reached. Fuel consumption during limit cycle operation varies inversely as the width of the deadband and directly as the square of the deadband rates, if the effects of the external disturbance torques are low compared to the deadband rates. For a two sided limit cycle the fuel weight required W, is given by

$$W = \frac{I \dot{\theta}_o^{\,2} t}{\ell \theta_d I_{sp}}$$

where

θ_d = the half-deadband angle

$\dot{\theta}_o$ = characteristic limit cycle rate of the system

ℓ = moment arm

t = total mission time

I_{sp} = fuel specific impulse

In this mode, the fuel consumption is directly dependent upon system parameters, and the fuel weight is inversely proportional to θ_d. In general, θ_d must be set smaller than the desired pointing accuracy to allow for potential sensors errors; hence fuel weight can be expected to be high for applications where θ_d <0. 1 degree.

When vehicle rates are very low, external disturbance torques may reverse the vehicle's motion before it crosses the deadband. In this case it emerges from the same side of the deadband as it entered.

This mode of operation is called a one sided or "soft" limit cycle. It is an attractive situation because no fuel is consumed to remove vehicle momentum which was imparted by the previous expenditure of fuel. The integral of the attitude control torques is equal to the integral of the disturbance torques, resulting in the minimum possible fuel consumption, namely

$$W = \frac{T_d\, t}{I_{sp}\, \ell}$$

where

t = time

T_d = the average disturbing torque

This one-sided mode of operation is not normally achieved by the use of position information and directly-sensed rate information. Derived rate techniques have been developed, however, which permit very low vehicle angular rates to be achieved. As a result one-sided limit cycle operation is feasible where the disturbance torques are relatively constant and can be accurately predicted.

Reaction jets can be used singly, or in pairs. The latter configuration has the advantage that the moment applied to the vehicle is constant regardless of the location of the nozzles relative to the c. g. This may be of importance where the c. g. shift is large (such as when a lander is separated from a parent vehicle). The use of couples is also advantageous in that it permits the nozzles to be located at any convenient part of the vehicle.

Reaction jet systems are customarily classified according to the fuel used as

Cold Gas

Hot Gas monopropellant

Hot Gas, bipropellant.

Cold gas systems operate by expelling compressed cold gas through expanding nozzles. The common fuels – nitrogen, helium, and the freons – are non-toxic, inexpensive, readily available, and pose no thermal or contamination problems to components or surfaces on which they may impinge. Specific impulse is modest but specific volume is relatively low. A wide range of thrust levels may be attained and thrust

REACTION JETS

response time is short. In contrast to the time and expense of developing and qualifying a new hot gas thrust chamber, cold gas nozzles require only proper sizing and brief testing to assure that they will have the intended performance. Cold gas nozzles were the first actuators used for attitude control of space vehicles and have been widely used since.

Along with these virtues there are some distinct disadvantages to cold gas actuators. Where large total impulse is required, the low specific impulse gives a definite weight penalty. For missions of long duration, especially where accurate orientation is required, the control valve may be operated many thousands of times. This places a severe reliability requirement on the components. Leakage poses a severe threat as a consequence of the limited total impulse carried by the vehicle.

As seen in Figure A,[1] there is a fairly well defined breakeven point where weight considerations favor the use of hot gas over cold gas. Other factors to be considered are the thrust level desired and the minimum impulse bit required. Hot gas engines typically have higner minimum thrust, but this is partially offset by a faster valve response than for cold gas. This is particularly true of bi-propellant systems. Figures B through D[1] show typical performance characteristics for expulsive systems.

Mono-propellant hot gas systems rank intermediate between the bi-propellant and the cold gas. They have the advantage of simplicity in that a single valve is required, and the pressurization system does not have to guard against the possibility of accidental mixing of fuel and oxidizer due to leakage or permeation of diaphragms or bladders. Mono-propellants also have more modest specific impulse and a thrust buildup time constant that is both longer and more uncertain than with the bi-propellants. This is particularly true for short pulses.

Other factors to be considered in the use of hot gas systems are the gas temperature and the combustion products, both of which can be detrimental to surfaces they impinge upon, and also to optical devices whose line-of-sight intersects the plume. Radiation cooled thrustors pose an additional thermal problem to the vehicle and equipment near them. As a result of these considerations the tradeoff between hot gas and cold gas systems frequently favors the cold gas even though hot gas can demonstrate a definite weight saving.

The primary advantages of the reaction jet stabilization system are simplicity, flight proven capability, and the ability to provide acquisition, reacquisition, and maneuvers on ground command (limited only by sensor field-of-view capability). The primary disadvantages are the weight penalties associated with fuel and tankage weight for long missions and the accuracy limitations (the limit cycle mode implies an average pointing error approximately equal to one-half the attitude deadband width in addition to sensor contributed errors).

---

[1] Woestemeyer, F. B., "General Considerations in the Selection of Attitude Control Systems," Conf. Proc. SAE/NASA Aerospace Vehicle Flight Control Conference, Los Angeles, California, July 13-15, 1965.

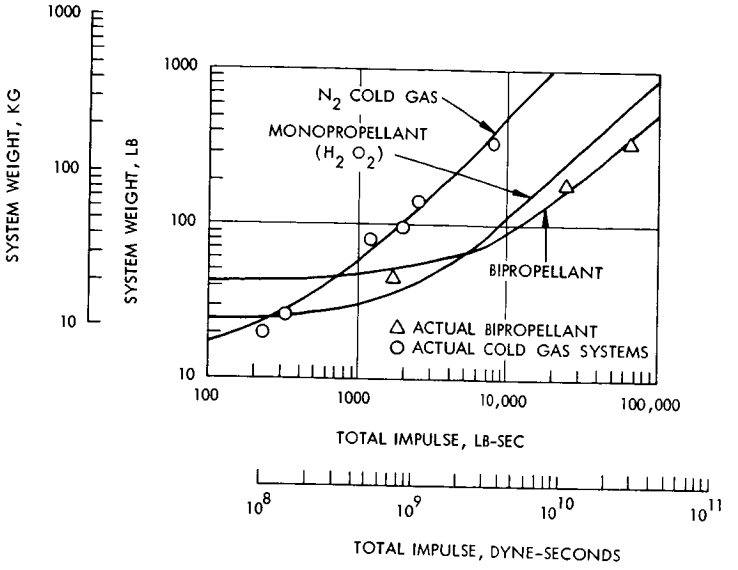

Figure A. Attitude Control System Weight Versus Total Impulse

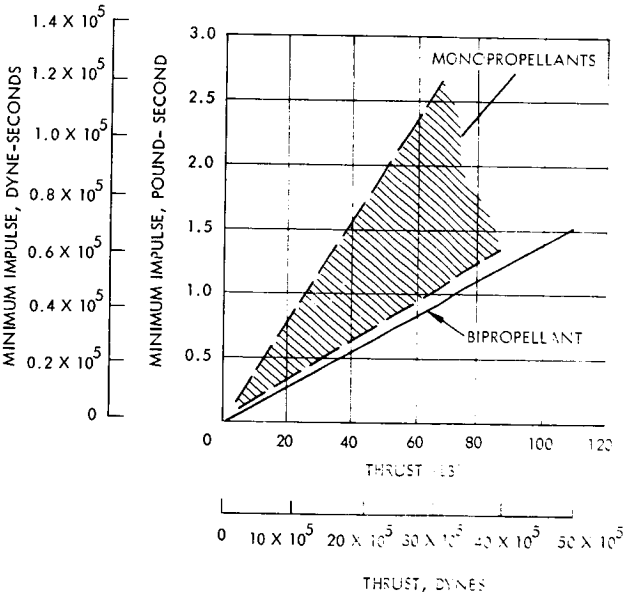

Figure B. Minimum Impulse Bit Versus Thrust

REACTION JETS

A further consideration is that for reaction jet systems energy consumption is a function of the instantaneous control torques required by the vehicle. Momentum removed from the vehicle leaves the system with the expelled gas and cannot be reclaimed. Momentum transfer devices, on the other hand, merely transfer momentum from the vehicle structure to a rotating mass such as a flywheel or a gyroscope located inside the vehicle. As a result, momentum that is transferred to a fly-wheel or gyro in resisting a clockwise torque on the vehicle can then be transferred back to the vehicle in resisting a subsequent counterclockwise torque. This difference is significant in the case of orbiting vehicles which frequently experience cyclic torques as a function of position in orbit. Large components of these will integrate to zero over the orbital period so that the net momentum required over the period is zero.

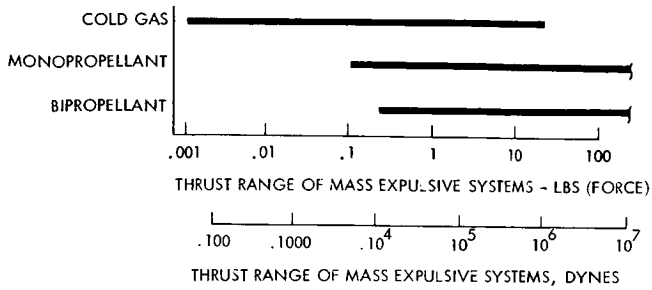

Figure C. Thrust Range of Mass Expulsive Systems

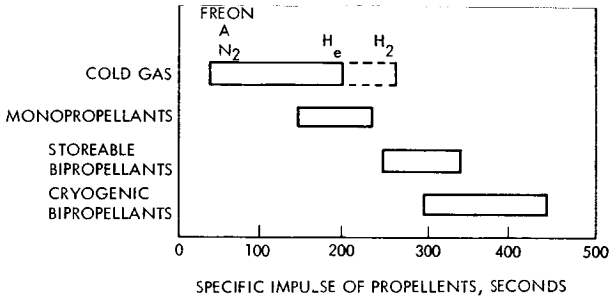

Figure D. Specific Impulse of Propellants

COMPONENT PERFORMANCE AND BURDEN RELATIONSHIPS

Burden Relationships

WEIGHT BURDENS

The acquisition and tracking weight needed for spaceborne apertures are modeled in a form compatible with the methodology described in Volume II of this final report.

A typical transmitter or receiving antenna pointing system consists of a gimbaled support unit, which holds the antenna, and an associated control system, which points the antenna. The weight of the antenna pointing system is dependent upon the weight it must support, the antenna weight, whose weight in turn is dependent upon the antenna size. The antenna pointing system weight is usually not dependent upon the pointing accuracy.

The weight of the acquisition and tracking system may then be modeled in terms of the diameter of the aperture being used.

Such modeling has been done below in a form suitable for the methodology described in Volume II of this final report.

$$W_{QT} = W_{BT} + K_{W_{AT}} K_{d_T} d_T^{n_T} \qquad (1)$$

where

W_{QT} = total transmitter acquisition and tracking weight.

W_{BT} = transmitter acquisition and tracking weight independent of aperture size.

$K_{W_{AT}}$ = constant relating transmitter acquisition and tracking weight to transmitter antenna weight.

K_{d_T} = constant relating transmitter antenna weight to transmitter antenna diameter.

n_T = exponent relating transmitter antenna weight to transmitter antenna diameter.

The constants of equation 1 have been evaluated using the material of this section references quoted in this section and engineering judgement. The result of this determination is given in Figures A and B which plot the acquisition and tracking weight required for spaceborne optical and radio apertures respectively.

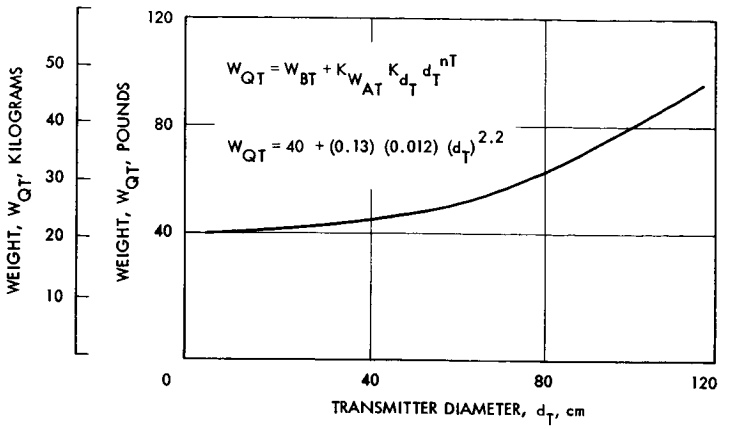

Figure A. Optical Transmission Acquisition and Track Weight

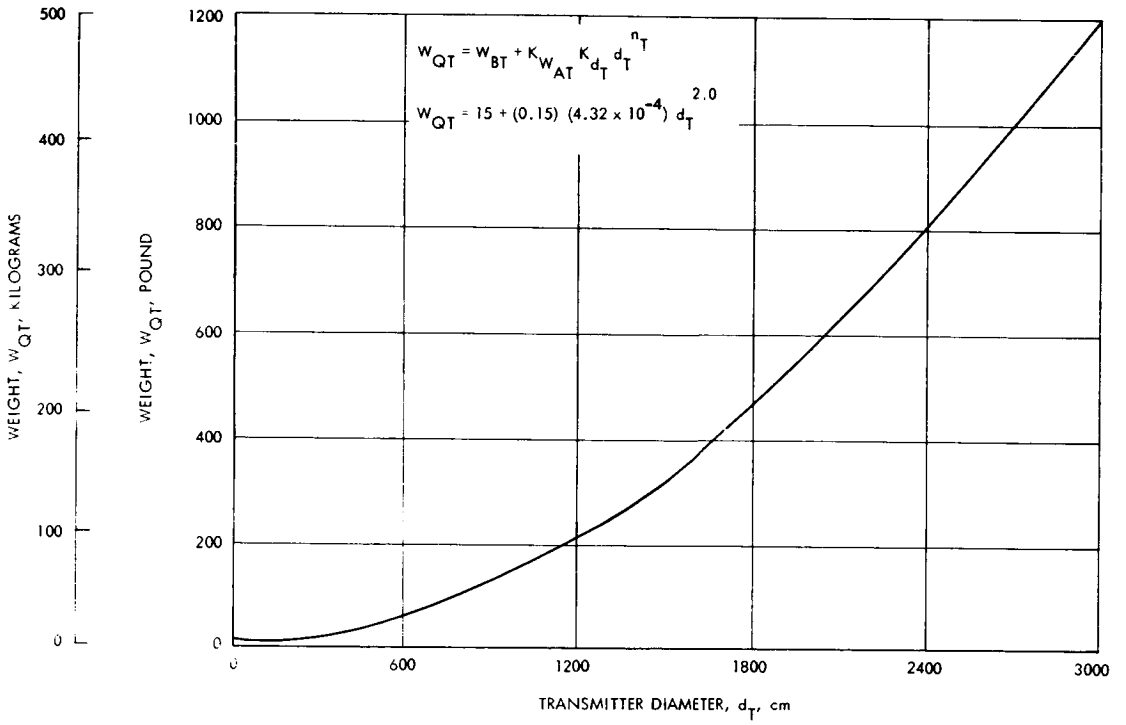

Figure B. Radio Transmitter Acquisition and Track Weight

COST BURDENS

The acquisition and tracking cost for spaceborne and earth apertures is modeled in a form compatible with the methodology described in Volume II of this final report.

The fabrication cost of the transmitter antenna pointing equipment is inversely proportional to the pointing accuracy. Pointing accuracy is generally specified as a fixed percentage of the transmitter beamwidth. Since the transmitter antenna is usually diffraction limited, the fabrication cost of the transmitter antenna pointing equipment is dependent upon the transmitter antenna diameter or gain. A modeling dependent upon these considerations and compatible with the methodology described in Volume II of this Final Report is shown below.

$$C_{QT} = C_{AT} + K_{AT}\left(\frac{\lambda}{d_T}\right)^{-q_T} \qquad (1)$$

where

C_{QT} = total transmitter acquisition and tracking fabrication cost.

C_{AT} = transmitter acquisition and tracking fabrication cost independent of transmitting beamwidth.

K_{AT} = constant relating transmitter acquisition and tracking cost to transmitter beamwidth.

λ = transmitted wavelength

d_T = transmitter aperture diameter

q_T = Exponent relating transmitting acquisition and tracking fabrication cost to transmitted beamwidth.

The fabrication cost of the receiver antenna pointing equipment is inversely proportional to the pointing accuracy. For a diffraction limited receiver antenna the fabrication cost of the pointing equipment is dependent upon the receiver antenna diameter or gain, and for a non-diffraction limited receiver antenna the fabrication cost is proportional to the receiver field of view. A modeling dependent upon these considerations and compatible with the methodology described in Volume II of this final report is shown below.

$$C_{QR} = C_{AR} + K_{AR}\,(\theta_R)^{-q_R} \qquad (2)$$

where

C_{QR} = Total receiver acquisition and tracking fabrication cost.

C_{AR} = Receiver acquisition and tracking equipment fabrication cost independent of receiver beamwidth.

K_{AR} = Constant relating receiver acquisition and tracking equipment fabrication cost to receiver beamwidth.

θ_R = Receiving beamwidth, field of view

q_R = Exponent relating receiver acquisition and tracking equipment fabrication cost to receiver beamwidth.

The constants of equations 1 and 2 have been evaluated using the material of this section, references quoted in this section and engineering judgement. The results of this determination is given in Figures A, B, C and D.

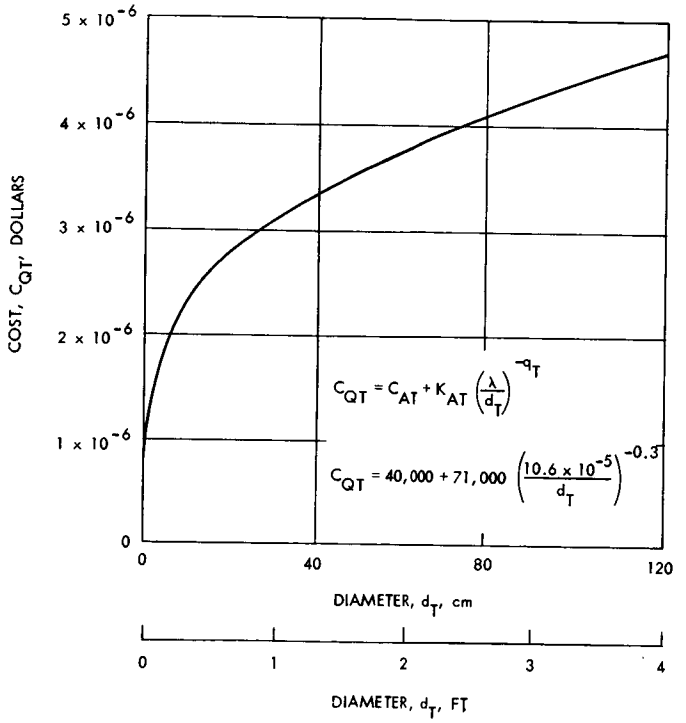

Figure A. Cost of Optical Transmitter Acquisition and Tracking

COST BURDENS

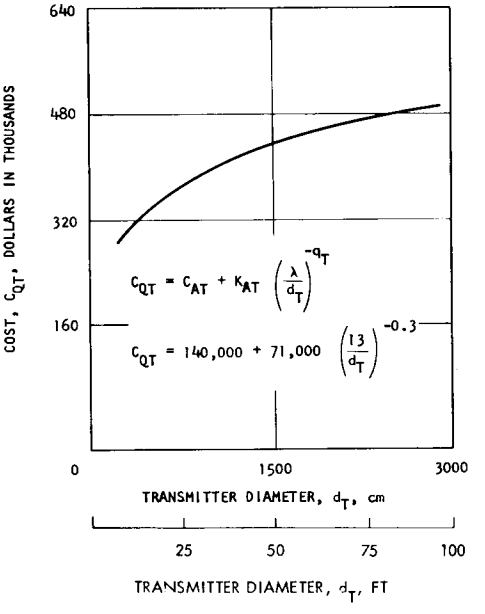

Figure B. Cost of Transmitter Acquisition and Pointing

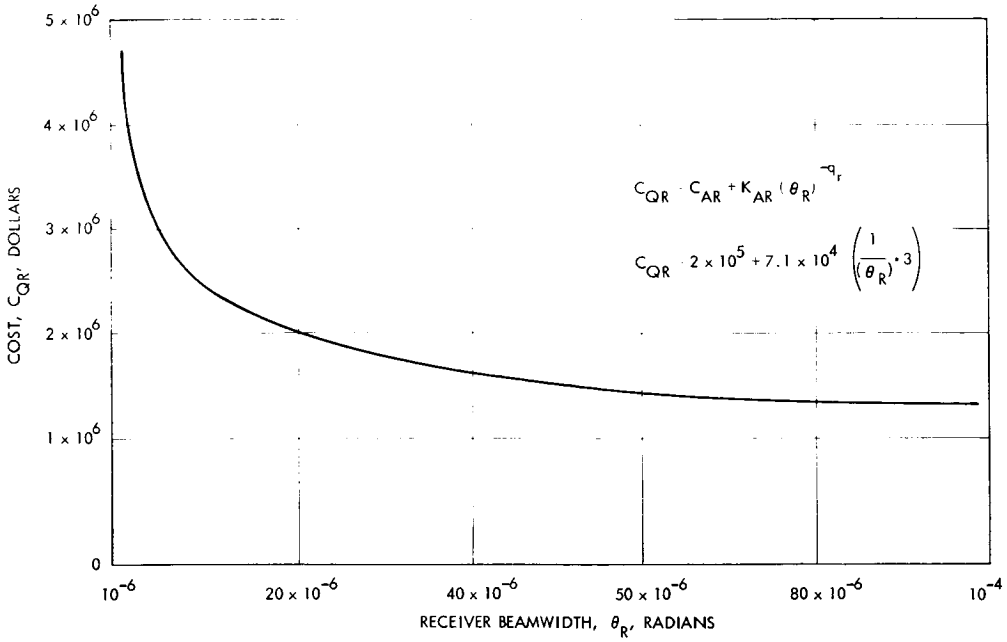

Figure C. Optical Receiver Acquisition and Pointing Cost

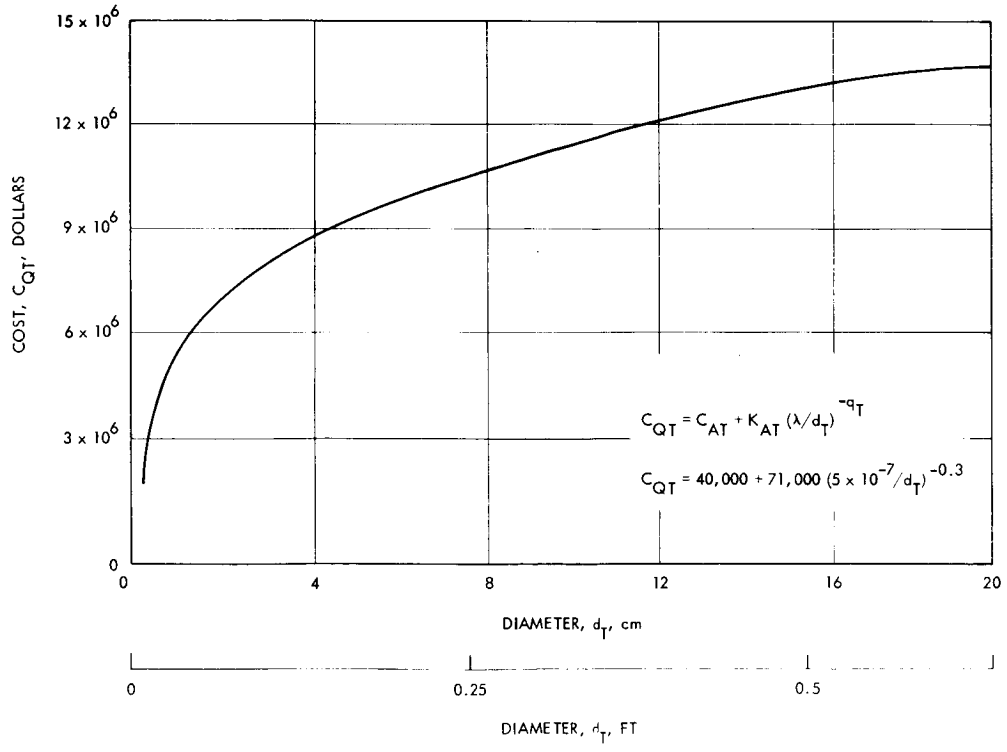

Figure D. Radio Transmitter Acquisition and Pointing Cost

POWER BURDENS

The acquisition and tracking power requirement for spaceborne apertures are modeled in a form compatible with the methodology described in Volume II of this final report.

The electrical power requirement for the transmitter or receiver antenna pointing equipment is primarily dependent upon the weight of the antenna that must be positioned by the gimbal motors. Hence, the power requirement is also proportional to the antenna diameter or gain. A modeling dependent upon this consideration and compatible with the methodology given in Volume II of this final report is shown below.

$$P_{QT} = K_{P_{QT}} W_{QT} \tag{1}$$

where

P_{QT} = The power required by the transmitter acquisition and tracking subsystem.

$K_{P_{QT}}$ = Constant relating transmitter acquisition and tracking equipment power to acquisition and tracking weight.

W_{QT} = Total transmitter acquisition and tracking weight.

The total transmitter acquisition and tracking weight, W_{QT}, may be expressed in terms of the transmitting aperture diameter. This was done in a previous topic but is repeated here for completeness.

$$W_{QT} = W_{BT} + K_{W_{AT}} K_{d_T} d_T^{nT} \tag{2}$$

where

W_{QT} = Total transmitter acquisition and tracking weight

W_{BT} = Transmitter acquisition and tracking weight independent of aperture size

$K_{W_{AT}}$ = Constant relating transmitter acquisition and tracking weight to transmitter antenna weight

K_{d_T} = Constant relating transmitter antenna weight to transmitter antenna diameter

n_T = Exponent relating transmitter antenna weight

d_T = Transmitter Aperture Diameter

The total expression for the required power is then

$$P_{QT} = K_{P_{QT}} \left[W_{P_{QT}} + K_{w_{AT}} K_{d_T} d_T^{nT} \right] \qquad (3)$$

This is plotted in Figures A and B for a radio and optical system, respectively.

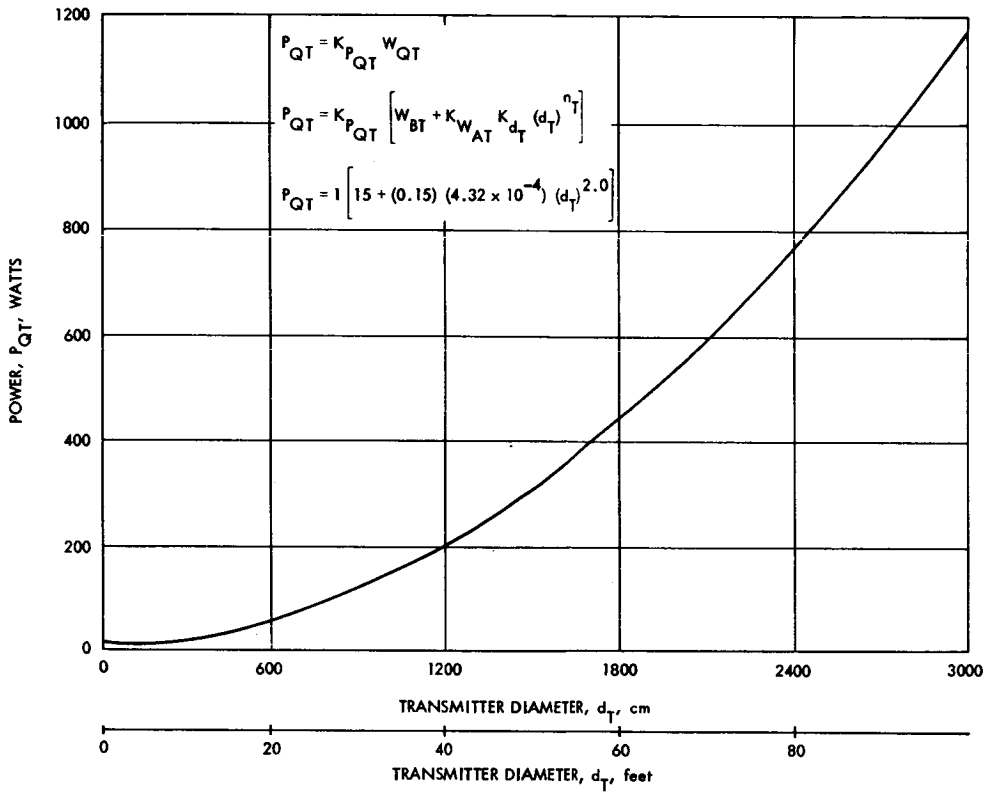

Figure A. Power for Radio Acquisition and Tracking (Transmitting or Receiving)

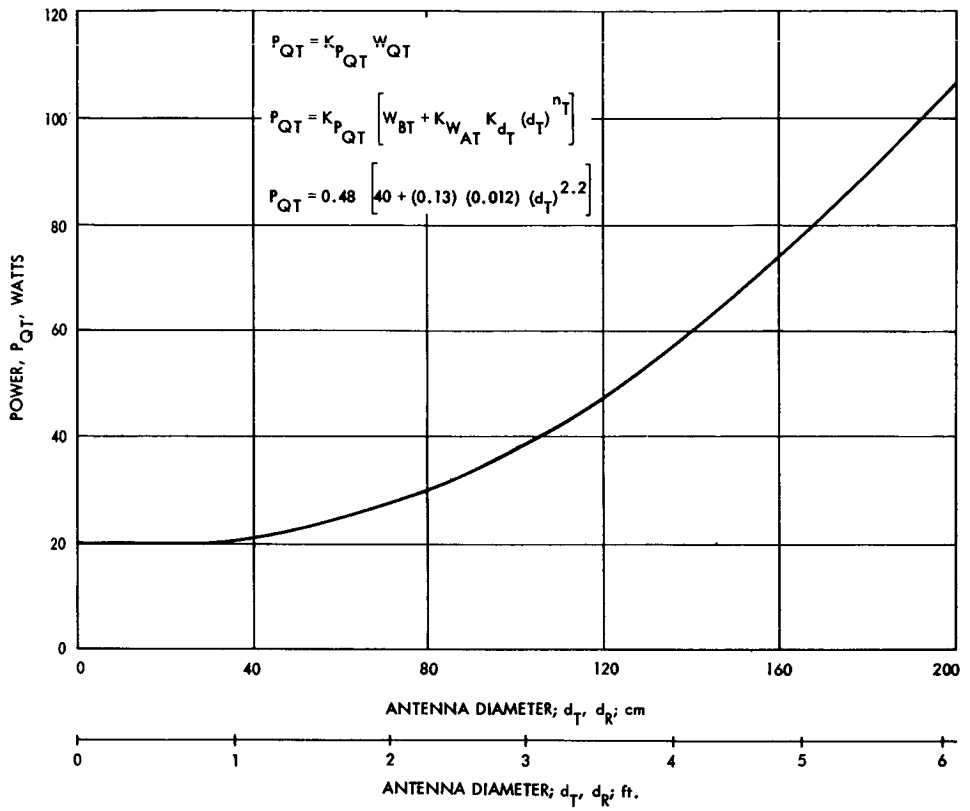

Figure B. Optical Transmitter (Receiver) Acquisition and Tracking, Power

PART 6 – PRIME POWER SYSTEMS

Section